Spectrum of Cuscuton Bounce and Cosmological Parameter Inference Using Dark Sirens

by

Jungjoon Leo Kim

A thesis
presented to the University of Waterloo
in fulfillment of the
thesis requirement for the degree of
Master of Mathematics
in
Applied Mathematics

Waterloo, Ontario, Canada, 2021

Author's Declaration

This thesis consists of material all of which I authored or co-authored: see Statement of Contributions included in the thesis. This is a true copy of the thesis, including any required final revisions, as accepted by my examiners.

I understand that my thesis may be made electronically available to the public.

Statement of Contribution

I am the sole author for Chapters 1, 2, 3, 5, and 7, which was written under the guidance of my advisor Ghazal Geshnizjani and were not written for the sake of publication.

The research presented in Chapter 4 is based on my research with my advisor Ghazal Geshnizjani, which was published to the Journal of Cosmology and Astroparticle Physics (JCAP) in March 2021 [143].

The research presented in Chapter 6 is based on my research performed in collaboration with Supranta Sarma Boruah, William Gregory Dallaway, and Ghazal Geshnizjani. At the time of writing this thesis, the work is in preparation for submission to be published.

Abstract

Over the last couple of decades, cosmology has become an exciting area to study. Technological developments in both the computational and observational fronts have propelled cosmology into the limelight of modern physics. Since cosmology is the study of the Universe, many areas of physics – such as astronomy, astrophysics, gravitation, fundamental physics, statistical mechanics, and quantum theory – all couple together and present some of the most fascinating puzzles in modern physics in a natural meeting place. In this thesis I will present my research in two very different epochs of our cosmological history.

In order to describe my research, I will first provide a brief introduction to cosmology and Einstein's field equations in a cosmological background. I will then review some of the developments in understanding the very early Universe – a cosmological epoch that corresponds to the very first moments of what we believe to be our cosmological history. I will outline the successes and criticisms of the current paradigm, and discuss the status of alternative proposals that could address some of these criticisms. In particular, bouncing cosmologies are an interesting alternative to inflation since they naturally resolve the singularity problem. I will then present my own work on a bouncing cosmology driven by a modification to general relativity called Cuscuton gravity. In particular, I show the prospects of this model for producing initial conditions for the ripples of spacetime at early times are consistent with observational constraints.

In the second half of my thesis, I will drastically shift in time to the "present day" Universe, only up to about 2 billion years ago, where I will discuss the prospects of using gravitational waves to extract significant information about the previously hidden sectors of the Universe. To be specific, since the gravitational waves emitted when a compact binary system merges provide an opportunity to measure cosmological distances, this information can then be used alongside previous electromagnetic signals to shed new light on cosmological mysteries. In particular, by assuming that the binary mergers and galaxies both come from the same underlying distribution of matter in our Universe, I show that one can use Bayesian inference methods to infer cosmological parameters without making an excessive amount of assumptions.

Acknowledgements

This thesis would not have been possible without the help of many individuals – both of academic and personal relations.

First and foremost I sincerely thank my advisor, Ghazal Geshnizjani, for her guidance in my research during the course of my degree and her limitless patience. She has been a role model to me, both as a scientist and an individual, for whom I have been grateful to work with over the last couple of years. I consider myself tremendously lucky for such a fantastic advisor in all aspects.

I thank my committee members Michael J. Hudson and Florian Girelli for their very helpful feedback. I thank Niayesh Afshordi, José T. Gálvez Ghersi, and Erik Schnetter for their very helpful discussions and feedback in my research. I am also grateful towards Guilhem Lavaux for the mock catalog via the `VELMASS` suite for Chapter 6. I would also like to thank the past and current members of the Geshnizjani group during my time – Supranta Sarma Boruah, Hyungjin (Tony) Kim, Dorsa Sadat Hosseini Khajouei, Amirhossein Dehghanizadeh, William Gregory Dallaway, Madison Tindall, Jordan Krywonos, and Kieana Fana. I especially thank Supranta and Tony not only for the discussions about research, but also for their guidance and mentorship before even starting my program. I also thank Gantumur Tsogtgerel, Kyung Soo Choi, and Edward Vrscay for their guidance.

I am also indebted to my hometown friends Chris, Ivan, Jason, Mike, Ben, and Sanai for their (virtual) camaraderie in these times of isolation. In the same regard, I thank all the members of the University of Waterloo Kendo Club, especially Avery and Julian, for all the good times. I also thank Connie and Derek for their limitless hospitality and friendship. To those in the AMATH Grad Journal Club who I consider my virtual officemates – Brian, Delaney, Melissa, Nick, Stéphanie, and William – thank you for the very interesting discussions, support, and group rant sessions.

Finally, I thank my parents, my grandparents, and my sister Flora, for their unwavering support for my ambitions from the start. Without them, I would not have had the opportunity, nor the courage, to pursue my scientific curiosities. Lastly, I thank Dannie Fu for her constant willingness to listen to my ramblings about research or just about anything. She has been a pillar of support and the source of my motivations, to whom I am grateful for beyond words.

Finally, I acknowledge the support of the Natural Sciences and Engineering Research Council of Canada (NSERC) throughout the course of my degree. I acknowledge that I live and work on the traditional territory of the Neutral, Anishinaabeg and Haudenosaunee peoples. The University of Waterloo is situated on the Haldimand Tract, the land promised to the Six Nations that includes ten kilometres on each side of the Grand River.

Table of Contents

List of Figures

List of Tables

Chapter 1

Introduction

Throughout human history, our enigmatic universe has never failed to captivate its inhabitants in its deep mysteries. It is only natural then, that with the continuous development of mathematical physics and the rapid advancement of technology to test those mathematical models, the study of the universe and cosmology, has become one of the pillars of modern physics. As many textbooks and journal articles like to state in their introductions, we are in the "golden era of cosmology"[1]. This statement, however cliché it may be, is truly an accurate representation of the current state of cosmology. A common problem in physics is that the development of theoretical models drastically precedes the technology required to obtain experimental data to test these models. However, in cosmology the vast amount of currently available and upcoming observational data from cosmological surveys provide a healthy harmony of theory and data – making cosmology remarkably exciting to study.

While the study of cosmology is a very diverse field with an abundance of topics and subcategories, this thesis will focus on topics in two specific topics one in early universe cosmology and the other related to gravitational wave cosmology. The early universe is a period in our cosmological history that precedes the formation of galaxies and stars, considering the very first moments of our universe. The current paradigm for the early universe is the inflationary model [121]. The inflationary model is a hugely successful theory, historically being able to answer puzzling cosmological problems such as the horizon problem and the flatness problem, while also providing a framework to explain the initial conditions for the large scale structure of the Universe and in the Cosmic Microwave Background (CMB) that were later confirmed by astronomical observations [22].

[1] A search on the NASA/ADS database for "golden age" in the body text with keyword "cosmology" gives 263 results since 1984. This is not including grant proposals, arguably the biggest offender.

While the early universe has been studied in depth over the last 40 years or so, with inflation having been continuously developed since the 1980s [160, 28, 158, 159], the theoretical predictions of gravitational radiation are much older. It is only recently that experiments have caught up to theory and gravitational wave astronomy is coming to fruition. One of Einstein's many predictions from general relativity, gravitational waves (GWs) are the ripples in spacetime produced by accelerated masses. With the first detection of gravitational waves from a binary black hole merger by the Laser Interferometer Gravitational-Wave Observatory (LIGO) Scientific Collaboration and the Virgo Collaboration in 2015[2] [2], a new era of multi-messenger astronomy was realized. While most previous astrophysical signals were only available in the electromagnetic (EM) spectrum (ie. light) which can be affected by many obstructions between the us and the source, gravitational waves allow for an almost unimpeded direct signal to the source since they are distortions of spacetime. Since then, many subsequent detections of gravitational waves have been observed, with many more expected to come in the upcoming years. As more gravitational wave data become available to us, we can then use existing data from electromagnetic signals along with the gravitational waves to acquire a more complete understanding of our universe.

Despite the recent exciting successes in cosmology, there are still some gaps in our knowledge of the standard picture of cosmological models. For instance in early universe cosmology, inflationary paradigm, while successful in explaining some cosmological puzzles, has shortcomings of its own. In particular, issues such as the trans-Planckian problem and the singularity problem are just couple of challenges that the inflationary model still faces. In addition, from an effective field theory perspective, it is an ongoing discussion whether or not inflation is compatible with the predictions of string theory via the swampland conjectures. Meanwhile, in the late Universe we still face conundrums such as understanding the nature of dark energy and dark matter, and more recently, there is a current ongoing tension for the local Hubble constant H_0 between observational measurements the from early universe remnants such as the CMB, and late universe observations such as, but not limited to, supernovae data. With the expected incoming gravitational wave data from experiments and with the large galaxy surveys available to us, cosmologists hope that multi-messenger astronomy will shed light on the cosmological parameter debates.

The outline for this thesis is as follows: in chapter 2, I will present a working background of the standard model of cosmology. Then the thesis splits into two parts. The first part of the thesis will be on topics in the very early Universe. In particular I will discuss the inflationary paradigm for the very early Universe and its proposed alternatives in chapter 3. Then in chapter 4, I will present the predictions for the power spectrum for

[2]The direct detection was on September 15, 2015, while the announcement from the LIGO collaboration was made on February 11, 2016.

an alternative scenario to inflation known as a Cuscuton bounce. In the second part of the thesis, I will discuss the exciting developments in multi-messenger astronomy using GWs. In chapter 5, I will briefly introduce GW astronomy as well as some preliminary background for understanding statistics of the large scale structure of the Universe. Then I will present my own work on using gravitational wave data from dark sirens to infer cosmological parameters in chapter 6. I will conclude the thesis in chapter 7 and provide final discussions.

The primary programming language for any numerical computation for this thesis was performed in python[3], using the `NumPy`[4] [125], `SciPy`[5] [218], `Astropy`[6] [196, 190], `astroML`[7] [214], and the Code for Anisotropies in the Microwave Background (`CAMB`)[8] [152] libraries. For the rest of the thesis, I will use the $(-+++)$ sign convention for the metric tensor. In addition, in the context of tensors, the Latin indices i, j, k, etc. will correspond to spatial dimensions $i = 1, 2, 3$, while Greek indices μ, ν, λ, etc. will correspond to all spacetime dimensions $\mu = 0, 1, 2, 3$. Spatial vectors will be denoted in bold, ie. $\mathbf{v}$. I will also take the usual convention of natural units where $c = \hbar = k = 1$. Wherever the Planck mass M_P shows up, it will take the form of $M_P = 1/\sqrt{8\pi G}$, unless otherwise stated.

[3] https://www.python.org/
[4] https://numpy.org/
[5] https://www.scipy.org/
[6] https://www.astropy.org/
[7] https://www.astroml.org/
[8] https://camb.info/

Chapter 2

Cosmology

In this section I will introduce the standard model of cosmology starting with some basic results from general relativity. The discussions in this section are inspired by several reference texts – Sean Carroll's textbook/lecture notes on general relativity [75], Steven Weinberg's textbook/lecture notes on cosmology [219], and Scott Dodelson's textbook on cosmology [94].

2.1 The Einstein Field Equations

General Relativity (GR) is one of Einstein's most significant contributions to modern physics, and is one of the cornerstones of our current understanding of physics. Originally proposed in the early 1900s, it is the successor to Newtonian gravity, the previous paradigm of gravitational physics, and has remained as the most successful theory of gravity to date.

For a proper introduction to GR, one must study differential geometry on manifolds. For this thesis, I will simply present the relevant equations and provide a brief description of the underlying mathematical implications. Given a spacetime manifold $\mathcal{M}$, one equips $\mathcal{M}$ with a *metric tensor* $g_{\mu\nu}$[1]. In the context of general relativity, the metric is a symmetric, Lorentzian or pseudo-Riemannian[2], $(0,2)$ tensor. The metric is also often used

[1] In a widely used convention, the "tensor" $A^{\nu_1\nu_2\cdots\nu_m}{}_{\mu_1\mu_2\cdots\mu_n}$ is actually the coefficient of a (m,n) tensor A, which is a multilinear map from a collection of m dual vectors and n vectors to $\mathbb{R}$. For general purposes however, physicists often interchange the tensor A and the coefficient $A^{\nu_1\nu_2\cdots\nu_m}{}_{\mu_1\mu_2\cdots\mu_n}$ for brevity.

[2] A Euclidean or Riemannian metric is a continuous, nondegenerate, positive-definite metric. A Lorentzian or pseudo-Riemannian metric is a metric that is continuous, nondegenerate, and indefinite.

interchangably with the spacetime line element:

$$ds^2 = g_{\mu\nu} dx^\mu dx^\nu, \tag{2.1}$$

where dx^μ is a basis dual vector. The inverse metric $g^{\mu\nu}$ can also be defined as a symmetric, Lorentzian, $(2,0)$ tensor such that

$$g^{\mu\nu} g_{\nu\sigma} = \delta^\mu_\sigma, \tag{2.2}$$

where δ^μ_σ is the four-dimensional Kroenecker delta, such that

$$\delta^\nu_\mu = \begin{cases} 1 & \text{if } \mu = \nu, \\ 0 & \text{if } \mu \neq \nu. \end{cases} \tag{2.3}$$

If spacetime is flat, then one refers to the associated metric as the *Minkowski metric* denoted as $\eta_{\mu\nu}$, where

$$\eta_{\mu\nu} = \text{diag}(-1, 1, 1, 1). \tag{2.4}$$

The metric and the inverse metric can be used to raise lower indices in tensor calculus. Given a metric $g_{\mu\nu}$ and a generic tensor $A^{\alpha\beta}{}_{\gamma\delta}$,

$$A^{\alpha\beta}{}_{\gamma\delta} = g_{\mu\gamma} A^{\alpha\beta\mu}{}_\delta = g^{\alpha\mu} A_\mu{}^\beta{}_{\gamma\delta}. \tag{2.5}$$

One can also contract two indices of a tensor if the same index shows up as an upper and lower index. For example, given a generic tensor $A^{\alpha\beta}{}_{\gamma\delta}$, the contraction for the second and third indices is given by

$$A^\alpha{}_\delta = A^{\alpha\beta}{}_{\beta\delta} = g_{\beta\gamma} A^{\alpha\beta\gamma}{}_\delta. \tag{2.6}$$

This is a useful trick to reduce the ranks of tensors, such as to consider a scalar quantity from a $(1,1)$ tensor, oftentimes called the trace.

The *Einstein Field Equations* (EFE) are given by[3]

$$G_{\mu\nu} = R_{\mu\nu} - \frac{1}{2} R g_{\mu\nu} = 8\pi G T_{\mu\nu}, \tag{2.7}$$

[3]This form is without the explicit cosmological constant Λ. For the rest of this thesis we will assume this form of the EFE.

where G is Newton's constant and $G_{\mu\nu}$ is the Einstein tensor, while the other quantities are soon to be defined. To compute the left-hand side of the EFE, one first requires the *Ricci scalar*, which is defined as

$$R = g^{\mu\nu} R_{\mu\nu}. \tag{2.8}$$

As we see the Ricci scalar itself is a contraction of a quantity $R_{\mu\nu}$ called the *Ricci tensor* which is a symmetric tensor defined as

$$R_{\mu\nu} = R^{\lambda}{}_{\mu\lambda\nu}. \tag{2.9}$$

The Ricci tensor is also a contraction, this time of the first and third indices of a quantity $R^{\rho}{}_{\sigma\mu\nu}$ called the *Riemann tensor*, defined as

$$R^{\rho}{}_{\sigma\mu\nu} = \partial_\mu \Gamma^{\rho}_{\nu\sigma} - \partial_\nu \Gamma^{\rho}_{\mu\sigma} + \Gamma^{\rho}_{\mu\lambda}\Gamma^{\lambda}_{\nu\sigma} - \Gamma^{\rho}_{\nu\lambda}\Gamma^{\lambda}_{\mu\sigma}. \tag{2.10}$$

The Riemann tensor is a combination of partial derivatives and products of a quantity known as the *Christoffel symbols*, which are given by

$$\Gamma^{\sigma}_{\mu\nu} = \frac{1}{2} g^{\sigma\rho}(\partial_\mu g_{\nu\rho} + \partial_\nu g_{\rho\mu} - \partial_\rho g_{\mu\nu}). \tag{2.11}$$

The Christoffel symbols are comprised of products of the metric tensor and derivatives of the metric tensor. Hence ultimately the Ricci scalar R and Ricci tensor $R_{\mu\nu}$ that show up in the EFE are determined by the metric $g_{\mu\nu}$. From this, one can see that the left-hand side of the EFE is encompassed completely by the spacetime geometry of the manifold.

In contrast, the right-hand side of the EFE packages information regarding the content on the spacetime manifold. In (2.7), $T_{\mu\nu}$ is the *energy-momentum tensor*. In cosmological contexts, the perfect fluid description is often a good description, which then gives the form for the energy-momentum tensor as

$$T_{\mu\nu} = (\rho + p) U_\mu U_\nu + p g_{\mu\nu}, \tag{2.12}$$

where U_μ is the spacetime four-velocity of the fluid.

In summary, Einstein's equations comprise a system of coupled nonlinear second-order partial differential equations. In the form expressed in (2.7), since the left-hand side is dependent on the geometry of the spacetime manifold and the right-hand side includes all dependencies to the matter content in the Universe, the EFE capture the interactions between spacetime and matter.

2.2 Einstein Field Equations from Field Theory

By using the *Einstein-Hilbert action*

$$S_{\text{EH}} = \frac{M_P^2}{2} \int \sqrt{-g} R \, d^4x, \tag{2.13}$$

where $M_P = 1/\sqrt{8\pi G}$ in natural units is the reduced Planck mass, one can also derive the EFE (2.7) from the Lagrangian formalism by using Hamilton's Principle of Least Action. Varying this action using standard methods in variational calculus, one finds that the variation δS_{EH} yields a summation of terms that include variations of the metric and the Ricci tensor, which by performing integration by parts and simplifying yields [75]:

$$\delta S_{\text{EH}} = M_P^2 \int d^4x \sqrt{-g} \left[R_{\mu\nu} - \frac{1}{2} R g_{\mu\nu} \right] \delta g^{\mu\nu}, \tag{2.14}$$

where $\delta g^{\mu\nu}$ is the variation of the inverse metric tensor $g^{\mu\nu}$. From this, since the stationary points of the action are given by $\delta S / \delta g^{\mu\nu} = 0$ ($g^{\mu\nu}$ is our "field" here), classical field theory yields

$$\frac{1}{\sqrt{-g}} \frac{\delta S_{\text{EH}}}{\delta g^{\mu\nu}} = R_{\mu\nu} - \frac{1}{2} R g_{\mu\nu} = 0, \tag{2.15}$$

and we recover the EFE (2.7) for vacuum, where $T_{\mu\nu} = 0$. In order to incorporate a non-empty Universe, we must include it into our action. Hence if the total action is denoted by S, then

$$S = S_{\text{EH}} + S_M, \tag{2.16}$$

where S_M is the action for some cosmological content (ie. matter). Variation of the total action, ie.

$$\delta S = \delta S_{\text{EH}} + \delta S_M, \tag{2.17}$$

and defining the energy-momentum tensor in this way as

$$T_{\mu\nu} = -\frac{2}{\sqrt{-g}} \frac{\delta S_M}{\delta g^{\mu\nu}}, \tag{2.18}$$

yields the EFE (2.7) for a general non-empty Universe with energy momentum tensor defined above. As we will see later on, the Lagrangian formalism is very useful in deriving how cosmological perturbations behave.

2.3 The Friedmann Equations

The *Friedmann-Lemaître-Robertson-Walker metric* is given by

$$ds^2 = -dt^2 + a^2(t)\left[\frac{dr^2}{1-\kappa r^2} + r^2 d\Omega^2\right], \tag{2.19}$$

where r is a spatial coordinate with dimensions of distance and κ is a curvature parameter with dimensions of inverse distance squared. $a(t)$ is the *scale factor*, a quantity that defines the relative size of the Universe at some time t. If one denotes the time today as t_0, then the usual convention is to take $a(t_0) = 1$. By approximating the matter and energy as an isotropic perfect fluid, one can write the four velocity for a comoving observer as

$$U^\mu = (1, 0, 0, 0). \tag{2.20}$$

Hence the stress-energy tensor with one upper and one lower index can be written conveniently as

$$T^\mu{}_\nu = \text{diag}(-\rho, p, p, p). \tag{2.21}$$

Substitution of the FLRW metric (2.19) and the stress-energy tensor (2.21) into the EFE (2.7) gives a set of equations known as the *Friedmann equations*:

$$\left(\frac{\dot{a}}{a}\right)^2 = \frac{8\pi G}{3}\rho - \frac{\kappa}{a^2}, \tag{2.22}$$

$$\frac{\ddot{a}}{a} = -\frac{4\pi G}{3}(\rho + 3p), \tag{2.23}$$

where $\dot{a} = da/dt$ and $\ddot{a} = d^2a/dt^2$. Although these are technically both Friedmann equations, (2.22) is commonly referred to as the Friedmann equation and (2.23) is known as the second Friedmann equation. A common quantity in literature is the expansion rate of the Universe, called the *Hubble parameter* (or constant):

$$H = \frac{\dot{a}}{a}, \tag{2.24}$$

commonly taken to be in units of km/sec/Mpc. With this definition, the Friedmann equations can be re-expressed in terms of H and $\dot{H} = dH/dt$ as

$$H^2 = \frac{8\pi G}{3}\rho - \frac{\kappa}{a^2}, \tag{2.25}$$

$$\dot{H} + H^2 = -\frac{4\pi G}{3}(\rho + 3p). \tag{2.26}$$

2.4 Standard Cosmology

With the Friedmann equations in place, one can now make conventional definitions to frame the dynamics of the Universe in a convenient way. Still following the perfect fluid prescription, one can define an *equation of state parameter* w, such that

$$p = w\rho, \tag{2.27}$$

where p is the fluid pressure and ρ is the fluid density as usual. This provides a simple relationship between the pressure and density of the cosmological components. For convenience, one can define the *critical density* as

$$\rho_c = \frac{3H^2}{8\pi G}, \tag{2.28}$$

and define the dimensionless density parameter as

$$\Omega_i = \frac{\rho_i}{\rho_c}, \tag{2.29}$$

where the index i is used to denote the type of cosmological content, except for curvature. For the special case of spatial curvature[4],

$$\rho_K = -\frac{3\kappa}{8\pi G a^2}, \quad \Omega_K = -\frac{\kappa}{a^2 H^2}. \tag{2.30}$$

If the total density is made up of the sum of all the individual components, ie.

$$\rho = \sum_i \rho_i, \tag{2.31}$$

then dividing out the first Friedmann equation by H^2 and rewriting in terms of Ω_i,

$$1 = \sum_i \Omega_i, \tag{2.32}$$

where the index i denotes the types of cosmological contents, including curvature. To simplify even further, given the energy momentum tensor $T_{\mu\nu}$ in the perfect fluid description, one can use conservation of energy $0 = \nabla_\mu T^\mu{}_0$ with (2.27) to get [75]:

$$\frac{\dot{\rho}}{\rho} = -3(1+w)\frac{\dot{a}}{a}. \tag{2.33}$$

[4]The quantities ρ_K and Ω_K are not actual densities like the rest of the components, but are just a conventional definition that one takes to write the Friedmann equation conveniently.

Table 2.1: Usual suspects for cosmological content in the Universe following a perfect fluid description $p = w\rho$.

Type of content	w	Relationship to a
Matter (m)	0	$\rho_m = \rho_{m0}a^{-3}$
Radiation (r)	1/3	$\rho_r = \rho_{r0}a^{-4}$
Curvature (K)	-1/3	$\rho_K = \rho_{K0}a^{-2}$
Vacuum (Λ)	-1	$\rho_\Lambda = \rho_{\Lambda 0}$

If the equation of state parameter w_i for a type of cosmological content is constant, then integrating (2.33) gives the general solution of the form for each component i:

$$\rho_i = \rho_{i0}a^{-3(1+w_i)} = \rho_{i0}a^{-n_i}, \tag{2.34}$$

where ρ_{i0} is the constant of integration that corresponds to the value of ρ_i evaluated at some initial time t_0 (usually taken to be the current day). Table 2.1 shows the equation of state parameter w_i for each cosmological component along with the respective relationships to the scale factor a. Since each cosmological component evolves at a separate rate with respect to a, then one can also write the Friedmann equation in terms of the present-day densities and the scale factor:

$$H^2 = \frac{8\pi G}{3}\sum_i \rho_i = \frac{8\pi G}{3}\left(\rho_{m0}a^{-3} + \rho_{r0}a^{-4} + \rho_{K0}a^{-2} + \rho_{\Lambda 0}\right), \tag{2.35}$$

of alternatively, if divided out by the current value of the Hubble parameter H_0,

$$H^2 = H_0^2\left(\frac{\Omega_{m0}}{a^3} + \frac{\Omega_{r0}}{a^4} + \frac{\Omega_{K0}}{a^2} + \Omega_{\Lambda 0}\right). \tag{2.36}$$

From equations (2.35) and (2.36), one can see that the cosmological components contribute to the expansion of the Universe at different rates. In particular, different epochs in our cosmological history will have been dominated by different components. For instance due to the a^{-4} scaling for the radiation energy density, one expects that when a was very small the contribution from the radiation term to have been dominant over the other terms, barring the radiation density Ω_r from being zero. At some value of equilibrium $a_{\rm rm}$, the a^{-3} term will start to dominate over the a^{-4} term, which then the matter component in the Friedmann equations would contribute the most to the expansion rate. Similarly, the constant density term Ω_Λ will start to dominate over the matter density at some scale $a_{m\Lambda}$.

Note that in a general Universe with nonzero spatial curvature, the curvature term would take over after the matter dominated era before the constant term due to the a^{-2} scaling. However, the spatial curvature density has been measured to be nearly zero, and hence we ignore contributions of curvature in the Friedmann equations[5]. Thus in their respective eras, we can isolate the contribution to the Friedmann equation to solve for a as a function of time t.

2.4.1 Cosmological Distances

Proper and Comoving Distances

Note that there are several notions of distance in a cosmological setting due to the fact that space is expanding. The first matter at hand is to distinguish between proper (physical) and comoving distances. A comoving distance is the distance between two points without the effect of the expansion of the Universe. The proper distance is the actual distance in physical space, with the effects of spatial expansion included. The relationship between these two distance measures is simple:

$$D_p(t) = a(t)r, \tag{2.37}$$

where $D_p(t)$ is the proper distance and r is the comoving distance, which for an emission time t_e and observation time t can be written as (assuming that $\kappa = 0$),

$$r = \int_{t_e}^{t} \frac{dt'}{a(t')}. \tag{2.38}$$

Note that this allows one to compute the maximum comoving distance that a light ray could travel by taking the emission time to $t_e = 0$, oftentimes called the (comoving) particle horizon:

$$D_p(t) = \int_{0}^{t} \frac{dt'}{a(t')}. \tag{2.39}$$

Two particles that are separated by comoving distances larger than the horizon $D_p(t)$ will not be able to communicate in time t. As I will discuss later on, this is an important issue that comes up in the historical cosmological puzzles.

[5] A vanishing curvature has deeper implications for cosmology, in the form of the flatness problem. This will be discussed in more detail in section 3.1.

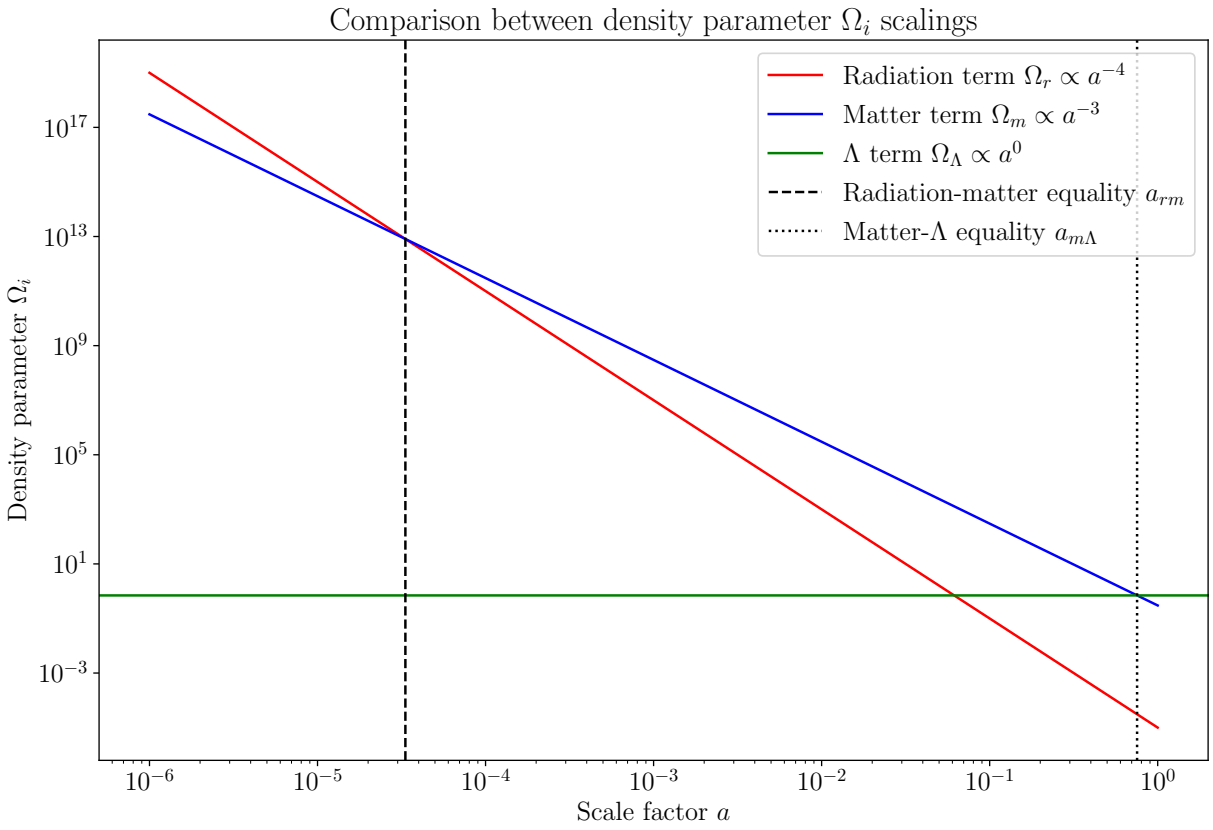

Figure 2.1: Comparison of the cosmological components with respect to the scale factor a for a Universe without spatial curvature ($\Omega_\Lambda = 0$). From this plot one can see that radiation dominates for $a < a_{rm}$, matter dominates for $a_{rm} \leq a \leq a_{m\Lambda}$, and Λ dominates afterwards for $a > a_{m\Lambda}$. The initial conditions were given by $\Omega_{m0} = 0.3, \Omega_{r0} = 10^{-5}$, and $\Omega_\Lambda = 0.7$.

Cosmological Redshift

Rather than looking at distances or cosmological pasts using the scale factor, an intuitive indicator for distance and time is the cosmological redshift of a signal z. Since the Universe is expanding, the wavelength of an emitted signal will increase as it propagates. Hence the longer a signal travels, the larger the observed wavelength, which in physics is a phenomenon known as redshift. It is also related to the scale factor in a similar manner, so that

$$1 + z = \frac{\lambda_o}{\lambda_e} = \frac{a(t_0)}{a(t_e)}, \tag{2.40}$$

where λ is the wavelength of the signal and the subscript e corresponds to quantities at emission while the subscript o corresponds to quantities at observation. With this definition, the Friedmann equation in the form (2.36) can be written as

$$H^2 = H_0^2 \left[\Omega_{m0}(1+z)^3 + \Omega_{r0}(1+z)^4 + \Omega_{K0}(1+z)^2 + \Omega_{\Lambda 0}\right] = E(z)^2 H_0^2, \tag{2.41}$$

where $E(z)$ is a commonly defined expression that captures the evolution of the density parameters. With this, the comoving distance can also be rewritten to be a function of redshift as

$$r = \frac{1}{H_0} \int_0^z \frac{dz'}{E(z')}, \tag{2.42}$$

which can either by integrated numerically or analytically to acquire the total comoving distance to an object at redshift z.

Angular Diameter Distance

The angular diameter distance D_A is another useful distance measure in cosmology where one wishes to compare angular sizes with physical sizes. It is defined as the ratio of an object's physical transverse size to its angular size, and is given by [128, 219]:

$$D_A = \frac{r}{1+z}. \tag{2.43}$$

Luminosity Distance

In addition, there is another distance measure known as the luminosity distance, which is used in the flux-luminosity relation as

$$F = \frac{L}{4\pi D_L^2}, \tag{2.44}$$

where F is the flux at the luminosity distance D_L and L is the luminosity[6]. The luminosity distance can also be related to the comoving and angular diameter distances for a source at redshift z by [128, 219]:

$$D_L = (1+z)r = (1+z)^2 D_A. \tag{2.45}$$

While there are other types of distances measurements in cosmology [128, 219], these are the only ones that are relevant for this thesis. Figure 2.2 shows the different cosmological distance measures discussed.

2.4.2 Matter dominated era

At early enough times, when a^{-3} was the dominant term in the Friedmann equation, the Universe was in a matter dominated era. Ignoring all other terms in the Friedmann equation, then

$$H^2 = \frac{\dot{a}^2}{a^2} \propto \frac{1}{a^3} \Longrightarrow \dot{a} \propto \frac{1}{a^{1/2}}, \tag{2.46}$$

which when solved yields

$$a_m(t) \propto t^{2/3}. \tag{2.47}$$

2.4.3 Radiation dominated era

At even earlier times, when a^{-4} was the dominant contributing term in the Friedmann equation, the Universe was in a radiation dominated era. Similar as above, considering only the dominant radiation term in the Friedmann equation,

$$H^2 = \frac{\dot{a}^2}{a^2} \propto \frac{1}{a^4} \Longrightarrow \dot{a} \propto \frac{1}{a}, \tag{2.48}$$

which when solved yields

$$a_r(t) \propto t^{1/2}. \tag{2.49}$$

[6]There is also another way to see the luminosity distance using the apparent and absolute magnitudes of a source. From this perspective, the luminosity distance is defined by $D_L = 10^{\frac{m-M}{5}+1}$ pc, where m is the apparent magnitude and M is the absolute magnitude.

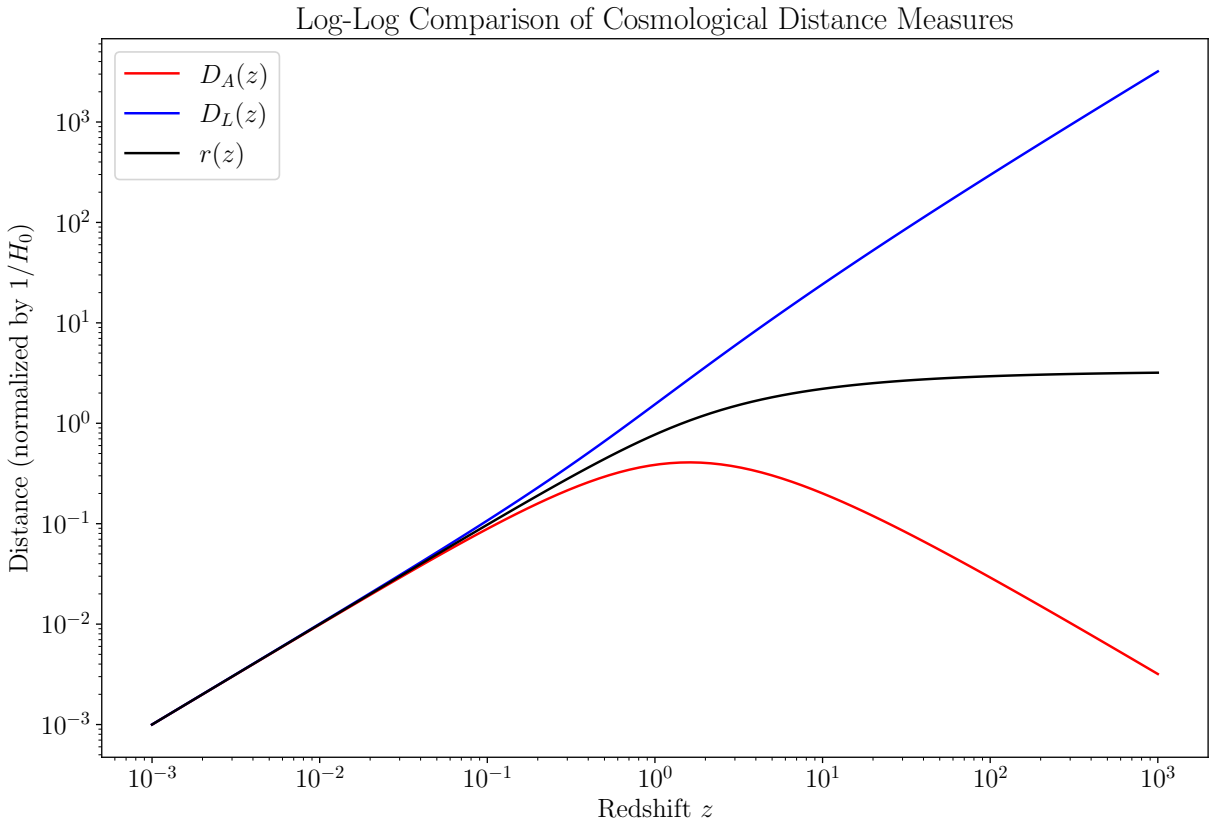

Figure 2.2: Log-Log Comparison of the different cosmological distances normalized by the Hubble distance $1/H_0$. The initial density parameters were taken for simplicity as $\Omega_{m0} = 0.3$ and $\Omega_\Lambda = 0.7$. For low redshifts, the distance agreements agree fairly well, but diverge quickly. In particular, the luminosity distance D_L grows by an extra power of z compared to r, while the angular distance D_A falls quickly due to the inverse relation to z. By $z = 0$ (ie. $a = 1$) the distance measures are already divergent from one another.

2.4.4 Λ dominated era

At late times when $a \gg 1$, the contributions of a in the denominator in Friedmann's equation forces all of the terms except for the Λ-term to become negligible. In the late Universe, the dominating contribution to the expansion is from the cosmological constant Λ. In that case,

$$H^2 = \frac{\dot{a}^2}{a^2} \propto \Omega_\Lambda \Longrightarrow \dot{a} \propto a, \tag{2.50}$$

and so

$$a_\Lambda(t) \propto e^{Ht}. \tag{2.51}$$

Hence in a cosmological constant-dominated Universe, the expansion is exponential with the rate of expansion given by H.

2.4.5 Cosmological history

By separating out the individual components of the Universe and solving the Friedmann equation, we were able to find the time evolution of the scale factor in those scenarios. However, for the times in the Universe's history where multiple components contributed to the expansion at similar scales, then the approximations for the single component solutions are not sufficient. In the end for a proper history of our Universe, one must solve the Friedmann equation with all of the components

$$H_0 t = \int_0^a \frac{da}{\sqrt{\Omega_{m0} a^{-1} + \Omega_{r0} a^{-2} + \Omega_{K0} + \Omega_{\Lambda 0} a^{-2}}}. \tag{2.52}$$

Doing so will let us look at the transition eras in between the single component dominated eras. Figure 2.3 shows the scale factor a as a function of the time parameter $H_0 t$, where H_0 is the present day measurement of the Hubble parameter H.

Tracing back in time, one can see that the relative size of the Universe a goes to zero. This is the fundamental idea of the Standard Big Bang (SBB) model, in which the Universe is birthed from an initial spacetime singularity. One must take caution in these results for our cosmological history however; several assumptions were made throughout this first section to arrive at this model, which are summarized again as [59]:

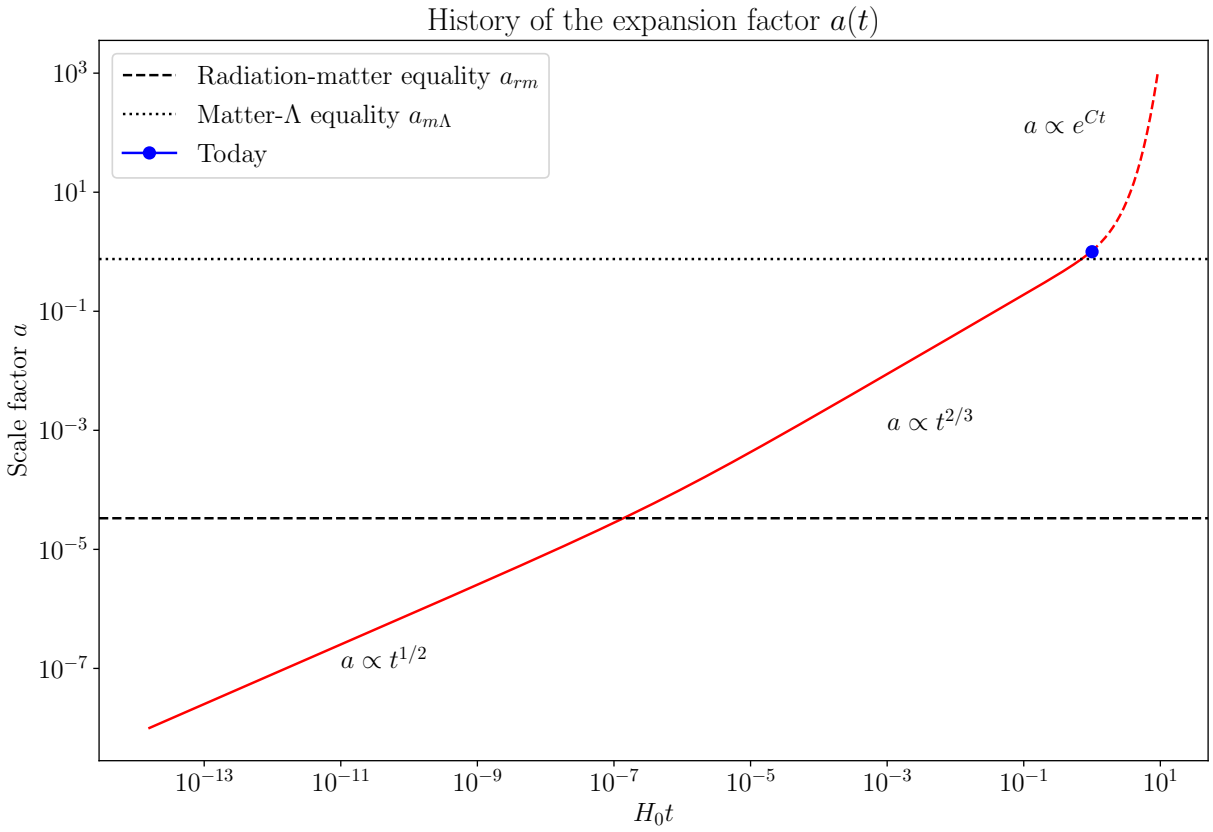

Figure 2.3: History of the expansion factor $a(t)$ assuming a multi-component Universe with no curvature. The solid red line to the left of the blue dot represents the past history, while the red dashed line to the right of the blue dot represents the future. One can observe that in present-day the Universe has just entered the Λ dominated era, hence the Universe is expanding at an accelerated rate (which has been observationally confirmed as well [184, 201]. The initial conditions for the density parameters when solving the Friedmann equation were $\Omega_{m0} = 0.3$, $\Omega_{r0} = 10^{-5}$, and $\Omega_{\Lambda} = 0.7$.

1. The cosmological principle says that the Universe is homogeneous and isotropic on sufficiently large scales. This allowed for a simplification of the expansion rate of the Universe that we implicitly asserted in the FLRW metric such that

$$a(t, \mathbf{x}) = a(t). \tag{2.53}$$

   In other words, the expansion of space is the same in all directions at every point on large enough scales.

2. The interactions between spacetime and cosmological content in the Universe are governed by the EFEs (2.7).

3. The perfect fluid description is a sufficient description to capture the cosmological components in the Universe.

In summary, the SBB is a result stemming from Einstein's equations and the FLRW metric, which together show how our expanding Universe has dynamically evolved over the course of our cosmological history, starting with a spacetime singularity.

Part I

Cuscuton Bounce as an Alternative to Inflation

Chapter 3

The Very Early Universe

The early Universe is a moment in our cosmological history that well precedes the formation of galaxies and stars that make up the cosmos today. While the radiation temperature is currently sitting at approximately 2.73 K, the early Universe entails the era when the radiation temperature was roughly 10^4 K [219]. In this era, the energy density of radiation was well above the energy density of matter. The early Universe is an epoch that includes important phases in the history of our Universe such as nucleosynthesis and recombination.

While the physics of the early Universe is generally very well agreed upon, one can turn back the clock even further to a much more controversial era in our cosmological history known as the very early Universe. The very early Universe captures the very first moments in our Universe, even hotter and more dense than the early Universe. In this section I will introduce the current paradigm for the very early Universe, and note some of the problems with the model. I will then discuss an alternative to the current paradigm known as a cosmological bounce, that can address some of the potential issues.

3.1 Cosmological Puzzles

Despite the many successes of the SBB model, two[1] cosmological puzzles gathered attention in the mid-late 1900s for not having a suitable answer from SBB cosmology.

[1]Some cosmologists refer to a third cosmological puzzles as well – the Monopole problem.

3.1.1 Flatness Problem

Several cosmological observations favour a vanishing spatial curvature parameter Ω_K. However this is the value of the curvature parameter today, which has evolved over several cosmological epochs. If one traces this back to when the temperature was about $T \approx 10^4$ K, then $|\Omega_K| \lesssim 10^{-4}$. Following this argument further, in order to acquire this level of vanishing curvature at $T = 10^4$ K, tracing this back even further to an earlier state of the Universe gives $|\Omega_K| \lesssim 10^{-16}$ when $T \approx 10^{10}$ K [219]. Although it is possible that the spatial curvature could have coincidentally taken this initial condition, the SBB model did not have any physical justifications for it. This challenge to the SBB model is known as the Flatness problem, appropriately named for the apparent fine-tuning problem of the initial conditions for the spatial curvature of the Universe.

3.1.2 Horizon Problem

The Nobel prize winning detection of the Cosmic Microwave Background (CMB) [183] launched cosmology into its golden age, and also pointed out the an issue with the SBB model. The observed isotropy of the CMB temperature suggests that the patches in the sky had to have reached thermal equilibrium at some point in their history. In other words, the patches had to have been causually connected at an instance in time. To be in casual contact, the particles must be inside their respective comoving horizons, previously defined as

$$D_p(t) = \int_0^t \frac{dt'}{a(t')}. \tag{3.1}$$

Two patches on the CMB can be associated using the angular diameter distance D_A. However, calculation of the particle horizon size at the time of last scattering gives a result of order $D_p \approx H_0^{-1}(1+z_L)^{-3/2}$ while calculation of the angular diameter distance gives a result of order $D_A \approx H_0^{-1}(1+z_L)^{-1}$ [219], where z_L is the redshift at the surface of last scattering. Thus the angle in the sky that the horizon at last scattering is today would be

$$\theta = \frac{D_p}{D_A} \approx (1+z_L)^{-1/2}, \tag{3.2}$$

which for a last scattering redshift of $z_L \approx 1100$ gives $\theta \approx 1.6°$ [219]. This would imply that a vast majority of the CMB sky are causually disconnected, and so under the SBB model, there would be no physical explanation to the homogeneity of the CMB radiation temperature. This problem is known as the Horizon problem.

3.2 Inflation

3.2.1 Physical Intuition

In the 1980s *inflation* was developed as a potential resolution to the abovementioned problems [122, 160, 28, 158, 159]. The inflationary paradigm refers to a period of accelerated, exponential expansion of the Universe in a metastable state called the false vacuum [161] in which the Universe, although empty, has a very large and approximately constant energy density.

In order to address the flatness problem, recall that the density parameter for curvature is given by

$$\Omega_K = -\frac{\kappa}{a^2 H^2}. \tag{3.3}$$

One potential possibility to address the very small value of Ω_K in the early Universe is to have a cosmological epoch in which $1/(aH)^2$ was decreasing, so that the curvature gets "smoothened" out. In other words, we wish to have

$$0 > \frac{\partial (aH)^{-1}}{\partial t} = \frac{\partial \dot{a}^{-1}}{\partial t} = -\frac{\ddot{a}}{\dot{a}^2}. \tag{3.4}$$

Since $\dot{a}^2 > 0$, we must have that $\ddot{a} > 0$ – an accelerated period of expansion. The parameter $1/(aH)$ is often called in literature as the comoving Hubble radius/horizon [205]. One can also rewrite the comoving particle horizon in terms of this $1/(aH)$ (ignoring bounds for now), so that

$$D_p(t) = \int \frac{dt}{a(t)} = \int \frac{da}{Ha^2} = \int \frac{1}{aH}\, d\ln a. \tag{3.5}$$

From here, one can see that if the comoving Hubble radius is large, then the comoving particle horizon would also be large. Hence if this inflationary period had a decreasing comoving Hubble radius, then it must have been larger in the past. Thus an inflationary period with an accelerated expansion would solve the flatness problem, while also being able to solve the horizon problem if the comoving Hubble radius was large enough in the past. In the next sections, I will present the requirements to solve these problems analytically.

3.2.2 Background Inflationary Cosmology

By thinking of the inflaton ϕ as a free scalar field in de Sitter space, the action for the inflaton is given by

$$S_\phi = \int d^4x \ \sqrt{-g} \left[-\frac{1}{2} \partial^\mu \phi \partial_\mu \phi - V \right], \tag{3.6}$$

so that the total action with coupling to gravity is given by

$$S = S_{\text{EH}} + S_\phi = \frac{1}{2} \int d^4x \sqrt{-g} \left[M_P^2 R - \partial^\mu \phi \partial_\mu \phi - 2V \right]. \tag{3.7}$$

By adopting the definition of the stress tensor in equation (2.18), one can read off the density ρ_ϕ and pressure p_ϕ for the inflaton from (2.21):

$$\rho_\phi = \frac{1}{2} \dot{\phi}^2 + V(\phi), \tag{3.8}$$

$$p_\phi = \frac{1}{2} \dot{\phi}^2 - V(\phi). \tag{3.9}$$

Thus the background evolution of a Universe equipped with a FLRW metric under the influence of the inflaton is given by substituting (3.8) and (3.9) into the Friedmann equations (2.25) and (2.26)

$$H^2 = \frac{1}{3M_P^2} \left[\frac{1}{2} \dot{\phi}^2 + V(\phi) \right], \tag{3.10}$$

$$\dot{H} = -\frac{1}{2M_P^2} \dot{\phi}^2. \tag{3.11}$$

Variation of the action respect to the inflaton field also yields the equation of motion (also called the Klein-Gordon equation)

$$\ddot{\phi} + 3H\dot{\phi} + V'(\phi) = 0, \tag{3.12}$$

where the prime here denotes the derivative of the potential V with respect to the inflaton field ϕ.

3.2.3 Accelerated Expansion and Slow-Roll

Up to this point, we have treated the inflaton field to just be a free scalar field, in which an accelerated expansion is not guaranteed. In order to get a phase of accelerated expansion,

one requires that

$$\ddot{a} > 0. \tag{3.13}$$

Recall from the second Friedmann equation in the form of (2.23) that one requires

$$\rho + 3p < 0, \tag{3.14}$$

in that case. For a approximately exponential expansion, we require that $w \approx -1$ so that the scale factor evolves exponentially as a function of time as we saw in (2.51). If one wants $w \approx -1$, one can then see that for $p \approx -\rho$ to hold true, then equations (3.8) and (3.9) show that the potential term must dominate over the kinetic term:

$$\frac{1}{2}\dot{\phi}^2 \ll |V(\phi)|. \tag{3.15}$$

If the potential term dominates enough to ignore the kinetic term in the first Friedmann equation (2.25), then it can be approximated by

$$H^2 \approx \frac{1}{3M_P^2} V(\phi). \tag{3.16}$$

By moving the potential term to the other side in equation (3.15), the two results from the Friedmann equations (3.11) and (3.16) gives motivation to define the first slow-roll parameter ϵ as

$$\epsilon = -\frac{\dot{H}}{H^2} \ll 1, \tag{3.17}$$

called the first slow-roll condition. This condition guarantees accelerated expansion of the cosmological background, but puts no constraints on the duration of this phase.

We know that the events in the very early Universe must eventually transition into a radiation dominated era while at the same time, solving the cosmological puzzles presented in section 3.1. This gives rise to the second slow-roll condition, which requires that the acceleration of the field itself is sufficiently small enough so evolution of the inflaton is governed primarily by the friction term in the Klein-Gordon equation (3.12), ie.

$$\ddot{\phi} \ll -3H\dot{\phi}. \tag{3.18}$$

By differentiating the second Friedmann equation (3.11),

$$\ddot{H} = -\frac{1}{M_P^2}\dot{\phi}\ddot{\phi}. \tag{3.19}$$

Isolating for $\ddot{\phi}$ and substituting it into the second slow-roll condition (3.18) after moving all terms to the left-hand side gives motivation to define the second slow-roll parameter η as

$$\eta = -\frac{\ddot{\phi}}{H\dot{\phi}} = -\frac{\ddot{H}}{2H\dot{H}} \ll 1. \tag{3.20}$$

If the acceleration of the field is sufficiently subdominant to the velocity, this allows one to ignore the $\ddot{\phi}$ term from the Klein-Gordon equation for ϕ, so that

$$3H\dot{\phi} \approx -V'(\phi). \tag{3.21}$$

One can also define the slow-roll parameters with respect to the shape of the inflaton potential $V(\phi)$, so that

$$\epsilon_V = \frac{M_P^2}{2}\left(\frac{V'}{V}\right)^2, \tag{3.22}$$

$$\eta_V = M_P^2 \frac{V''}{V}. \tag{3.23}$$

Assuming the slow-roll conditions, using the first Friedmann equation in the form of (3.16) and the Klein-Gordon equation for the inflaton in the form of (3.21), we can see that

$$\epsilon_V \approx \epsilon, \tag{3.24}$$

$$\eta_V \approx \epsilon + \eta. \tag{3.25}$$

These slow-roll parameters give restrictions on the inflaton potential to guarantee a period of exponential expansion. The first slow-roll condition (3.17) is equivalent to saying that we are on a background solution of the Friedmann equations, where H changes slowly with time, while the second slow-roll condition (3.20) is equivalent to saying that we are on an attractor solution, so that this period will last sufficiently long [205].

3.2.4 *e*-folds

While the two slow-roll parameters give conditions for the inflaton background for an sufficiently long enough period of exponential expansion, the inflationary epoch must end sometime and eventually transition into other cosmological epochs. Inflation ends when the approximation $w \approx -1$ is no longer valid, which is equivalent to saying $\epsilon \approx \eta \approx 1$. In

order to quantify exactly how long the inflationary epoch must be in order to solve the cosmological puzzles, we define the number of e-folds N as

$$\frac{a_e}{a} = e^N, \tag{3.26}$$

where a_e corresponds to the scale factor at the end of inflation. With this definition,

$$dN = -d\ln a, \tag{3.27}$$

and so basic change of integration variables gives

$$N = \int_a^{a_e} d\ln a = \int_t^{t_e} H\ dt = \int_\phi^{\phi_e} \frac{H}{\dot{\phi}}\ d\phi. \tag{3.28}$$

If one uses the slow-roll approximations in the previous section, then we can write the number of e-folds as a function of the potential shape:

$$N \approx \int_{\phi_e}^{\phi} \frac{V}{M_P^2 V'}\ d\phi. \tag{3.29}$$

Thus given a potential for the inflaton field, one can calculate the number of e-folds expected to gauge the amount of expansion during the inflationary period. To connect the number of e-folds required with the cosmological puzzles, we start by noting that during the inflationary period, in the slow-roll approximation where H evolves slowly (ie. $\epsilon \ll 1$), then one can take $H = H_I$ to be nearly constant. Hence

$$\Omega_K = -\frac{\kappa}{a^2 H_I^2} \propto \frac{1}{a^2}. \tag{3.30}$$

If we assume that the curvature parameter Ω_K had a value of order unity at the beginning of inflation (ie. $\Omega_K(a_i) \sim 1$), then

$$\Omega_K(a_e) \approx \Omega_K(a_i)\frac{a_i^2}{a_e^2} \sim \frac{a_i^2}{a_e^2} = e^{-2N}, \tag{3.31}$$

where the subscript i denotes the quantities at the beginning of inflation. Relating this quantity to the curvature today,

$$\Omega_K(a_0) \approx \Omega_K(a_e)\frac{a_i^2 H_I^2}{a_0^2 H_0^2} \sim e^{-2N}\left(\frac{a_i H_I}{a_0 H_0}\right)^2. \tag{3.32}$$

This allows one to put a lower bound on the number of e-folds required to make $\Omega_K(a_0)$ sufficiently small:

$$N \gtrsim \ln\left(\frac{a_e H_I}{a_0 H_0}\right). \tag{3.33}$$

Coincidentally, this lower bound also appears when we try to solve the horizon problem. Since the horizon problem corresponds with the homogeneous behaviour of the CMB, we are concerned with the particle horizon at the last scattering surface. If t_L denotes the time of the last scattering surface, then

$$D_p(t_L) = a(t_L)\int_{t_i}^{t_L}\frac{dt}{a(t)} \approx a(t_L)\int_{t_i}^{t_e}\frac{dt}{a(t)}, \tag{3.34}$$

where we assumed that majority of the integral contribution is from the period of inflation. Just replacing N with $N = H_i(t_i - t_e)$ in (3.26), we also know that the scale factor $a(t)$ during inflation can be written as

$$a(t) = a(t_e)\exp(H_I(t - t_e)). \tag{3.35}$$

Substituting this into (3.34),

$$D_p(t_L) \approx \frac{a(t_L)}{a_e H_I}(e^N - 1) \approx \frac{a(t_L)}{a_e H_I}e^N, \tag{3.36}$$

since e^N is expected to be the dominant term. The angular diameter distance at the last scattering surface is approximately [219]

$$D_A(t_L) \approx \frac{a(t_L)}{a_0 H_0}. \tag{3.37}$$

Thus the requirement that $D_p(t_L) \gtrsim D_A(t_L)$ gives

$$N \gtrsim \ln\left(\frac{a_e H_I}{a_0 H_0}\right), \tag{3.38}$$

the same as approximately what we needed for the flatness problem. While these values are just lower bounds for the number of e-folds, a more careful calculation yields a requirement of around 60 e-folds [155, 219, 38] to solve these problems. Hence as long as the inflationary epoch lasts sufficiently long, the cosmological puzzles previously mentioned are resolved.

3.3 Inflationary Perturbation Theory

3.3.1 Perturbation Theory

While there are several frameworks to perform cosmological perturbation theory [174], a convenient method is to use the Arnowitt-Deser-Misner (ADM) formalism [30] alongside a comoving gauge choice, which simplifies the calculations in the context of inflation [165]. The ADM formulation is a Hamiltonian formulation, in which spacetime is decomposed into foliations of non-intersecting spacelike hypersurfaces Σ_t labelled by their time t [189]. This spacetime decomposition allows for a standard Hamiltonian approach in classical field theory, where one can consider the field configurations and their conjugate momenta to derive the momentum and energy constraints. In the case of general relativity, the Hamiltonian is a functional of the induced spatial metric and its associated conjugate momentum [189].

The ADM metric is given by

$$ds^2 = -N^2 dt^2 + h_{ij}(N^i dt + dx^i)(N^j dt + dx^j), \tag{3.39}$$

where N is the lapse function, N^i is the shift vector, and h_{ij} is the spatial induced metric. The spatial hypersurfaces Σ_t are described by the three-dimensional spatial Ricci tensor $R^{(3)}_{\mu\nu}$ and the extrinsic curvature

$$K_{ij} = \frac{1}{2N}(\dot{h}_{ij} - \nabla_i N_j - \nabla_j N_i) = \frac{1}{N} E_{ij}, \tag{3.40}$$

where the dot above a variable corresponds to a time derivative. E_{ij} is just a conveniently defined tensor that is related to the extrinsic curvature K_{ij} with a factor of the lapse function. Figure 3.1 shows a graphical representation of the ADM decomposition. With this, the action (3.7) can be written as

$$S = \frac{1}{2}\int d^4x\, \sqrt{h} N \left[M_P^2 R^{(3)} - 2V + M_P^2 N^{-2}(E^{ij}E_{ij} - E^2) + N^{-2}(\dot{\phi} - N^i \partial_i \phi)^2 - h^{ij}\partial_i\phi\partial_j\phi \right]. \tag{3.41}$$

Now we will set $M_P = 1$ for brevity. From (3.41), one can vary the action with respect to the shift N^i and lapse N to find the Hamiltonian constraint

$$R^{(3)} - N^2(E_{ij}E^{ij} - E^2) = (\dot{\phi} - N^i\partial_i\phi)^2 + h^{ij}\partial_i\phi\partial_j\phi + 2V, \tag{3.42}$$

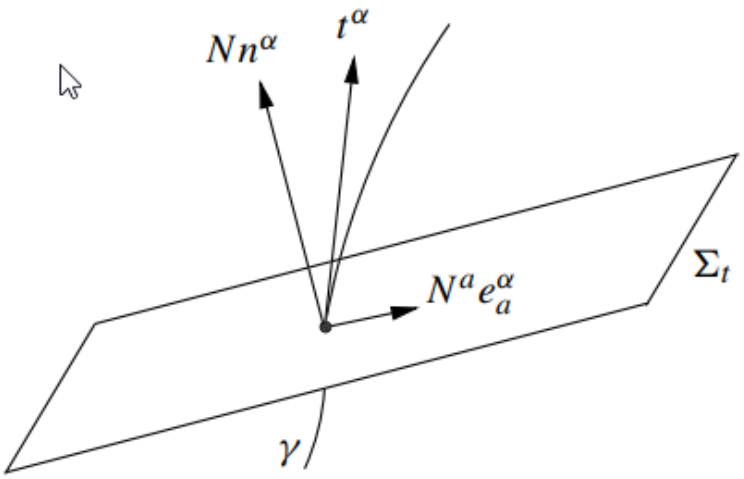

Figure 3.1: Visual representation of the lapse function and shift vector in the ADM decomposition, reproduced from Ref. [189]. Here γ is used to indicate some curve. Note that t^α is a tangent vector to the curve γ at the hypersurface and e_a^α are tangent vectors on Σ_t. n^α is the unit normal to the hypersurfaces.

and the momentum constraint

$$\nabla_i[N^{-1}(E^i_j - E\delta^i_j)] = 0. \tag{3.43}$$

While these are technically the equations of motion for the shift and lapse, since no time derivatives for N^i or N are present, the shift and lapse are completely fixed by these equations.

At this point the only dynamical parameters are the induced metric h_{ij} and the inflaton field ϕ. Two possible gauge choices are the spatially flat gauge in which the scalar metric perturbations are taken to be zero, or the comoving gauge in which the inflaton perturbations are vanishing. We will fix our gauge with the comoving gauge. As mentioned, in the comoving gauge one is "comoving" with the inflaton field ϕ, and so perturbations for ϕ are taken to be zero:

$$\phi = \phi_0 + \delta\phi = \phi_0. \tag{3.44}$$

Only considering the scalar perturbations to the metric, the metric can be written by[2]:

$$h_{ij} = a^2(1 + 2\zeta)\delta_{ij}, \tag{3.45}$$

where ζ is the *comoving curvature perturbation* and δ_{ij} is the spatial flat metric. The lapse function and the shift vector also carries perturbations[3]

$$N = 1 + \alpha, \quad N_i = \partial_i \beta. \tag{3.46}$$

By substituting these quantities into the constraint equations (3.42) and (3.43), we get that [165, 38]

$$\alpha = \frac{\dot{\zeta}}{H}, \quad \partial^2\beta = -\frac{\partial^2\zeta}{H} + a^2\frac{\dot{\phi}_0^2}{2H^2}\dot{\zeta}. \tag{3.47}$$

One can then substitute these quantities into the inflaton action (3.41) and after several levels of integration by parts along with using the background equations [38], the second order action is then given by

$$S^{(2)} = \int d^4x\ a^3\epsilon\left(\dot{\zeta}^2 - \frac{1}{a^2}\partial_i\zeta\partial^i\zeta\right), \tag{3.48}$$

where $\epsilon = \dot{\phi}_0^2/(2H^2)$ is the first slow-roll parameter as before. By introducing the *conformal time* τ related to the cosmic time t by

$$dt = a\ d\tau, \tag{3.49}$$

the action above can be written as

$$S^{(2)} = \int d\tau d^3x\ a^2\epsilon\left[(\zeta')^2 - (\partial\zeta)^2\right], \tag{3.50}$$

where $\partial^2\zeta = \partial^i\zeta\partial_i\zeta$ and the prime denotes the derivative with respect to conformal time. Varying this action with respect to ζ and then using a Fourier transform to get the equation of motion for ζ_k,

$$\zeta_k'' + (3 + \eta)H\zeta_k' + \frac{k^2}{a^2}\zeta_k = 0. \tag{3.51}$$

[2]Note that in reality vector perturbations and tensor perturbations would also enter this expression, but we omit them for brevity.

[3]Here we use the notation of Baumann [38], which use α and β as the perturbations to the lapse and shift, while Maldacena [165] uses N_1 and ψ as the perturbation quantities. Note that the vector modes here are already separated out.

For $k \ll aH$, ie. super-Hubble scales, this equation takes the form

$$\zeta_k'' + (3+\eta)H\zeta_k' \approx 0, \tag{3.52}$$

and so $\zeta_k = \text{const.}$ is a solution. Since the other solution is decaying in most cases, this means that super-Hubble modes do not evolve, an important feature to be discussed shortly.

Although (3.51) gives an ODE for ζ_k, it is often useful to think of the *Mukhanov-Sasaki variable*, which is given in this case as

$$v = a\sqrt{2\epsilon}\zeta = z\zeta, \tag{3.53}$$

where we defined $z = a\sqrt{2\epsilon}$. With this definition, the equation of motion for v_k can be derived from (3.50) to be

$$v_k'' + \left(k^2 - \frac{z''}{z}\right) v_k = v_k'' + \omega_k^2 v_k = 0. \tag{3.54}$$

This is just a harmonic oscillator with frequency

$$\omega_k^2 = \left(k^2 - \frac{z''}{z}\right). \tag{3.55}$$

These expressions give the dynamics for the perturbation quantity ζ_k and v_k. In the next section we will see how to set initial conditions for these perturbations and see the physical significance of the results once evolved.

3.3.2 Quantizing Perturbations

Bunch-Davies Vacuum

When dealing with quantum field theory in curved spacetimes, the choice of a physical vacuum is not always clear. In a de Sitter geometry, there is a conventional choice of a vacuum called the Bunch-Davies vacuum. Consider a massless, free scalar field ϕ in a de Sitter background:

$$S = \frac{1}{2}\int d^4x\sqrt{-g}g^{\mu\nu}\partial_\mu\phi\partial_\nu\phi = \frac{1}{2}\int d\tau d^3x a^2\left[(\phi')^2 - (\partial_i\phi)^2\right], \tag{3.56}$$

where τ is again the conformal time defined by $d\tau = a\ dt$. In this de Sitter universe, the scale factor is given by

$$a(\tau) = -\frac{1}{H\tau}, \quad -\infty < \tau < 0. \tag{3.57}$$

As before, one can define a canonical field (the Mukhanov-Sasaki variable from before) as $v = a\phi$, so that varying the action in Fourier space gives the equation of motion

$$v_k'' + \left(k^2 - \frac{a''}{a}\right) v_k = v_k'' + \omega_k^2 v_k = 0, \tag{3.58}$$

where ω_k acts as a frequency for the mode's oscillation. While the general solution of equation (3.58) is given by

$$v_k(\tau) = c_1 \left(1 - \frac{i}{k\tau}\right) e^{-ik\tau} + c_2 \left(1 + \frac{i}{k\tau}\right) e^{ik\tau}, \tag{3.59}$$

for c_1, c_2 constants, there is a usual choice of mode functions that is preferred in inflationary contexts. After the appropriate canonical quantization, if we require that the vacuum state is also the ground state of the canonical Hamiltonian operator for the field[4], then the unique physical vacuum state called the *Bunch-Davies vacuum* is given by

$$v_k(\tau) = \frac{1}{\sqrt{2k}} \left(1 - \frac{i}{k\tau}\right) e^{-ik\tau}. \tag{3.60}$$

The Bunch-Davies mode function corresponds to the initial condition that is physically the instantaneous lowest-energy vacuum in the $\tau \to -\infty$ limit [173]. Although the expectation value of the fluctuations is zero, the variance of the fluctuations is non-zero and can be encapsulated by the dimensionless power spectrum

$$\mathcal{P}_k^{v_k}(\tau) = \frac{k^3}{2\pi^2} |v_k(\tau)|^2. \tag{3.61}$$

The power spectrum of vacuum fluctuations is the signature produced in the very early Universe that would sources the anisotropies embedded in the CMB. Although the previous expression is a general expression for a power spectrum for each mode k, not all modes k are of physical interest. In particular, the Hubble radius acts as an important boundary between observable and unobservables modes. The comoving Hubble radius is given by

$$D_H = \frac{1}{aH}. \tag{3.62}$$

[4]For a review on the necessary canonical quantizations as well as the derivation for the Bunch-Davies vacuum, see either Mukhanov [173] or Baumann [38].

Modes with a wavelength larger than the Hubble radius (or $k \lesssim aH$) are called superhorizon or super-Hubble modes, while modes with a wavelength smaller than the Hubble radius (or $k \gtrsim aH$) are called subhorizon or sub-Hubble modes. Due to the expansion of the Universe, sub-Hubble modes can *cross the horizon* and enter the super-Hubble regime. In a de Sitter background, the sub-Hubble modes oscillate since the k^2 term dominates in the frequency defined in (3.58), while super-Hubble modes have their amplitudes freeze out [173, 219]. There are thus three separate regions to classify perturbations using the Hubble radius [173]:

1. The mode stays subhorizon for the duration of inflation. These modes oscillate during the entire inflationary period, and have their spectra suppressed. Hence these modes are not of interest.

2. The mode starts in the superhorizon regime and crosses the horizon during the inflationary period. The mode experiences a *freeze-out*, in which it stops oscillating and growing, and remains roughly constant afterwards. These are the modes of interest for cosmological observations.

3. The mode starts in the superhorizon regime and remains superhorizon throughout the inflationary period. These are modes with wavelengths much larger than the visible Universe, and are not of interest.

Hence when one considers the observational imprints of inflation in the CMB, they are interested in the second types of modes generated during inflation. Thus one often takes the superhorizon limit of the power spectrum.

Scalar Perturbations

For the more general case of massive fields, the equation of motion is given by [173]

$$v_k'' + \left(k^2 + m^2 a^2 - \frac{a''}{a}\right) v_k = 0. \tag{3.63}$$

In de Sitter space, this becomes

$$v_k'' + \left(k^2 - \frac{\nu^2 - 1/4}{\tau^2}\right) v_k = 0, \tag{3.64}$$

where

$$\nu^2 = \frac{9}{4} - \frac{m^2}{H^2}. \tag{3.65}$$

This has the general solution

$$v_k(\tau) = \sqrt{-\tau}\left[c_1 H_\nu^{(1)}(|k\tau|) + c_2 H_\nu^{(2)}(|k\tau|)\right], \tag{3.66}$$

where $H_\nu^{(1)}$ and $H_\nu^{(2)}$ are Hankel functions of the first and second kind respectively and c_1, c_2 are constants. Now returning to the context of the inflaton, the term z''/z in the ODE (3.54) is an effective mass term, in which

$$\frac{z''}{z} = \frac{\nu^2 - 1/4}{\tau^2}, \tag{3.67}$$

where

$$\nu \approx \frac{3}{2} + \epsilon + \frac{\eta}{2}. \tag{3.68}$$

By asserting the Bunch-Davies initial condition, the Bunch-Davies mode function is given by

$$|v_k(\tau)| = \frac{\sqrt{\pi}}{2}\sqrt{-\tau}|H_\nu^{(1)}(-k\tau)|. \tag{3.69}$$

For superhorizon modes, where $k\tau \to 0$, the power spectrum for the curvature perturbations is given by

$$\mathcal{P}_k^\zeta(\tau) = \lim_{k\tau\to 0}\frac{k^3}{2\pi^2}|\zeta_k(\tau)|^2 = \frac{1}{z^2}\lim_{k\tau\to 0}\frac{k^3}{2\pi^2}|v_k(\tau)|^2 = \frac{1}{16\pi^2}\frac{H(\tau)^2}{\epsilon(\tau)}(-k\tau)^{-2\nu+3}, \tag{3.70}$$

where the time-dependence of $H(\tau)$ and $\epsilon(\tau)$ are expected to cancel the time dependence in the final factor [38], so that if we let k_* be a reference scale that exits the horizon at time $\tau_* = -1/k_*$, then the power spectrum is given by

$$\mathcal{P}_k^\zeta = A_s\left(\frac{k}{k_*}\right)^{n_s - 1} \tag{3.71}$$

where H_* and ϵ_* are those quantities evaluated at $\tau = \tau_*$. In the slow-roll approximation, one can write the parameters A_s and n_s as a function of the potential shape [38]:

$$A_s = \frac{1}{24\pi^2}\frac{1}{\epsilon_V}\frac{V}{M_P^4}, \tag{3.72}$$

$$n_s = 1 - 6\epsilon_V + 2\eta_V. \tag{3.73}$$

Tensor Perturbations

Similar to how the curvature perturbations entered the metric, one can also have tensor perturbations to the spatial metric. Tensor perturbations are the leftover traceless-transverse parts of the metric after decomposition into Scalar-Vector-Tensor (SVT) form. These perturbations can be written as[5]:

$$h_{ij} = a^2(\delta_{ij} + 2\gamma_{ij}). \tag{3.74}$$

Note that we are able to treat the scalar and tensor perturbations separately because to second order they remain uncoupled [174]. To second order, the action for the tensor modes is given by

$$S^{(2)} = \frac{M_P^2}{8} \int d\tau \; d^3x \; a^2 \left[(\gamma'_{ij})^2 - (\nabla \gamma_{ij})^2 \right], \tag{3.75}$$

where ∇ is the spatial derivative operator. By again using Mukhanov variables and setting the Bunch-Davies vacuum, the superhorizon limit of the power spectrum is given by [38]

$$\mathcal{P}_k^\gamma = A_t \left(\frac{k}{k_*} \right)^{n_t}, \tag{3.76}$$

where

$$A_t = \frac{2}{\pi^2} \frac{H_*^2}{M_P^2}, \tag{3.77}$$

$$n_t = -2\epsilon_*. \tag{3.78}$$

3.4 The Inflationary Paradigm – Current State

The inflationary paradigm is a largely successful theory that not only solves the cosmological puzzles, but also makes several predictions which can be tested by cosmological observations. Despite its successes, the inflationary paradigm has been a topic of debate for cosmologists, with several developments from both sides of the debate [135, 123]. I will outline some of the successes and criticisms that inflation has come to face in the recent years below. Then I will briefly discuss an alternative to inflation known as a cosmological bounce.

[5]Similar to before, to only consider one type of perturbation quantity, we omit scalar and vector perturbations in this expression, which would be present in reality.

3.4.1 Successes of Inflation

Some of the earliest data about our Universe that is available to us is embedded in the CMB. Inhomogeneities in the CMB are imprints of an early cosmological era that can used as a probe of the very early Universe. The CMB offers a plethora of data that can be used to differentiate not only between inflationary models, but between the various very early Universe models in general.

From the amplitudes for scalar and tensor perturbations, we can define the *tensor-to-scalar ratio* as

$$r = \frac{A_t}{A_s} = 16\epsilon_*. \tag{3.79}$$

Inflationary models are generally tested using the scalar spectral index n_s and the tensor-to-scalar ratio r. The Planck collaboration [22] has most recently measure values of

$$n_s = 0.965 \pm 0.004, \tag{3.80}$$

$$r_{0.002} < 0.06, \tag{3.81}$$

where $r_{0.002}$ corresponds to the tensor-to-scalar ratio assuming $k_* = 0.002h^{-1}$ Mpc. The slight deviation from 1 for the scalar index is often described as a "nearly scale-invariant power spectrum with a slight red tilt". One of the successes of the inflationary paradigm is that in general, inflationary models are capable of producing a power spectrum for scalar perturbations that have a scalar index consistent with the observational data. When one builds a model of the very early Universe, it must at least be able to satisfy these two requirements from the CMB.

3.4.2 Criticisms of Inflation

Singularity Problem

Inflation does not seem to resolve the initial singularity problem. It has been pointed out [47, 48, 49], that inflationary cosmologies are still geodesically past-incomplete. Therefore one must still turn to novel physics in order to properly formulate the physics before inflation.

Eternal Inflation

Generic inflationary models also have the issue of eternally inflating [211, 217, 159]. The false vacuum decays at an exponential rate while also expanding in space. Hence even though the false vacuum is decaying, it never completely decays away [122]. This means that pocket universes may start popping out of the false vacuum just like our Universe. This process can go on forever, indicating an infinite number of pocket universes, often called the Multiverse. Currently our understanding of Multiverse remains fairly incomplete – for example it is not well understood how to define probabilities and test if a universe such as ours is even a likely outcome of inflation, since anything that can happen will happen an infinite number of times [123].

Smoothing Inhomogeneities

When the Planck 2013 results were released [15, 16, 17], Ijjas et al. [135] claimed that the inflationary epoch is able to smoothen the inhomogeneities of the Universe only if the Universe is almost smooth to begin with. Guth et al. [135] followed up with a response to Ijjas et al., claiming false assumptions. Full numerical relativity simulations have shown arguments for both camps [112, 100, 79, 131], and is still a topic of recent debate.

Trans-Planckian Problem

As seen in Section 3.3, the framework for describing vacuum fluctuations was quantum field theory. The trans-Planckian problem refers to the notion that if the inflationary period lasted even slightly longer than necessary to solve the cosmological puzzles, then the cosmological perturbations at physical scales today would have to have started in the sub-Planckian regime [166]. In other words, the wavelengths λ of the fluctuations generated during inflation would have been $\lambda < \ell_P$, where ℓ_P is the Planck length. In this trans-Planckian regime, the semi-classical approximation of gravity could break down and quantum field theory in curved spacetime may not be a valid theory to describe the evolution of these initial fluctuations.

Swampland Conjectures

Recently, the inflationary paradigm has started coming under pressure from some in the string theory community in the form of the Swampland Conjectures. These conjectures

propose a criteria for a valid effective field theory that can be compatible with string theory. Effective field theories that are not compatible with string theory are said to lie in the swampland. An inflationary model with the necessary parameters taken from observational data [25] are believed to be in tension with the swampland conjectures [181, 65, 178, 23, 13, 144]. In addition, the previously mentioned trans-Planckian problem has been promoted to the Trans-Planckian Censorship Conjecture (TCC) [39, 40], which proposes that models which encounter the trans-Planckian problem are inconsistent with string theory.

3.4.3 Bouncing Cosmology

To address the several potential problems of inflation, many alternative proposals to this paradigm have been suggested over the years. While the list of alternatives is fairly long, for the purpose of this thesis, I will focus on one type of alternative known as a cosmological bounce, or a bouncing cosmology. Rather than a big bang, in which the Universe is believed to be a manifestation resulting from spacetime singularity or some quantum gravity state in the past, the idea of a cosmological bounce is to circumvent it in the regime of semiclassical gravity[6]. A cosmological bounce is a scenario in which the Universe underwent a contraction phase before "bouncing" at a minimal spatial volume, then entered a phase of expansion as we observe today.

Other than being free of a spacetime singularity, cosmological bounces can also naturally avoid the trans-Planckian problem. As long as the energy scale of the bounce corresponds to the energy scales in inflationary models, then the observed wavelengths from the CMB will always have had wavelengths larger than the Planck length, avoiding the trans-Planckian regime [55].

Generally in order to generate a bounce, novel physics that go beyond GR or the standard model must be introduced. While the number of bouncing cosmologies is abundant, there are generally three types of novel physics from which a cosmological bounce can be realized [55]. By choosing to stay in the context of Einstein GR, one can introduce modified matter that violates the null energy condition (NEC), one of the energy conditions from Einstein GR given by $p+\rho \geq 0$. To show why the NEC must be violated for a non-singular bounce, consider a simple bouncing Universe with zero curvature. In this scenario, $H \to 0$ at the bounce since the Universe must swap from a negative $\dot{a}$ to a positive $\dot{a}$. In this case, since H also swaps signs, $\dot{H} > 0$. Combining the first and second Friedmann equations

[6] Although in principle quantum gravity models can also produce bouncing scenarios.

(2.25) and (2.26) gives

$$\dot{H} = -4\pi G(\rho + p). \tag{3.82}$$

Since $\dot{H} > 0$, then $\rho + p < 0$ and so the NEC is violated. This approach has historically been dangerous because violating the NEC can lead to ghost instabilities or a superluminal propagation speeds [95, 200, 197]. Alternatively, one can choose to keep standard matter and introduce some modifications to GR, but still within the regime of validity for semi-classical gravity. Finally, there are bouncing cosmologies that are motivated from (super)string theory in hopes of a UV-complete theoretical background[7]. Another way to categorize bouncing cosmologies is from an effective field theory perspective, in which bounce models are either singular or non-singular.

Just as inflationary models can be constrained or ruled out by recent cosmological observations, bouncing cosmologies can also be restricted in the same way. For instance, a cosmological bounce that fails to acquire a nearly scale-invariant power spectrum for perturbations consistent with observations is not favoured. Another important feature of bouncing cosmologies is the production of gravitational waves. Although most bouncing models do not produce an observable spectrum of gravitational waves, bouncing cosmologies which can generate a spectrum of gravitational waves have also been proposed (for example, [63, 56, 57]). The detection of a primordial spectrum of gravitational waves can thus have significant implications for the modelling of the very early Universe [60].

3.5 Summary

In this chapter I presented an introductory background to the very early Universe. In particular, the inflationary paradigm was discussed. Inflationary models are able to solve the historical cosmological puzzles while at the same time being able to produce observational signatures that are consistent with the currently available observational data. Although several aspects of inflation are still up for debate, it is important to consider alternatives to inflation that are consistent with observations, such as cosmological bounces. With the onset of more cosmological data becoming available to us, it is important to preserve consistent models while eliminating inconsistent models to gain more insight about the very first moments of our cosmological history.

[7] It is not clear if quantum gravity is the resolution to the singularity problem it would have to be manifested as bounce. Also note cosmological bounces can also be realized as a hybrid of these classes. For example, one can implement a modification to both matter and GR.

Chapter 4

Spectrum of Cuscuton Bounce

It has been recently shown that a cosmological bounce model based on Cuscuton gravity does not have any ghosts or curvature instabilities. In this chapter we will explore whether Cuscuton bounce can provide an alternative to inflation for generating near scale-invariant scalar perturbations. While a single field Cuscuton bounce generically produces a strongly blue power spectrum (for a variety of initial/boundary conditions), we demonstrate that scale-invariant entropy modes can be generated in a spectator field that starts in adiabatic vacuum, and is kinetically coupled to the primary field. Furthermore, our solution has no singularity, nor requires an *ad hoc* matching condition. We also study the generation of tensor modes (or gravitational waves) in Cuscuton bounce and show that while they are stable, similar to other bounce models, the produced spectrum is strongly blue and unobservable.

4.1 Introduction

Over the past forty years, the inflationary paradigm [121, 160] has gradually become the widely accepted theory to describe the initial conditions of the Universe. Originally motivated to mainly address the flatness and horizon problems, inflationary models also provide an impressive mechanism to generate seeds of fluctuations in the gravitational background on cosmological scales (length scales of gigaparsecs, $\sim 10^{60}\ell_P$) from vacuum quantum fluctuations on extremely small scales (length scales $\lesssim H^{-1} \approx 10^{-19}\text{Å} \sim 10^{6}\ell_P$) [205]. As the scales corresponding to these fluctuations cross the Hubble horizon during inflation, their power spectra become nearly scale-invariant ($n_s \simeq 1$, $n_t \simeq 0$) for both scalar modes and tensor modes, and they also have coherent phases which leads to acoustic peaks in the

temperature, polarization, and matter power spectra. This near scale-invariance prediction is consistent with cosmological observations such as the Cosmic Microwave Background (CMB) measurements by WMAP [127] and Planck[1] [22] as well as the Baryon Acoustic Oscillation (BAO) in galaxy survey power spectra (e.g., [26]). In addition, the precision measurement of cosmological parameters such as the value of spectral index n_s can be used to exclude or constrain many inflationary models [25].

From the theoretical perspective, there is no consensus on a theory beyond the Standard Model of particle physics that can be used to verify or eliminate inflation as a viable theory. Still, one can test the validity of the effective field theory and semi-classical gravity assumptions that are used in inflation and their consistency with current theoretical candidates to describe quantum gravity. For example while the effective field theory itself and loop corrections during inflation seem to be under control [33, 67], it is still important to understand whether or not inflation faces issues such as the trans-Planckian problem [166, 61, 62]. The latter can arise from the period of inflation being possibly too long such that the physical wavelengths of cosmological observations today correspond to sub-Planck length scales at the beginning of inflation. If that is the case then the Bunch–Davies vacuum may not be the correct initial conditions and the theory needs to be further extended in order to adequately set the initial conditions [32]. Therefore, it is still not clear whether inflation provides a fully self-consistent theoretical framework for setting initial conditions in the early Universe.

More recently, the trans-Planckian problem has been promoted to the Trans-Planckian Censorship Conjecture (TCC) [40, 39], positing that models that encounter the trans-Planckian problem are inconsistent with string theory, i.e. they lie in the "swampland" [181, 65, 178, 182]. The swampland conjectures provides a list of criteria for effective field theories that can arise from string theory. However, constraints on inflationary models from observational data are believed to be in strong tension with the swampland conjectures [13, 92, 23, 144, 157]. Regardless of whether the swampland conjectures are to be believed, the question of fine-tuning/naturalness has also been a matter of much contention in the cosmology communities. In the language of smoothing [112, 79, 131], the dynamical attractor solution for inflation is a flat, homogeneous and isotropic universe, but it has been argued that is not necessarily a quantum smoother [211, 217]. In addition to these,

[1]We note that the Planck collaboration observed a spectral tilt of $n_s = 0.965 \pm 0.004$, which is 8σ away from scale invariance ($n_s = 1$). However, from the model building point of view the more significant development is getting n_s close to one. In the language of inflation that translates into first realizing a de Sitter back-ground geometry that produces exact scale invariant perturbations, then by slightly deviating from it and allowing a varying potential rather than a cosmological constant produce the deviation from one.

inflationary spacetimes are also eternal in nature [159, 122] and seem to be geodesically past incomplete, which implies they do not address the singularity problem [47]. To summarize, taking everything into account from theory to observations, one could argue that in spite substantial circumstantial evidence for an early phase of inflation [117, 115, 116], its compatibility within a larger theoretical high energy physics framework is far from certain. With this being said, the trans-Planckian problem is an ongoing topic of discussion with arguments for both sides of the debate (for a relatively recent argument against the trans-Planckian problem, see [97]).

With all this in mind, it is natural to ask whether alternative models of the Early Universe can avoid these suggested shortcomings and/or be less contrived. One natural alternative that could directly address the horizon and singularity problems is a bounce scenario in which the Universe initially undergoes a contracting phase, pauses momentarily and then proceeds to enter an expansion phase. Over the years, many different bouncing models have also been proposed and studied in detail [106, 64, 191, 70, 68, 69, 113, 73, 71, 72, 149, 140, 134, 133, 93, 98, 80, 83, 82], each with their own set of defining characteristics and obstacles. These bouncing models can be classified into two main categories, either singular bounce models or regular (non-singular) bounce scenarios. In particular, the regular bouncing cosmologies have a finite curvature and energy density at the bounce, naturally addressing the singularity problem. However, these models generically violate the Null Energy Condition (NEC) $\rho+p \geq 0$, which in general relativity and most theories of modified gravity leads to either instabilities or a superluminal speed of sound [95, 200, 197, 154, 145].[2] Remarkably, it was shown recently that a bouncing cosmology generated by Cuscuton gravity [51, 52] can work around all these difficulties. Cuscuton gravity [20, 19] is an infrared modification to gravity, which is implemented though an auxiliary field without its own dynamical degrees of freedom. Similar to general relativity, in order to induce a dynamical cosmological background, one has to include other matter fields. At its simplest form, this auxiliary field is a non-canonical scalar field that is incompressible. The studies in [51, 52] show that a Cuscuton bounce does not have any ghost instabilities and the scalar perturbations remain stable throughout the bounce phase. This crucial result relies on the fact that, while providing a mechanism for the bounce, the Cuscuton field does not have any dynamical degrees of freedom.[3] This allows for an effective violation of the

[2] A superluminal propagation speed may not necessary imply that causality is violated [34]. However, for configurations that allow superluminality, UV completeness can also be an issue [14]. For further discussion on superluminality, interested readers should refer to some of the many papers discussing this topic and the references therein [99, 154, 34, 14, 93, 169, 170, 171].

[3] This has been shown for Cuscuton without coupling to gravity and pertubatively around cosmological backgrounds. However, [118] suggests that a generic inhomogeneous initial condition for Cuscuton may lead to a propagating degree of freedom. However, whether under such conditions the equations remain

NEC for the background while the matter fields remain safe. The stability results for these perturbations were explored in further detail [192] for both Cuscuton gravity as well its extended version [137]. Note that a bounce scenario need not exclude an inflationary phase. For example, a bouncing universe followed by an inflationary phase can address the singularity problem and also generate the seeds for inhomogeneities in the universe. However, even a more interesting possibility is to see if there is a way to address both of these aspects without requiring an inflationary phase.

The goal of this work is mainly to investigate that second possibility, i.e. study the power spectrum of scalar perturbations in a Cuscuton bounce cosmology. We start with section 4.2 which provides a review of the Cuscuton bounce scenario presented in [52] and the reason this model is free of scalar instabilities throughout the bounce. Next, we show in section 4.3 why the tensor perturbations are also free of instabilities through the bounce. The power spectra for scalar perturbations in single field Cuscuton bounce model are explored in section 4.4, where we argue despite various initial conditions, the adiabatic cosmological perturbations cannot produce nearly scale-invariant power spectra. We will then show in section 4.5 that by adding another scalar field that is kinetically coupled to the primary matter field, a near scale-invariant power spectrum can be obtained for entropy perturbations, either before or after the bounce phase. Finally, we return to the tensor perturbations in section 4.6 and show that they produce an unobservably small, but strongly blue power spectrum assuming adiabatic vacuum initial condition. We end this chapter by making our concluding remarks in section 4.7.

4.2 The Single Field Cuscuton Bounce Scenario

In this section, we will review the Cuscuton bounce model and the stability studies that were carried out in [52]. The general action, including the Einstein-Hilbert term, the kinetic and potential terms for Cuscuton field φ, and a dynamical scalar field π, with minimal coupling and no potential is given by:

$$S = \int d^4x\sqrt{-g}\left[\frac{M_P^2}{2}R - \mu^2\sqrt{-D_\mu\varphi D^\mu\varphi} - V(\varphi) - \frac{1}{2}D_\mu\pi D^\mu\pi\right], \tag{4.1}$$

where D_μ denotes the covariant derivative.[4] As demonstrated in [52], choosing a potential $V(\varphi)$ with some generic features around the bounce and far from it can induce a cosmolog-

well-posed and system is still physical or not is not clear.

[4]In general, the kinetic term for Cuscuton action can be taken to be negative or positive. However, we are using the negative sign since only that can induce a regular bounce solution.

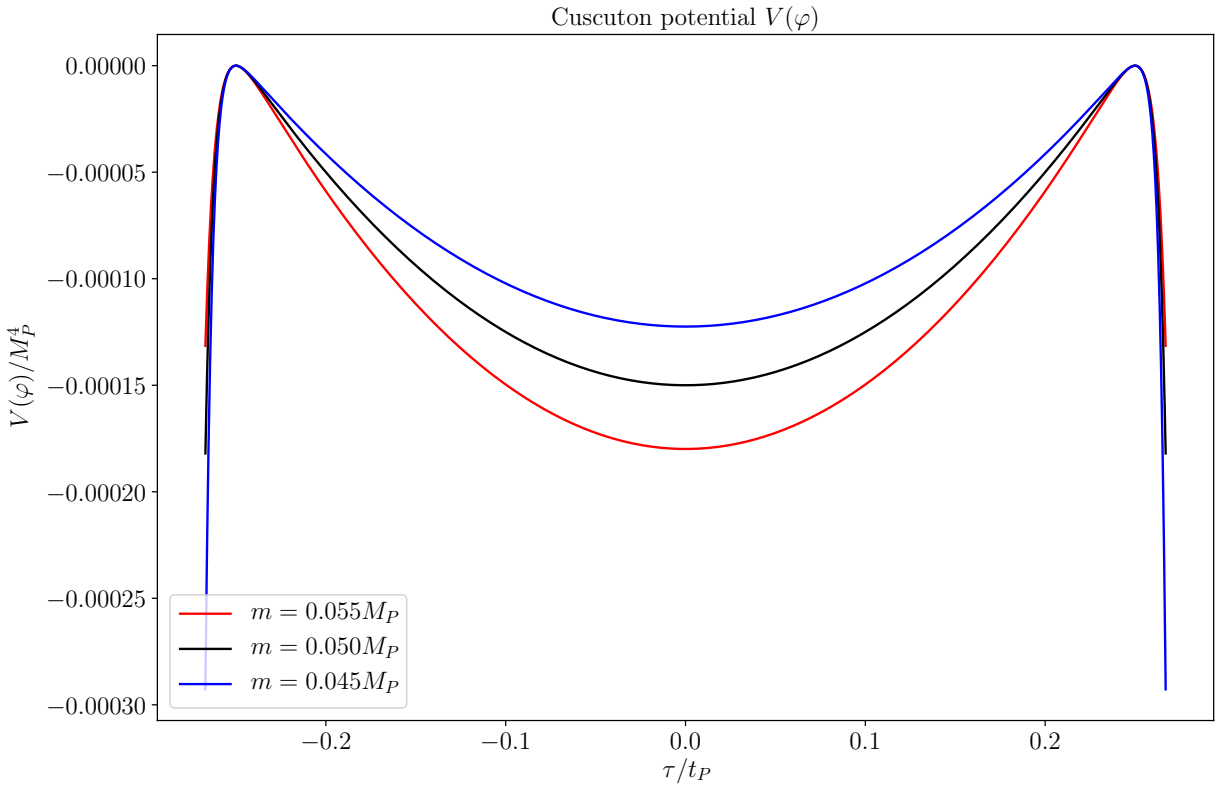

Figure 4.1: Cuscuton potential $V(\varphi)$ for a range of φ. For this plot, $\varphi_\infty = 5m$ is fixed while m is allowed to vary. The construction of this potential along with the selection of the necessary parameters are covered in detail in [52].

ical bounce solution. In this scenario, a potential consistent with those features was taken to be

$$V(\varphi) = m^2(\varphi^2 - \varphi_\infty^2) - m^4\left[e^{(\varphi^2-\varphi_\infty^2)/m^2} - 1\right], \tag{4.2}$$

where m, μ and φ_∞ are free parameters. Figure 4.1 gives a visual intuition about the shape of the Cuscuton potential for different values of μ and a fixed φ_∞. For the rest of the chapter, we will fix values of $m = 0.05M_P$ and $\varphi_\infty = 5m$, taking the same values as the original bounce paper.

Considering a Friedmann–Lemaître–Robertson–Walker (FLRW) universe, variation of the action (4.1) with respect to the Cuscuton field φ results in the following constraint

equation:

$$V'(\varphi_0) - 3\ \mathrm{sgn}(\dot{\varphi}_0)\mu^2 H = 0, \tag{4.3}$$

where $\varphi_0(t)$ is the homogeneous component of the φ-field. Without loss of generality, in what follows, we only consider self-consistent solutions where $\dot{\varphi}_0 > 0$[5] This equation determines the relationship of the Cuscuton field φ_0 to the Hubble parameter H, and establishes that the sign of $V'(\varphi_0)$ will determine whether background is in contracting or expanding phase. Furthermore, as long as $V'(\varphi)$ is bounded H will not diverge. Note that since there are no time derivatives of the Cuscuton field φ in this equation, this confirms the lack of dynamical degrees of freedom at zeroth order in perturbations for φ around a flat FRW background. Therefore, a homogeneous FRW background cannot evolve with just the Cuscuton field and another matter field with dynamical degrees of freedom (in this case taken to be π) is required. Since π is a free field, its corresponding equation of motion for the background is given by

$$0 = 3H\dot{\pi}_0 + \ddot{\pi}_0, \tag{4.4}$$

where π_0 is the homogeneous component of the π-field. Note that it is from eq. (4.4) that one can see that $\rho_\pi \propto a^{-6}$. This was done intentionally by setting the potential for the π-field to be zero, which results in the equation of state parameter $w \sim 1$. By doing this, the anisotropies will never take over the background density, which is one of the generic problems in other bounce models that lead to the BKL instability [42, 156, 37]. Finally, the Einstein equations for the background lead to the following Friedmann equations:

$$H^2 = \frac{1}{3M_P^2}\left[\frac{1}{2}\dot{\pi}_0^2 + V(\varphi_0)\right] \tag{4.5}$$

$$\dot{H} = -\frac{1}{2M_P^2}\left[-\mu^2|\dot{\varphi}_0| + \dot{\pi}_0^2\right], \tag{4.6}$$

which when combined with eq. (4.3), provides an expression for the time evolution for φ,

$$\dot{\varphi}_0 = \frac{\frac{V(\varphi_0)}{M_P^2} - 3H^2(\varphi_0)}{\frac{V''(\varphi_0)}{3\mu^2} - \frac{\mu^2}{2M_P^2}}. \tag{4.7}$$

In fact, by solving this first order ODE, all of the other dynamics in the background can be re-expressed in terms of φ_0, which then acts as a clock. This leads to very efficient numerical computations.

[5]Note that our analysis is in the regime where $X = -D_\mu\varphi D^\mu\varphi > 0$ is globally satisfied. Therefore, $\dot{\varphi}_0$ cannot be zero. For more discussion about the two different branches of the theory and the cosmological backgrounds, interested readers should refer to the original Cuscuton papers [20, 19].

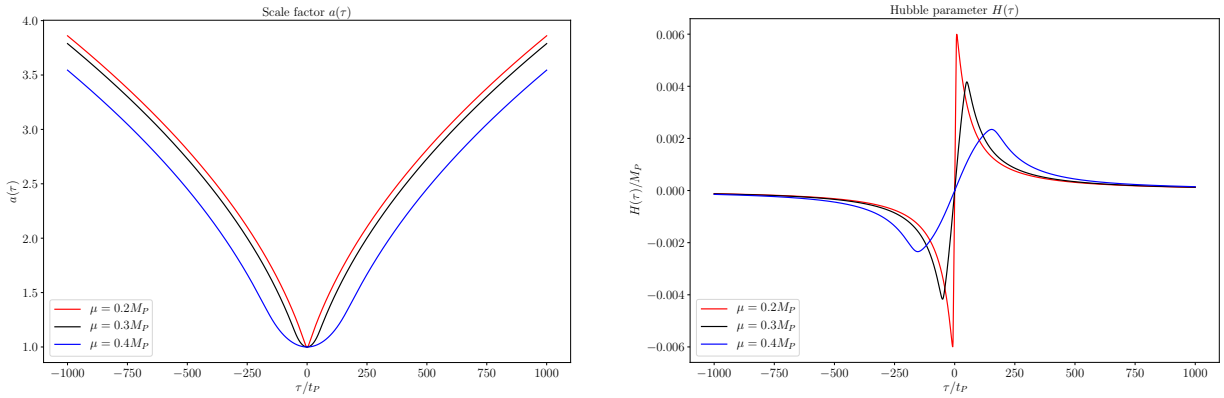

Figure 4.2: Background quantities for Cuscuton bounce. The left figure is the scale factor $a(\tau)$ where the bounce was set at $\tau_b = 0$ and $a(\tau_b) = 1$ and τ denotes the conformal time. The figure on the right is the Hubble parameter $H(\tau)$.

Figure 4.2 illustrates how the scale factor a and Hubble parameter H change with respect to time for different values of μ for this model. For what follows, we will also fix $\mu = 0.3M_P$ to match with the original Cuscuton bounce paper [52].

With the background quantities established, the next step is to study cosmological perturbations in this model. Similar to the standard theory of cosmological perturbations, the ADM formalism [30, 189] can be applied here by splitting the $3+1$ spacetime into a spacelike foliation and a time direction, where the metric is given by:

$$ds^2 = -N^2 dt^2 + h_{ij}(dx^i + N^i dt)(dx^j + N^j dt). \tag{4.8}$$

Here N and N^i represent the lapse and shift functions while h_{ij} is the induced metric on the three-dimensional spacelike hypersurfaces. After fixing one of the available gauge choices, h_{ij} can be expressed in terms of the curvature perturbations ζ and the tensor perturbations γ_{ij} as

$$h_{ij} = a^2[\delta_{ij}(1 + 2\zeta) + \gamma_{ij}]. \tag{4.9}$$

Expressing the perturbations for the Cuscuton field as $\varphi = \varphi_0 + \delta\varphi$ and the canonical scalar field as $\pi = \pi_0 + \delta\pi$, one can fix the leftover gauge choice by working in the unitary gauge for π where $\delta\pi = 0$. Next, varying the action with respect to N and N^i leads to Hamiltonian and momentum constraints while varying with respect to $\delta\varphi$ provides the constraint equation for Cuscuton. Writing this equation in Fourier space, the relationship

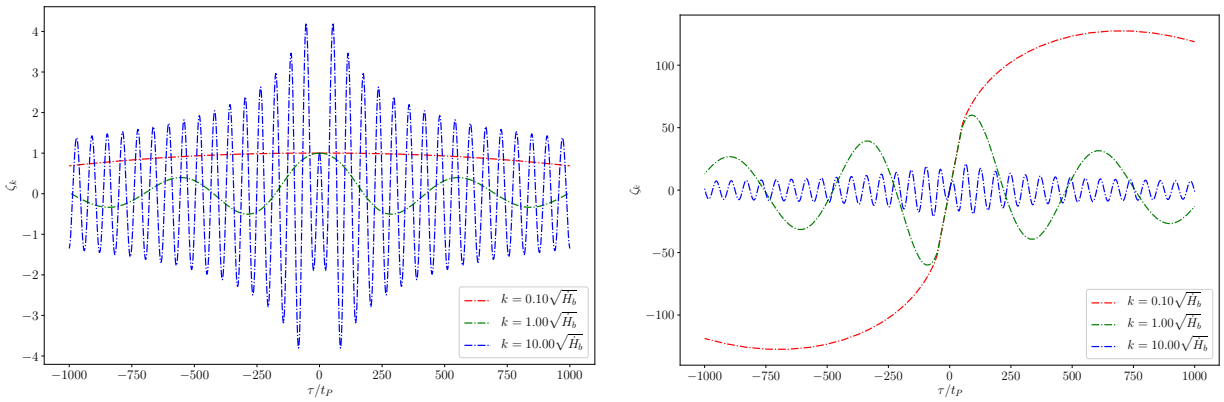

Figure 4.3: Independent solutions for ζ_k for three different scales. The figure on the left is with boundary condition set as $\zeta_k(0) = 0$ and $\zeta_k'(0) = 1$ at the bounce, while the figure on the right is with $\zeta_k(0) = 1$ and $\zeta_k'(0) = 0$. Both figures demonstrate that scalar mode solutions are non-singular and stable through the bounce.

between $\zeta_k, \dot{\zeta}_k$, and $\delta\varphi_k$ reduces to

$$\delta\varphi_k = \dot{\varphi}_0 \frac{(k/a)^2 H\zeta_k + P\dot{\zeta}_k}{[(k/a)^2 H^2 + P(3H^2 + P + \dot{H})]}, \tag{4.10}$$

where $P = \frac{1}{2M_P^2}\dot{\pi}_0^2$.[6] Finally, thorough computation of action up to second order in perturbations in Fourier space yields

$$S_\zeta^{(2)} = \frac{M_P^2}{2}\int dt\ d^3k\ az^2\left[\dot{\zeta}_k^2 - \frac{c_s^2 k^2}{a^2}\zeta_k^2\right], \tag{4.11}$$

where c_s and z are functions that are both time and scale dependent but reduce to their corresponding standard forms on small scales (large k). The exact form of these functions are given by

$$c_s^2 = \frac{(k/a)^4 H^2 + (k/a)^2\mathcal{B}_1 + \mathcal{B}_2}{(k/a)^4 H^2 + (k/a)^2\mathcal{A}_1 + \mathcal{A}_2} \tag{4.12}$$

$$z^2 = 2a^2 P\left(\frac{(k/a)^2 + 3P}{(k/a)^2 H^2 + P(3H^2 + P + \dot{H})}\right), \tag{4.13}$$

[6]Note that since for simplicity in our calculations, we are setting $a = 1$ at the bounce, the comoving wave number k represents physical scale at the bounce and not the physical scale at present time.

where the following background dependent quantities were introduced to simplify the above expressions:

$$\mathcal{A}_1 = P(6H^2 + \dot{H} + P) \tag{4.14}$$

$$\mathcal{A}_2 = 3P^2(3H^2 + \dot{H} + P) \tag{4.15}$$

$$\mathcal{B}_1 = P(12H^2 + 3\dot{H} + P) + \dot{H}\left(2\dot{H} + \frac{H\ddot{H}}{H}\right) \tag{4.16}$$

$$\mathcal{B}_2 = P^2(15H^2 - P + \dot{H}) - P\dot{H}\left(12H^2 - 2\dot{H} + \frac{3H\ddot{H}}{\dot{H}}\right). \tag{4.17}$$

These quantities were studied in detail in [51, 52] and interested readers are encouraged to refer to them for further discussion. To summarise, it was shown that first of all the sign of the kinetic term is always positive and hence there are no ghost instabilities. Second, that the independent solutions for ζ_k are stable and non-singular across the bounce both on small and large scales. Figure 4.3 illustrates this for three sets of these solutions for different scales of k. Note that the scales for k are given in terms of $\sqrt{\dot{H}_b} \approx 0.01 M_P$ to give context of the scales in our model. This is by construction since $\dot{H}_b$ depends on the model parameters.

4.3 Stability of Tensor Perturbations Through the Bounce

While the thorough investigations discussed in the last section show that the scalar sector of perturbations in Cuscuton bounce is stable, one could still ask whether the same statement is valid for tensor mode perturbations as well. In fact, it is often the case that the analysis of the tensor perturbations is less complicated than the analysis for scalar perturbations. The reason is that since $\sqrt{-g}$ that couples to Cuscuton and matter fields only gets ζ corrections at second order and terms with spatial covariant derivatives are already at second order in fields variations, the only perturbative contribution to action (4.1) from γ_{ij} at second order is through the standard Einstein-Hilbert term. Therefore, action for tensor modes in our Cuscuton model is no different than the usual standard,

$$S_\gamma^{(2)} = \frac{M_P^2}{8}\int d\tau d^3k\; a^2(\gamma_{ij}'^2 - (\nabla\gamma_{ij})^2), \tag{4.18}$$

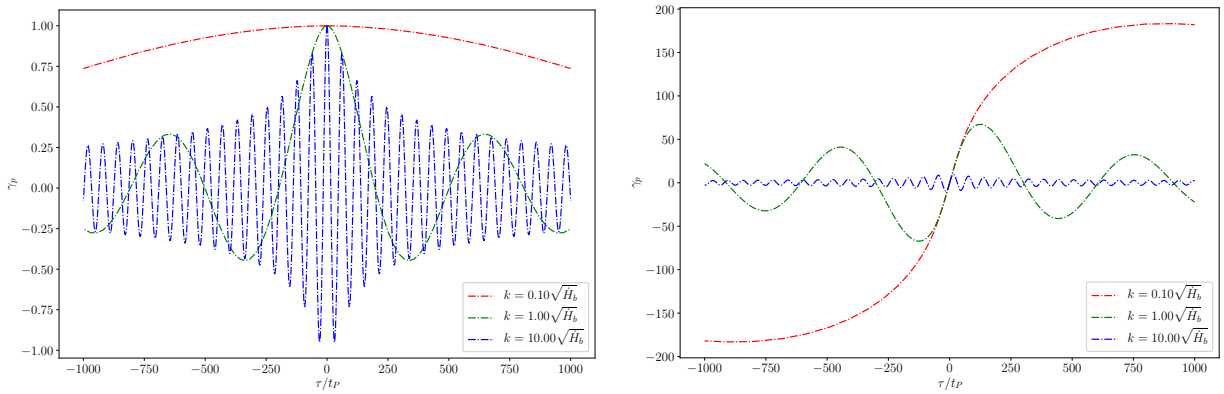

Figure 4.4: Independent solutions to tensor modes equation of state for three different scales. The figure on the left is with boundary condition set to $\gamma_p(0) = 0$ and $\gamma_p'(0) = 1$, while the figure on the right is with $\gamma_p(0) = 1$ and $\gamma_p'(0) = 0$. Both figures demonstrate solutions are non-singular and stable through the bounce.

where the conformal time τ is defined as $dt = a\ d\tau$ and ∇ is the differential operator for spatial dimensions, so that $(\nabla\gamma_{ij})^2 = \partial_a\gamma_{ij}\partial^a\gamma_{ij}$. The tensor perturbation can be split up into the appropriate tensor polarizations in the $+$ and $\times$ directions,

$$\gamma_{ij} = \sum_{p=+,\times} \gamma_p e^p_{ij}, \tag{4.19}$$

where γ_p represents the distinct amplitudes for the two polarization modes of the gravitational waves $p = \times$ and $p = +$, and e^p_{ij} represent the fixed polarization basis vectors with the property $e^p_{ij}e^{ij}_{p'} = 2\delta^p_{p'}$. Without loss of generality, assuming that the propagation direction for the gravitational waves is in the z-direction, the tensor perturbation can be written in matrix representation as

$$\gamma_{ij} = \begin{pmatrix} \gamma_+ & \gamma_\times & 0 \\ \gamma_\times & -\gamma_+ & 0 \\ 0 & 0 & 0 \end{pmatrix}. \tag{4.20}$$

Then converting to Fourier space, the action in eq. (4.18) simplifies to

$$S^{(2)}_\gamma = \frac{M_P^2}{4} \sum_{p=\times,+} \int d\tau d^3k\ a^2(\gamma_p'^2 - (\nabla\gamma_p)^2), \tag{4.21}$$

Next, similar to scalar modes, one can obtain the equation of motion for γ_p and then check to see if the independent solutions for tensor modes are non-singular and stable. Once

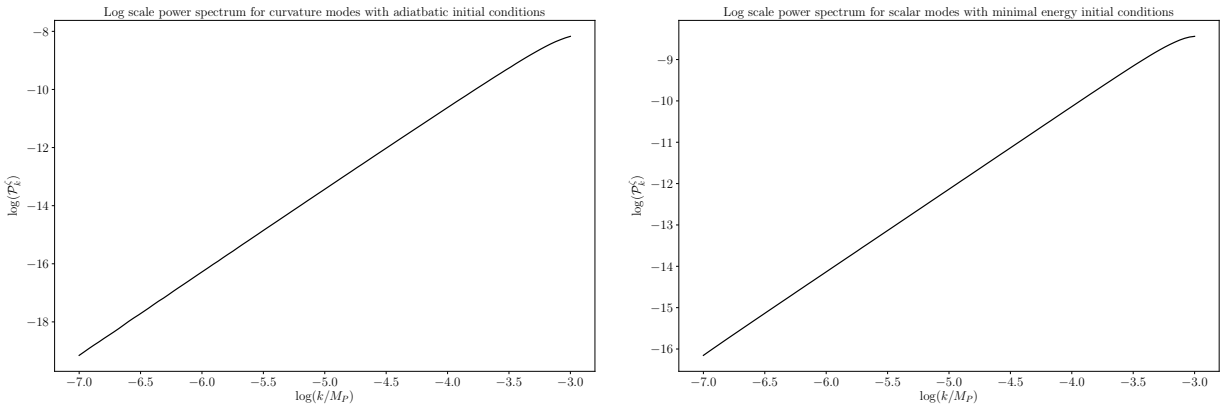

Figure 4.5: Log scale power spectrum for scalar perturbations (left) imposing adiabatic initial conditions at $\tau_i = -10^8 t_P$ and (right) imposing instantaneous minimal energy conditions at the bounce evaluated at a post time $\tau_f = 1000 t_P$. Both cases exhibit very blue power spectra.

again we see that the solutions are healthy for different scales in figure 4.4 for a set of arbitrary conditions injected at the bounce. Therefore, there is no instability associated with tensor perturbations in Cuscuton bounce either.

4.4 Power Spectrum for Scalar Modes in Single Field Cuscuton bounce

As discussed in Section 4.1, while existence of an stable bounce by itself has interesting implications for early universe and big bang singularity, another intriguing question is whether it could also provide an alternative for inflation. In particular, if it can provide a mechanism to produce curvature perturbations consistent with current data from adiabatic vacuum quantum fluctuations or other initial/boundary conditions. In this section we investigate this question for single field Cuscuton bounce and argue that this scenario as it stands, cannot produce a near scale-invariant scalar power spectrum.

To study the generation of scalar perturbations, we start by introducing the Mukhanov-Sasaki variable

$$v_k = M_P \; z(\tau, k)\zeta_k, \tag{4.22}$$

and turning the action (4.11) into the canonical form,

$$S^{(2)}_{v_k} = \frac{1}{2}\int d\tau\ d^3k\ \left[v_k'^2 + \left(\frac{z''}{z} - c_s^2 k^2\right) v_k^2\right]. \tag{4.23}$$

This enables us to apply the standard field theory quantization scheme, where v_k is promoted to operators $\hat{v_k}$. We refer readers to [173] for a review on quantizing cosmological perturbations in curved space-times. From here on we reserve the notation v_k to denote the mode functions corresponding to that operator, which also satisfy the classical equation of state,

$$v_k'' + \left(c_s^2 k^2 - \frac{z''}{z}\right) v_k = 0. \tag{4.24}$$

In order to calculate the amplitude of perturbations one needs to a make choice about initial/boundary conditions as well. We investigated the solutions to (4.24) under three different possibilities and showed that none of them produce a near scale-invariant scalar power-spectrum.

First, we started by setting the initial conditions at infinite past to adiabatic vacuum state. Like inflation, one could argue that generating all the structure in the universe out of vacuum quantum fluctuation is too impressive of an idea not to pursue. However, as we know, since the cosmological background is time dependent, the state of minimum energy also changes in time. In adiabatic regimes, where WKB approximations are satisfied, the adiabatic vacuum initial condition [45] remains close to minimum energy state. In practice, to impose that condition numerically, we selected the initial time, τ_i, long before the bounce such that the condition of $k^2 \gg \frac{z''}{zc_s^2}$ was satisfied and then imposed the following relations

$$v_k(\tau_i) = \frac{1}{\sqrt{2\omega_S}} e^{-i\omega_S \tau_i}, \qquad v_k'(\tau_i) = -i\sqrt{\frac{\omega_S}{2}} e^{-i\omega_S \tau_i}, \tag{4.25}$$

where we have defined

$$\omega_S^2 \equiv c_s^2 k^2 - \frac{z''}{z}. \tag{4.26}$$

The second possibility we considered was imposing instantaneous minimal energy condition at the bounce, $\tau_b = 0$. Motivation for this choice is that since the model is symmetric in time around the bounce, an underlying fundamental symmetry may enforce the fluctuation into ground state at $\tau_b = 0$, in order to preserve the symmetry[7]. This condition was set by

[7] Also see [53] for a different proposal regarding a CPT symmetric universe at big bang.

imposing,

$$v_k(\tau_b) = \frac{1}{\sqrt{2\omega_S}}, \qquad v_k'(\tau_b) = -i\sqrt{\frac{\omega_S}{2}}. \tag{4.27}$$

For either of the conditions listed above, we solved the equation of motion (4.24) and estimated the dimensionless power spectrum for ζ at a post bounce time through

$$\mathcal{P}_k^{\zeta_k}(\tau_f) = \frac{k^3}{2\pi^2}|\zeta_k(\tau_f)|^2 = \frac{k^3}{2\pi^2 M_p^2}\frac{|v_k(\tau_f)|^2}{z^2(\tau_f)}. \tag{4.28}$$

Figure 4.5 demonstrates the logarithmic scale dependence of the scalar power spectrum against wave number k for the two different initial condition hypotheses. In both cases we see that scale-invariance is not achieved, and both spectra are strongly blue.

In addition to these two initial conditions, we also considered thermal initial conditions [164, 104, 163, 21]. If universe existed for a long period of time before the bounce and there were additional interaction channels for fluctuations, they could have settled into a thermal equilibrium as well. In this case, we assumed the thermal energy density in fluctuations is subdominant to the background energy density in order to ignore back reaction effects. If we assume thermal initial conditions, the resulting vacuum power spectrum will be adjusted by an additional factor,

$$\mathcal{P}^{\zeta_k}_{\text{ther. ini.}} = (1 + 2\langle n_k\rangle_{\text{ini}})\mathcal{P}^{\zeta_k}_{\text{vac. ini.}}, \tag{4.29}$$

where $\langle n_k\rangle$ is the standard Bose-Einstein particle occupation number,

$$\langle n_k\rangle_{\text{ini}} = \frac{1}{e^{\frac{c_s k}{aT}} - 1}. \tag{4.30}$$

Note that c_s, a and T are evaluated at the initial time, assuming that scalar mode excitations were thermalized with temperature T.[8] Therefore, taking thermal initial condition, the power spectrum plotted on the left in figure 4.5 is adjusted by this new factor, which is demonstrated in figure 4.6 for different values of temperature T.

We can see all three sets of initial conditions for the scalar modes result in power spectra that exhibit a strongly blue tilt, inconsistent with observations. This is strong evidence that a Cuscuton bounce using only one matter field is not enough to produce a scale-invariant power spectrum for adiabatic perturbations, unless some new mechanism is introduced. We end the discussion for scalar modes in a single field Cuscuton bounce here. Since the modification to Cuscuton in section 4.5 does not affect tensor modes, we will return to tensor modes in single field Cuscuton bounce in section 4.6.

[8]Note again that in our calculations, we are setting $a = 1$ at the bounce. The comoving wave number k represents the physical scale at the bounce and not the physical scale at present time.

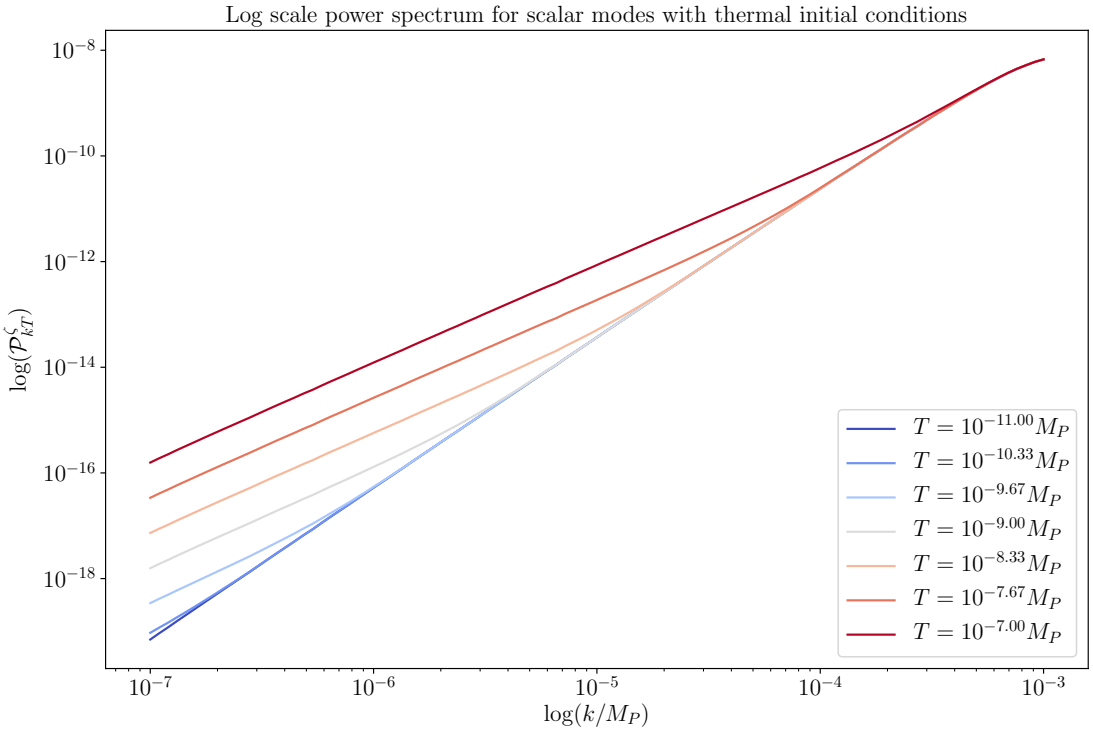

Figure 4.6: The power spectrum for ζ in the case of thermal initial conditions. Again the initial conditions were injected before the bounce at $\tau_i = -10^8 t_P$ and evaluated after the bounce at $\tau_f = 1000 t_P$. In this case the temperature of the background determines the tilt of the power spectrum, but is still unable to acquire scale-invariance.

4.5 Two Field Cuscuton Bounce and Power Spectrum for Entropy Perturbations

As we discussed in previous chapter, the power spectrum for curvature perturbations in a single field Cuscuton bounce is strongly blue. In fact, this result is consistent with what has been observed in other generic bounce models proposed in the past. For example, in the Pre-Big Bang scenario [113, 114], inspired by superstring theory, the power spectrum for curvature perturbations exhibits a strong blue tilt with $n_s = 4$. It has also been shown that the single field Ekpyrotic models [140], generically produce a blue power spectrum with a tilt of $n_s = 3$ [81, 213, 36]. As we know, this is contradictory to the observational precision measurements of the scalar power spectrum, such as those obtained through CMB measurements [22]. However, note that mathematically speaking, scalar modes can also include entropy (or isocurvature) perturbations in addition to the curvature (adiabatic) perturbations. While the observations put very tight constraints on the present day amplitude of entropy perturbations contributing to scalar anisotropies [25], they still leave the possibility that given the numerous degrees of freedoms present in early universe, these entropy modes were generated but then converted to curvature perturbations. In this section we will provide an example of how entropy perturbations with a nearly scale-invariant power spectrum could have been generated in Cuscuton bounce. This process is sometimes referred to as the entropic mechanism [66, 177], in which an additional field in the model sources the entropy perturbations that would later be converted into curvature perturbations [150, 132, 153].[9]

We start by adding a second field, χ, to our action (4.1). Once again we choose the simplest case such that the additional field only has a stabilized kinetic term ($\dot{\chi}_0 = 0$), also subdominant to the background. This field will not contribute to the Friedmann equations at zeroth order, and leaves the background dynamics unchanged. Since the field is massless, we need to allow for non-minimal coupling between this field and the dominant matter field to produce an effective mass and to source perturbations in χ. In fact, as we see below, if this coupling $F(\dot{\pi}, \nabla_i\pi, \dots)$ is proportional to the dominant background matter density, ρ_m, then power spectrum will automatically be scale-invariant. In this case, the action is

[9] Another possible mechanism inspired by S-branes in string theory, that has been more recently suggested in [57, 56, 54] could also lead to near scale-invariant power spectrum. The key difference between the two mechanisms is that as opposed to adding a new degree of freedom in entropic mechanism, in S-brane scenario, a delta-function potential gets added to effective potential at the bounce, and is the driving force for the actual bounce. Since our Cuscuton model gives us a non-divergent solution all across the bounce without needing an additional mechanism to generate the bounce itself, we explore the implications of the entropic mechanism for our power spectrum.

given by

$$S = \int d^4x\sqrt{-g}\left[\frac{M_P^2}{2}R - \frac{1}{2}D_\mu\pi D^\mu\pi - \frac{1}{2}F(\dot{\pi},\nabla_i\pi,\dots)D_\mu\chi D^\mu\chi - \mu^2\sqrt{-D_\mu\varphi D^\mu\varphi} - V(\varphi)\right], \tag{4.31}$$

where φ is the Cuscuton field, π is the scalar field from before, and χ is the new additional scalar field.[10]

As before, variation of the action at zeroth order in perturbations $\pi = \pi_0(t) + \delta\pi(x,t)$ and $\chi = \chi_0(t)+\delta\tilde{\chi}(x,t)$ around the FLRW metric leads to background equations of motion. The equation of motion for the Cuscuton field remains unchanged compared to the single field case, while for the scalar fields π_0 and χ_0 we have

$$-\frac{1}{2}\dot{\chi_0}^2F'(\dot{\pi}_0) + 3H\dot{\pi}_0 + \ddot{\pi}_0 = 0 \tag{4.32}$$

$$3F(\dot{\pi}_0)H\dot{\chi}_0 + F(\dot{\pi}_0)\ddot{\chi}_0 + \ddot{\pi}_0\dot{\chi}_0F'(\dot{\pi}_0) = 0. \tag{4.33}$$

Since we are assuming the energy density of the second field to be subdominant to the preexisting matter field and negligible for the background, this condition is satisfied if we simply set $\dot{\chi_0} = 0$ which in return makes the π-field and the Cuscuton field resume their background evolution obtained in previous section. We will show later that this solution is indeed stable and $\delta\tilde{\chi}$ do not exhibit any instabilities. Therefore our assumption is self-consistent. To summarize, under this simplification, adding a non-minimally coupled stabilized scalar field to our Cuscuton bounce model does not change the background dynamics.

Next, we study the behaviour of the cosmological perturbations under this additional coupling in the model. In all our numerical calculations we are working in Planck units, still in order to keep track of dimensions if we take χ to have dimension of mass, then $F(\dot{\pi}_0)$ is dimensionless. Therefore, from here on what we refer to as entropy perturbations is described by the dimension-less variable $\delta\chi \equiv \frac{\delta\tilde{\chi}}{M_p}$. Substituting this back in (4.31) and calculating the contribution to the second order action from χ-field yields

$$S_\chi^{(2)} = \frac{M_p^2}{2}\int d\tau d^3x a^2F(\dot{\pi}_0)\left[(\delta\chi')^2 - (\partial\delta\chi)^2\right] = \frac{M_p^2}{2}\int d\tau d^3x\ q^2\left[(\delta\chi')^2 - (\partial\delta\chi)^2\right], \tag{4.34}$$

[10]One difference between the Ekpyrotic and Cuscuton entropic mechanisms is that in the Ekpyrotic scenario, the dynamics are generated from the Ekpyrotic potential for the matter field [140, 66], while in the Cuscuton scenario, both potentials for the scalar fields are zero and the dynamics are generated from the Cuscuton potential.

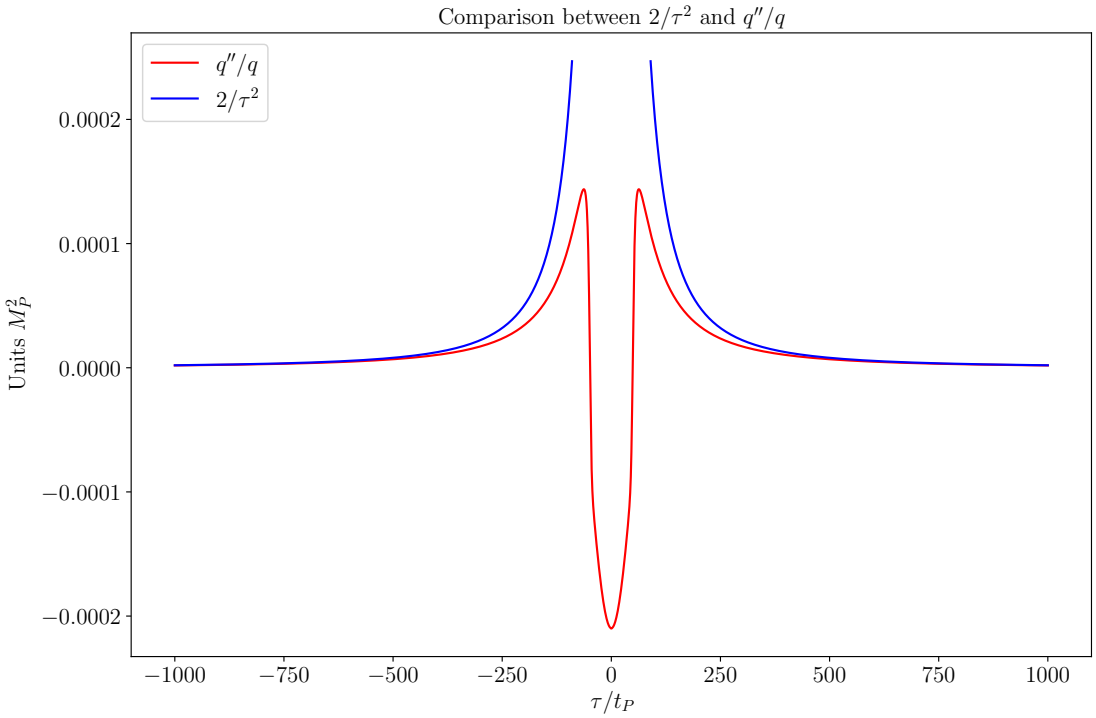

Figure 4.7: Comparison between the scale-invariance case of $2/\tau^2$ (blue) and the Cuscuton q''/q (red). By construction, q''/q approaches $2/\tau^2$ far from the bounce.

where we have also defined $q^2 \equiv a^2 F(\dot{\pi}_0)$. Introducing the canonical variable u,

$$u = M_p \; q \; \delta\chi, \tag{4.35}$$

the action (4.34) can be rewritten as

$$S_\chi^{(2)} = \frac{1}{2}\int d\tau d^3x \left[u'^2 - (\partial u)^2 + \frac{q''}{q}u^2\right]. \tag{4.36}$$

The equation of motion in Fourier space is then given by

$$u_k'' + \omega_u^2(\tau, k)u_k = 0, \tag{4.37}$$

where the effective frequency ω_u for these modes is

$$\omega_u^2(\tau, k) = \left(k^2 - \frac{q''}{q}\right). \tag{4.38}$$

Up to this point, we have not yet provided any description on the analytical dependency of the coupling function $F(\dot{\pi})$ to $\dot{\pi}$. However, a very important lesson familiar to most early universe cosmologists is that if

$$\frac{q''}{q} \sim \frac{2}{\tau^2}, \tag{4.39}$$

then (4.37) turns into a modified Bessel equation, which upon imposing vacuum initial conditions leads to nearly scale-invariant power spectrum. This is the magic that occurs to spectator fields on a de Sitter space-time backgrounds or tensor/scalar modes during slow-roll inflation which also effectively behave as spectator fields on a quasi-de Sitter background. Note that in general, equation (4.39) has two independent solutions:

$$q(\tau) = \frac{1}{\Lambda\tau} + M^2\tau^2, \tag{4.40}$$

and different values of constant Λ and M could in principle correspond to different mass scales [141, 117]. For example, in the case of a slow-roll inflationary model, for scalar modes $q \sim a\sqrt{\epsilon} \sim \frac{\sqrt{\epsilon}}{H\tau}$ approximately and for tensor modes $q \sim a \sim \frac{1}{H\tau}$. Therefore, in this case $M = 0$ and the value of $\Lambda \sim \frac{H}{\sqrt{\epsilon}}$ for scalars and $\Lambda \sim H$ for tensors determines the amplitude for perturbations. Similarly in our model, we can also find a general form of the coupling function $F(\dot{\pi}_0)$ such that entropy modes are nearly scale-invariant. In principle we could allow for the most generic case, where both Λ and M contributions exist. However, since

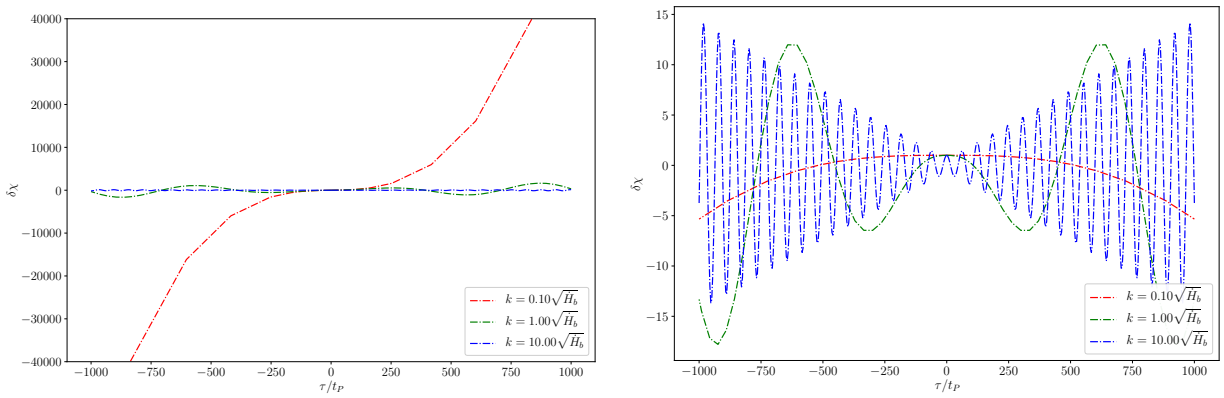

Figure 4.8: Two independent solutions for mode equation of $\delta\chi$ perturbations. The figure on the left corresponds to $\delta\chi(0) = 0$ and $\delta\chi'(0) = 1$, while the figure on the right is obtained by setting $\delta\chi(0) = 1$ and $\delta\chi'(0) = 0$. Both figures admit non-singular solutions through the bounce.

$\tau = 0$ corresponds to the time of the bounce, unless Λ contribution is strictly zero then $\frac{1}{\Lambda\tau}$ will always dominate the behaviour of q. Therefore, we proceed by considering $q(\tau) \approx \frac{1}{\Lambda\tau}$ and obtain the dependence of $F(\dot{\pi})$ to τ,

$$F(\dot{\pi}_0) \approx \frac{1}{a^2}\left(\frac{1}{\Lambda\tau}\right)^2 . \tag{4.41}$$

Note that at this point, we are simply focusing on solutions that can lead to scale-invariance itself. However, the next order effects which describe the precision value of spectral index have to be determined by accuracy of the relation (4.41), which in the language of inflation is translated to slow variation of $\Lambda(\tau)$ i.e. $H(\tau)$ in time, due to slow-roll parameters.

Next taking into account that the bounce transition period, where Cuscuton modifications become significant for the background, is a very brief period in Planck units (around 250 t_p, see figure 4.2) and that it is unlikely to have a significant impact on the power spectrum on cosmological scales, we postulated that it should be sufficient that relation (4.41) be satisfied when ρ_m is dominant. However, in that regime $a^2 \propto \tau$ and $\rho_m \propto a^{-6} \propto \tau^{-3}$ which implies $\frac{1}{a^2\tau^2} \propto \rho_m$ and we can consider

$$F(\dot{\pi}_0) \equiv \frac{1}{\Lambda^2 M_p^2}\left(\frac{1}{2}\dot{\pi}_0^2\right) \approx \left(\frac{H^2}{\Lambda^2}\right)_{a \gg a_b} . \tag{4.42}$$

In other words, interestingly in order for the theory to produce a near scale-invariant power spectrum, χ field needs to have the most natural non-minimal coupling to π, i.e. its energy

density. Expressing this relation in terms of the variable q, yields

$$q(\tau) = \frac{1}{\Lambda M_p}\sqrt{\frac{1}{2}\dot{\pi}_0^2}. \tag{4.43}$$

Figure 4.7 shows the comparison between $\frac{q''}{q} \approx \frac{2}{\tau^2}$ [11] and the Cuscuton model obtained from (4.43). As expected, except in the vicinity of the bounce, the coupling function in (4.42) leads to $\frac{q''}{q}$ tracking $\frac{2}{\tau^2}$ closely.

The magnitude of the coupling constant Λ adjusts the amplitude of the power spectrum and it can be determined by comparison to the observational constraints. Physically, it represents the strength of the non-minimal coupling of χ-fields to the density of π which could arise from the underlying fundamental theory.

Once we assert the form of the coupling function from (4.42), then substituting $q(\tau)$ from (4.43) into (4.38), the mode equation (4.37) can be solved numerically. Again the advantage of our model is that since $\frac{q''}{q}$ does not exhibit any divergences (see Figure 4.7), the differential equation is non-singular at all times and does not require any *ad hoc* matching conditions. As we discussed before, by construction we expect that imposing the adiabatic vacuum initial conditions would lead to a scale-invariant power spectrum. However, to test that, we need to impose the initial conditions numerically similar to the single field model. Therefore, we require

$$u_k(\tau_i) = \frac{1}{\sqrt{2\omega_u}}e^{-i\omega_u\tau_i}, \qquad u_k'(\tau_i) = -i\sqrt{\frac{\omega_u}{2}}e^{-i\omega_u\tau_i}, \tag{4.44}$$

at an initial time τ_i, such that $k|\tau_i| \gg 1$. Then, we estimate the power spectrum for entropy perturbations at some later "snapshot" time, τ_f, before and after the bounce by

$$\mathcal{P}_k^{\delta\chi}(\tau_f) = \frac{k^3}{2\pi^2}|\delta\chi_k(\tau_f)|^2 = \frac{k^3}{2\pi^2}\frac{|u_k(\tau_f)|^2}{M_p^2 q(\tau_f)^2}. \tag{4.45}$$

Figure 4.9 displays an example of a pre-bounce power spectrum, where we have set $\Lambda = 10^{-3.5}M_p$ and $\tau_f = -1000t_P$. The resulting power spectrum is indeed scale-invariant except for values of k that correspond to modes that do not cross the freezing horizon i.e. $k^2 \gtrsim \frac{q''}{q}|_{t_f}$ and remain oscillatory. In our model these modes are close to Planck scale at the bounce ($k \gtrsim 10^{-4}M_P$). Figure 4.10 shows the power spectrum for the same entropy modes after they have gone through the bounce and evaluated at the time $\tau_f = 1000t_P$. The black

[11] Which is the approximate time dependence of q''/q in slow-roll inflationary models.

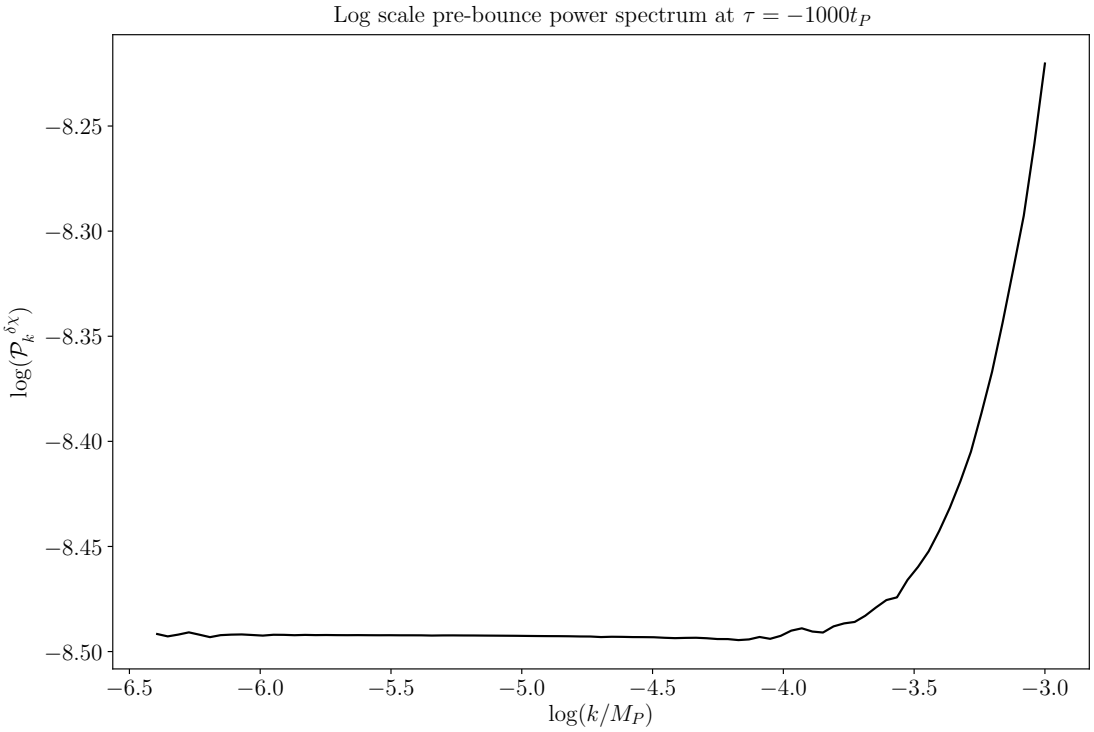

Figure 4.9: Pre-bounce power spectrum for χ-field perturbations evaluated at final time $\tau_f = -1000t_P$ before Cuscuton modifications start becoming significant. The adiabatic vacuum initial condition is set at $\tau_i = -10^{-8}t_P$ and with $\Lambda = 10^{-3.5}M_p$.

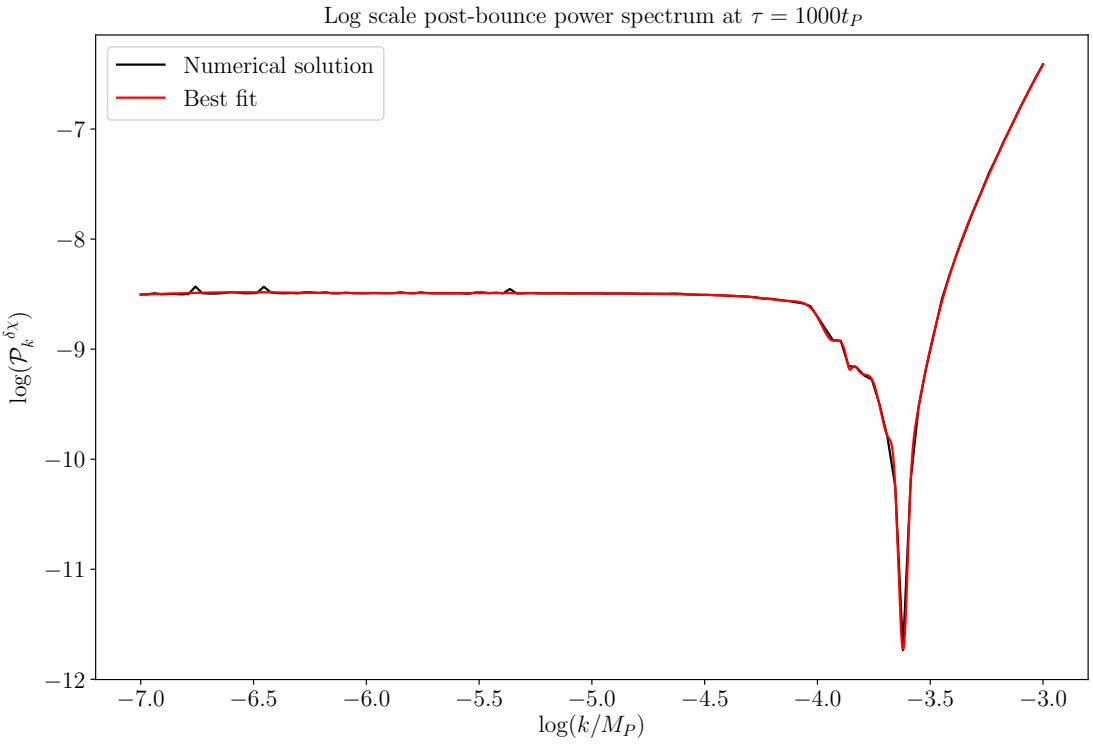

Figure 4.10: Post-bounce power spectrum for χ-field perturbations evaluated at $\tau_f = 1000t_P$, well after Cuscuton modifications become negligible again. The vacuum initial conditions are imposed at $\tau_i = -10^{-8}t_P$ and $\Lambda = 10^{-3.5}M_p$. The smooth red line represents a best fit through the numerical solution shown in black.

line is the actual numerical result and red curve shows the best fitted smooth function through the numerical result. As shown in the figure, the shape of the resulting power spectrum remains scale-invariant for $k \lesssim 10^{-4} M_P$ and is not impacted by the transition trough the bounce. In fact, if we assume the universe transitioned into radiation at this time, the actual modes of cosmological interest corresponding to CMB scales today would be more than 10 orders of magnitudes smaller in k than the range showed in this plot and are therefore even less impacted. Note that at this stage, from the model building perspective, our goal was simply to check if this model can produce a close to scale-invariant spectrum [12]. Testing for the proximity of the numerical solution to exact scale-invariance, in the range of $10^{-7} M_P \lesssim k \lesssim 10^{-4.5} M_P$, we obtain $n_s - 1 \approx -0.0036$. Although this result should not be compared to the actual observational tilt[13], it achieves our main goal of producing a solution which is nearly scale-invariant. As we mentioned before, when producing the actual observational tilt, one also needs to take into account additional effects such as the details of how the entropy modes are converted into adiabatic modes. The conversion itself requires some additional mechanism, such as premodulated preheating or the curvaton process. In Ekpyrotic models, the conversion of the entropy perturbations have been studied in detail and can happen either before the bounce, during the contracting phase [150, 151], or after the bounce [105]. We leave the study of these effects in Cuscuton bounce for future work.

As a final note to end this section, Figure 4.10 demonstrates the impact of the bounce transition on modes in the range $10^{-4} M_P \lesssim k \lesssim 10^{-3} M_P$ as well. Our result shows that for these modes, the deviation of $\frac{q''}{q}$ from $\frac{2}{\tau^2}$ in vicinity of $k^2 \sim \frac{q''}{q}$ crossing is significant. However, as we pointed out earlier since these scales are near the Planck scale, in a non-inflationary universe they would not be observable on cosmological scales.

4.6 Power Spectrum of Primordial Gravitational Waves in Cuscuton Bounce

We now return back to tensor modes and look into the power spectrum of primordial gravitational waves generated in Cuscuton bounce. While primordial gravitational waves have not been detected yet, if ever detected, they could play a crucial role in distinguishing

[12] We reiterate that in analogy to inflationary models, this is similar to first realizing that spectator scalar fields in de Sitter backgrounds generate scale invariant power-spectra. Then utilizing that observation and implementing a slowly rolling potential, inflationary models can accommodate quasi-de Sitter backgrounds where small deviations of n_s from one is achieved by adjusting the derivatives of the potential.

[13] Current observation from PLANCK data [22] require $n_s = 0.965 \pm 0.004$.

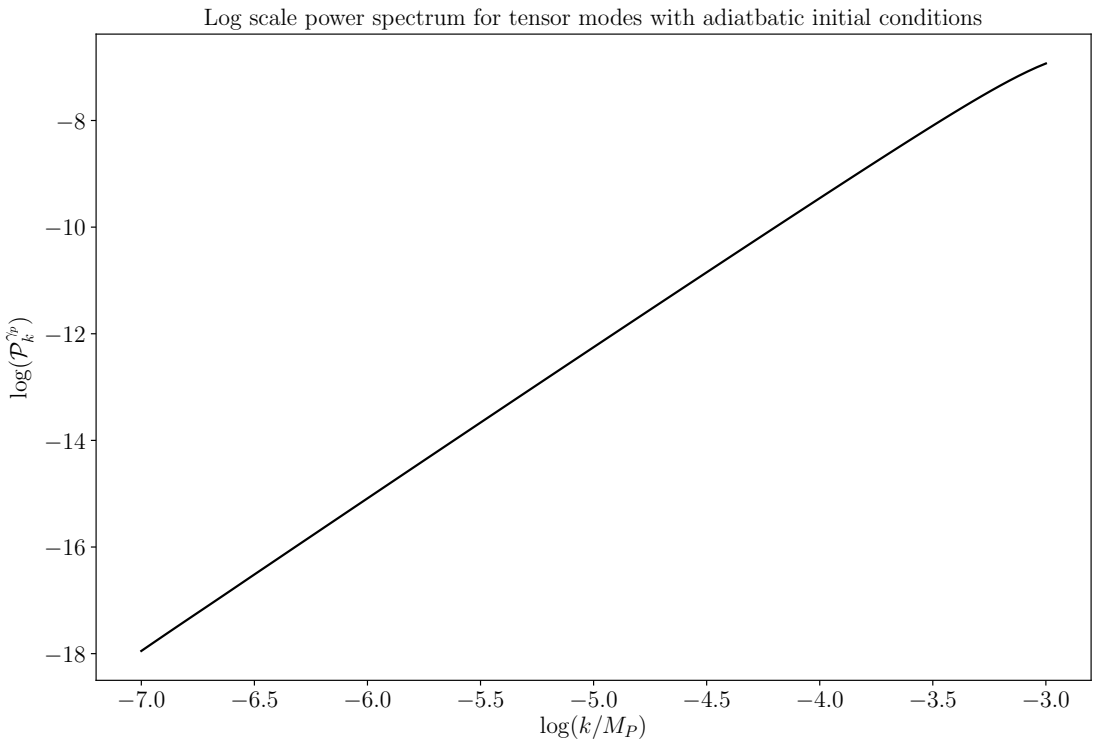

Figure 4.11: Logarithmic scale power-spectrum for tensor perturbations with vacuum initial conditions set at $\tau_i = -10^8 t_P$. The final time is taken as $\tau_f = 1000 t_P$. Power spectrum has the blue tilt of $n_t \sim 2$ with an amplitude which is many orders of magnitudes below observable thresholds at cosmological scales.

between inflationary and bouncing models. As has been argued in [116], there are some basic arguments on why extracting enough power from the tensor quantum fluctuations at extremely small scales and converting them to observable tensor modes at cosmological scales relies on gaining a large number of e-foldings, which is possible during the inflationary epoch but by construction is absent in bounce scenarios. Therefore, generally one does not expect bounce models to produce observable primordial tensor modes. As we show here, the same argument applies to Cuscuton bounce.

First, note that since χ-field does not couple to metric perturbations at second order, the action for tensor modes given by (4.21), remains unchanged. Furthermore, since the background evolution for the single field and two field Cuscuton bounce are the same, the evolution of tensor modes in both scenarios are also identical. Once again, the quantization procedure can be carried out by introducing the canonical variable v_p for both polarizations of the tensor modes [174, 58],

$$v_p = \frac{aM_P}{\sqrt{2}}\gamma_p, \tag{4.46}$$

so that the action in Fourier space can be rewritten as

$$S^{(2)}_{v_p} = \frac{1}{2}\sum_{p=\times,+}\int d\tau d^3k \left[v_p'^2(k,\tau) - \left(k^2 - \frac{a''}{a}\right)v_p^2(k,\tau)\right], \tag{4.47}$$

and the equation of motion for each polarization v_p is given by

$$v_p'' + \left(k^2 - \frac{a''}{a}\right)v_p = 0. \tag{4.48}$$

Next, considering the adiabatic vacuum initial conditions by imposing

$$v_p(k,\tau_i) = \frac{1}{\sqrt{2k}}e^{-ik\tau_i} \qquad v_p'(k,\tau_i) = -i\sqrt{\frac{k}{2}}e^{-ik\tau_i}, \tag{4.49}$$

at τ_i such that $k^2 \gg \frac{a''}{a}|_{\tau_i}$, we numerically solve equation (4.48) and evaluate the power spectrum at some later time τ_f,

$$\mathcal{P}_k^{\gamma_p}(k,\tau_f) = \frac{k^3}{2\pi^2}|\gamma_p(k,\tau_f)|^2 = \frac{k^3}{2\pi^2}\frac{|2v_p(k,\tau_f)|^2}{M_P^2\ a^2(\tau_f)}. \tag{4.50}$$

Our result shows that tensor modes never freeze out in pre-bounce transition and they are not affected through the bounce either. Figure 4.11 displays the logarithmic scale power spectrum for tensor modes evaluated post bounce, at $\tau_f = 1000t_P$ and with vacuum initial conditions set at $\tau_i = -10^8 t_p$. As expected, the produced power spectrum retains its vacuum sub-freezing tilt, i.e. $n_t \sim 2$ with an amplitude which is many orders of magnitudes below observable thresholds at cosmological scales.

4.7 Conclusion

In this work, we studied the power spectra of curvature, iso-curvature and tensor perturbations in the Cuscuton bounce proposed in [52]. For curvature perturbations, we considered three different initial conditions: standard adiabatic vacuum initial conditions, instantaneous minimal energy condition at bounce, as well as initial thermal condition. In all three cases, the generated power-spectrum for scalar perturbations were found to be strongly blue. Next, we investigated the possibility of a two field model, generating a nearly scale-invariant iso-curvature/entropy power spectrum for scalar perturbations. We found that this can be done with a very simple model with a spectator field that is kinetically coupled to the primary matter field. This is a very interesting result since our solution does not rely on any *ad hoc* matching condition across the bounce or encounter any instability or singularities as it passes through the bounce. While this is a significant result, we note that to explain the observed tilt and amplitude of scalar perturbations [22], the model requires an additional phase that converts entropy modes into adiabatic modes, and similar to inflation, it requires a reheating phase for the universe to transition into the radiation phase. We leave the exploration of all these interesting aspects as well other potentially important features, such as non-Gaussianities or pre-bounce smoothing, for future work.

To complete our work on the generation of the power spectrum, we also investigated the behaviour of tensor modes in Cuscuton bounce. We first showed that Cuscuton bounce is stable under tensor perturbations as well. Then we obtained the power spectrum for primordial gravitational waves produced in a Cuscuton scenario and found that similar to other bounce models, the tensor index n_t is strongly blue, and so the model does not predict an observable spectrum of primordial gravitational waves.

Part II

Cosmological Parameter Inference with Dark Sirens

Chapter 5

Gravitational Wave Cosmology

On February 11, 2016, the LIGO Scientific Collaboration and the Virgo Collaboration announced that two detectors of LIGO directly detected gravitational waves for the first time, from a binary black hole merger [2]. This detection caused tremors in the astronomy, astrophysics, and cosmology communities across the globe and marked the beginning of a new era of multi-messenger astronomy. The significance of GW detection in modern age astronomy is two-fold:

1. GWs can provide access to previously inaccessible sectors in astronomy and cosmology, and can be used to further test theoretical models of astrophysics, cosmology, and fundamental physics.

2. GW data can be used in combination with available EM data to acquire further understanding of our Universe. This gives rise to the common term *multi-messenger astronomy*, where the multiple "messengers" – EM signals at different wavelengths and GW signals – complement each other to provide a more complete picture.

In this chapter I will first outline how GWs arise as gravitational radiation in the linearized perturbation theory of gravity, then explain how GWs can be used alongside existing EM data in multi-messenger astronomy. Finally, I will discuss the prospects of using dark sirens in cosmology.

5.1 Gravitational Wave Theory

5.1.1 Linearized Theory in Vacuum

This subsection will go through the basics of linearized theory for GWs. The theoretical background is a standard derivation, easily accessible in several review articles [109, 199, 204, 148]. We consider a flat spacetime (Minkowski metric $\eta_{\mu\nu}$) with small metric perturbations denoted as $h_{\mu\nu}$. Then the physical metric $\bar{g}_{\mu\nu}$ can be defined as:

$$g_{\mu\nu} = \eta_{\mu\nu} + h_{\mu\nu}, \tag{5.1}$$

where we assume that the metric perturbations are small ($|h_{\mu\nu}| \ll 1$). The inverse physical metric can also be written as[1]

$$g^{\mu\nu} = \eta^{\mu\nu} - h^{\mu\nu}. \tag{5.2}$$

For convenience, one often defines the trace-reversed metric peturbation:

$$\bar{h}_{\mu\nu} = h_{\mu\nu} - \frac{1}{2}\eta_{\mu\nu}h, \tag{5.3}$$

where h is the trace of $h_{\mu\nu}$, taken with the Minkowski metric so that $h = \eta_{\mu\nu}h^{\mu\nu}$. We then enforce the Lorentz gauge

$$\bar{h}^{\mu\nu}{}_{,\nu} = 0, \tag{5.4}$$

in which the EFE become a set of decoupled linear wave equations:

$$\Box\bar{h}^{\mu\nu} = \left(-\frac{\partial^2}{\partial t^2} + \nabla^2\right)\bar{h}^{\mu\nu} = -16\pi T^{\mu\nu}, \tag{5.5}$$

where $\Box$ is the d'Alembertian operator and ∇ is the usual three-dimensional spatial derivative operator. In the case where the spacetime is empty, then one acquires the homogeneous GW equation

$$\Box\bar{h}^{\mu\nu} = \left(-\frac{\partial^2}{\partial t^2} + \nabla^2\right)\bar{h}^{\mu\nu} = 0, \tag{5.6}$$

[1] Even though $\eta_{\mu\nu}$ is not the physical metric since it is only the background metric to which perturbations are added, to linear order it can be used as an effective inverse.

which yields plane wave solutions of the form

$$\bar{h}_{\mu\nu} = Ae_{\mu\nu} \exp(ik_\gamma x^\gamma), \tag{5.7}$$

where A is the amplitude of the wave, $e_{\mu\nu}$ is the so-called polarization tensor to be discussed later on, and k_γ is the wave vector. Thus a perturbation to the spacetime metric yields propagating plane waves once substituted into the EFEs (2.7). These waves are what are called gravitational waves.

Substitution of the plane waves (5.7) into the homogeneous wave equation (5.6) yields

$$\Box\bar{h}^{\mu\nu} = k^\gamma k_\gamma \bar{h}_{\mu\nu} = 0, \tag{5.8}$$

which implies that $k^\gamma k_\gamma = 0$, and hence the wave vectors for the GWs are null vectors. Meanwhile, substitution of the plane waves (5.7) into the Lorentz gauge condition (5.4) gives

$$\bar{h}^{\mu\nu}{}_{,\nu} = k_\nu \bar{h}^{\mu\nu} = 0 \Longrightarrow k_\nu e^{\mu\nu} = 0, \tag{5.9}$$

since $A \neq 0$ for a non-trivial solution. This condition shows that the wavevector and the polarization tensor are orthogonal.

The linearized equations describe a classical field that has a total of 10 independent components (since $h_{\mu\nu}$ is symmetric), which the Lorentz gauge can be applied to reduce the number to 6. However, one can note that the Lorentz gauge alone does not uniquely specify $h_{\mu\nu}$. One can impose another four additional constraints through coordinate transformations to uniquely fix the solution [148]. A convenient gauge to demand is the *transverse-traceless* (TT) gauge, in which

$$e^{0\mu} = 0, \tag{5.10}$$

$$\eta_{ij} e^{ij} = 0, \tag{5.11}$$

where (5.10) is the transverse condition and (5.11) is the traceless condition [204]. The transverse condition (5.10) can be rewritten into a more familiar form when combined with the orthogonality condition (5.9):

$$k_\nu e^{\mu\nu} = k_0 e^{\mu 0} + k_j e^{\mu j} = 0 \Longrightarrow k_j e^{ij} = 0, \tag{5.12}$$

where we used the traceless condition twice to get rid of instances of $e^{\mu 0}$. Since the trace is zero in this gauge, one also notes that the trace-reversed metric perturbation $\bar{h}_{\mu\nu}$ and the metric perturbation $h_{\mu\nu}$ are equal by (5.3):

$$\bar{h}_{\mu\nu} = h_{\mu\nu} \tag{5.13}$$

Since our gauge-fixing leaves only two independent polarizations, the polarization tensor only has two independent components left. By taking an observer at rest and without loss of generality assuming that GWs propagate in the z-direction, ie.

$$u^\mu = (1,0,0,0), \quad k^\mu = (\omega,0,0,\omega), \tag{5.14}$$

where ω is the frequency of the wave detected by the observer at rest, the TT gauge conditions results in a form of the metric perturbation as [148]:

$$\bar{h}_{\mu\nu} = h_{\mu\nu} = \begin{pmatrix} 0 & 0 & 0 & 0 \\ 0 & h_+ & h\times & 0 \\ 0 & h_\times & -h_+ & 0 \\ 0 & 0 & 0 & 0 \end{pmatrix}. \tag{5.15}$$

Hence in terms of the two polarizations $p = \times, +$, the general solution can be written as a superposition of wave solutions at different frequencies ω as

$$\bar{h}_{\mu\nu} = \sum_{p=\times,+} h_p e^p_{\mu\nu} \exp(ik_\gamma x^\gamma), \tag{5.16}$$

where h_p is the polarization magnitude corresponding to each polarization and $e^p_{\mu\nu}$ is the associated unit polarization tensors, given in this context as [146]:

$$e^+_{\mu\nu} = \begin{pmatrix} 0 & 0 & 0 & 0 \\ 0 & 1 & 0 & 0 \\ 0 & 0 & -1 & 0 \\ 0 & 0 & 0 & 0 \end{pmatrix}, \quad e^+_{\mu\nu} = \begin{pmatrix} 0 & 0 & 0 & 0 \\ 0 & 0 & 1 & 0 \\ 0 & 1 & 0 & 0 \\ 0 & 0 & 0 & 0 \end{pmatrix}. \tag{5.17}$$

These GWs can be detected from ground-based interferometers such as the Laser Interferometer Gravitational-wave Observatory (LIGO) [1], the Virgo interferometer [74], or upcoming space-based interferometers such as the Laser Interferometer Space Antenna (LISA) [29]. Namely, when a GW event is detected, it would correspond to a measurement of $|\bar{h}|$ through deviations in the length of the arms of the detector. If L denotes the length of the arm and ΔL is the measured deviation in the arms due to spatial distortions from the GW packet, then the amplitude can be read off as [109]:

$$|\bar{h}_p| = \frac{2\Delta L}{L}. \tag{5.18}$$

In what follows, we will use h instead of $\bar{h}$ whenever we refer to tensor perturbations for brevity.

5.1.2 Sources of Gravitational Waves

There are many possible sources of GWs of astrophysical and cosmological interests. In this subsection I will briefly discuss some of these sources. Note that this is not a complete list, and for a more comprehensive list, interested readers should refer to Refs. [199] or [204].

Continuous Gravitational Waves

Gravitational radiation is quadrupole in nature, which means that a spherically symmetric mass distribution does not radiate gravitationally [199]. Hence a perfectly axially symmetric spinning neutron star would not produce GWs. However, if the neutron star has a deformation so that overall it is axially asymmetric, this deformation can produce gravitational waves. These axially asymmetric rotating neutron stars are often referred to as pulsars. These pulsars are expected to emit GW signals at twice the rotation frequency, and the EM counterpart signals are assumed to be coupled to the GW signals [6]. Hence pulsars are an excellent hub for multimessenger astronomy, and can provide rich information regarding the physics of rotating neutron stars.

Although pulsars have hinted at the existence of GWs indirectly through the orbital decay of binary pulsar system PSR B1913+16 due to the loss of energy from gravitational radiation [130, 220], so far all efforts for directly detecting GW signals from pulsars have shown to be unsuccessful thus far. The inability to detect the GW signals from pulsars at the sensitivity of LIGO is not completely in vain, since improved upper limits can be placed on the expected GW amplitude, quadrupole moment, and ellipticity of the pulsars [6]. With the upcoming improvements in detector sensitivity, cosmologists remain hopeful of a first direct measurement of continuous GWs.

Compact Binary Mergers

At this point in time, compact binary mergers are the only sources of GWs that have been directly detected. While this term can refer to any system of two compact objects that eventually coalesce, the primary binaries of interest are neutron star-neutron star pairs, neutron star-black hole pairs, or black hole-black hole pairs, due to their high mass (and thus luminosity and GW amplitude). Over the last couple of years, the LIGO Scientific and Virgo Collaborations have detected several binary mergers, resulting in a small zoo of mergers with different objects and different masses [5, 8]. Although it has been a while since

the first binary black hole merger [2] and binary neutron star merger [4] detections, only recently the first detection of two neutron star-black hole binary systems was reported [10]. As I will discuss in section 5.3.3, the detection of the binary neutron star merger GW170817 was accompanied by an EM counterpart, allowing for identification of the host galaxy [4]. This joint gravitational wave and EM event marked the first multi-messenger observation.

The GW signals from a binary merger are expected to contain rich information about the astrophysical quantities of the bodies as well as valuable information regarding the physical processes in the strong gravity regime [84]. In addition, as I will argue in section 5.3.3, binary mergers can provide us a valuable tool to study cosmology. The GW amplitude can be related to three main characteristic quantities in the following relation [199]:

$$h_p(t) \sim \frac{\mathcal{M}^{5/3} f(t)^{2/3}}{r}, \tag{5.19}$$

where f is the frequency of the GW, which is twice the orbital frequency of the inspiral. Note here for brevity, we have left out the explicit dependence on factors that depend on the angle the merger is viewed as well as the phase of the GW signal. The variable $\mathcal{M}$ is called the *chirp mass*, given by

$$\mathcal{M} = \frac{(m_1 m_2)^{3/5}}{(m_1 + m_2)^{1/5}}, \tag{5.20}$$

named because it sets the rate at which the binary inspirals, setting the chirp (ie. when the frequency and amplitude of the signal increases drastically) of the signal [129]. Along with the amplitude of the GW signal, one can also measure the frequency f as well as the change in frequency $\dot{f}$, which can be used in combination to break the degeneracy between the chirp mass and the distance [199]. Hence if the amplitude of the GW signal is known, then one can infer the value of its distance as well[2]. Merging binaries in cosmological scenarios will be discussed more in-detail in section 5.3.3.

Stochastic Gravitational Wave Background

So far all of the types of GW radiation discussed have been distinguishable signals from individual sources. However, analogous to the CMB, it is also expected that there is a background of GW radiation corresponding to the accumulation of indistinguishable GW

[2]While this is true, these equations are only valid for non-cosmological ($z = 0$) distances. Binary systems at cosmological distances require redshifted quantities, which I will discuss in section 5.3.3.

signals over time called the stochastic gravitational wave background (SGWB) [78]. The signals that make up the SGWB can be divided into two categories – the astrophysical background, which entails the superposition of all the signals from the countless number of discrete coherent and incoherent astrophysical sources, and the cosmological background, which is comprised of signals from fundamental processes [199].

While the astrophysical background is more easily detectable by our current detectors and can be used with other probes such as galaxy surveys to extract useful information, the cosmological background is of greater interest, since this is likely one of the only ways to probe GWs from certain fundamental processes. For instance, as seen in section 3.3.2, the very early Universe predicts a specific spectrum of primordial GWs when assuming the inflationary paradigm. While a non-zero detection on large scales is usually considered as a smoking gun for inflation (or deviations from general relativity [116]), there are also arguments that some alternatives to inflation and other processes in the very early Universe predict primordial GWs as well [60]. Similarly, there are inflationary models with lower energies that can have non-detectable GWs as well. Nevertheless, efforts to detect primordial GWs remain inconclusive so far, although the upper bounds are steadily improving [25]. As the experiments get better, and the constraints get tighter, primordial GWs (or the lack of them) will help constrain different models of the very early Universe. Deviations from the expected observables for the usual inflationary model can imply that our understanding of the very early Universe is not yet complete, and that the inflationary paradigm may need tweaking or reconsiderations [124]. In the extreme case where a background of primordial GWs is not detected, then the standard inflationary models could possibly require reexamination.

Inflationary physics are not the only fundamental physics that can be investigated using a cosmological SGWB. An example of great interest is the existence of cosmic strings [142], which are one-dimensional topological defects that would have been produced by phase transitions in the early Universe. These cosmic strings can form loops and as they vibrate, they emit gravitational waves over our cosmological history, which would leave imprints on the SGWB [216, 198, 87, 206, 179]. The confirmation of existence of cosmic strings would verify new physics beyond the Standard Model. In addition there can also be production of GWs from the phase transitions themselves or from dark sectors [221, 119, 120, 44].

While the SGWB has not been detected yet, LIGO and Virgo have placed constraints on the energy density of the background in their frequency band [7, 12]. Pulsar Timing Arrays (PTAs) such as the North American Nanohertz Observatory for Gravitational Waves (NANOGrav) have also been unable to directly detect a background of GWs, only placing upper constraints in their respective frequency bands [31]. Despite the lack of a detection thus far, several upcoming surveys are expected to be able to detect a background with

their improved sensitivities. Space-based detectors such as LISA [29] or the DECi-hertz Interferometer Gravitational wave Observatory (DECIGO) [138, 139] and next generation ground-based detectors such as the Einstein Telescope [162] will look for SGWB signals. Since the background consists of several different sources, the dependence of the signals on frequency will be important in identifying the possible sources [78].

5.2 Statistics Toolkit

In the modern age of cosmology, it is not enough to get by with the classical cosmological background in section 2. Indeed, most cosmologists are equipped with a statistics toolkit that they use for their research, whether for hypothesis testing, parameter estimation, or model selection. The types of statistical tools that a cosmologist can use are abundant, and so in this thesis I will only discuss the most relevant ones for the work in Chapter 6. In addition, statistics has varying levels of mathematical rigour. Rather than taking a very mathematical approach to the definitions, I will follow the mathematical rigour of Refs. [136, 126] and provide a background relevant for our purposes. In particular, I will discuss the basics of probability theory, explaining the difference between the frequentist and Bayesian interpretations. Then I will show how the Bayesian framework is a powerful tool for cosmology.

5.2.1 Basic Probability Theory

Let us denote Ω to be the sample space which possible outcomes are drawn from, and $A \in \Omega$ to be some event drawn from Ω. One can define a probability function p that associates an event to a probability. Hence for an event A, the probability associated with the event is given by $p(A)$. For a probability function to be valid, it must obey the following axioms, usually referred to as the Kolmogorov axioms [136]:

1. The probability of the event A happening cannot be negative:

$$p(A) \geq 0. \tag{5.21}$$

2. If the event in particular is the whole sample space Ω, one must have that

$$p(\Omega) = 1. \tag{5.22}$$

3. If $A_i \in \Omega$ are mutually exclusive events (ie. A_i and A_j are disjoint for $i \neq j$: $A_i \cap A_j = \emptyset$), then

$$p\left(\bigcup_{i=1}^{\infty} A_i\right) = \sum_{i=1}^{\infty} p(A_i). \tag{5.23}$$

For two general events A and B that are not necessarily mutually exclusive, the third axiom can be written as

$$p(A \cup B) = p(A) + p(B) - p(A \cap B). \tag{5.24}$$

In addition to these rules, the probability of event A and B happening is given by

$$p(A \cap B) = p(A, B) = p(A|B)p(B). \tag{5.25}$$

The quantity $p(A|B)$ is a conditional probability, referred to as the probability of A given B. A and B are called independent events if $p(A|B) = p(A)$, and so $p(A, B) = p(A)p(B)$ by (5.25). In other words, if the conditional probability of A given B is true is independent of B then B being true does not affect A, and so A and B are independent. Furthermore, since $p(A, B) = p(B, A)$ due to the symmetry of the "and" operator $\cap$, then

$$p(A, B) = p(B, A) \implies p(A|B)p(B) = p(B|A)p(A). \tag{5.26}$$

Rearranging this gives a very famous relation known as Bayes' rule:

$$p(A|B) = \frac{p(B|A)p(A)}{p(B)}. \tag{5.27}$$

In the next subsection, we will see how this important relationship plays out in the context of cosmological statistical analysis.

Another useful identity is the law of total probability, which says that if $B_i \in \Omega$ for $i = 1, \ldots, k$ is a partition of Ω (ie. they are disjoint and $\bigcup_{i=1}^{k} B_i = \Omega$), then

$$P(A) = \sum_{i=1}^{k} P(A \cap B_i), \tag{5.28}$$

or using conditional probabilities,

$$P(A) = \sum_{i=1}^{k} P(A|B_i)p(B_i). \tag{5.29}$$

The law of total probability is also referred to as marginalization, which is a powerful tool in cosmology as we will see.

Up to this point, I have mainly used events as inputs for the probability functions. However in most cases, we wish to quantify the physics by mapping events to real numbers so that probability functions become more mathematically familiar in the sense that the inputs are also real numbers. For this purpose, *random variables* are maps from the "event space" to the real numbers in "state space". In this case a set of real numbers in state space corresponding to an output of the random variables is called a *realization*. These quantities are often denoted in literature using a capital case X for random variables and lower case x for the realizations. These random variables can either be discrete or continuous. Finally, we can define the *probability density function* (pdf) as the probability function that assigns a probability to a realization of a random variable. At a low level, the main difference between the discrete cases and continuous cases is that the summation gets replaced by an integration.

There is an analogous version of law of total probability for the continuous case, which instead looks at marginal pdfs rather than marginal probabilities. If $p(x, y)$ is the joint pdf for the continuous random variables X and Y, we can marginalize over Y so that we obtain the marginalized pdf for X over Y:

$$p_X(x) = \int dy\ p(x, y) = \int dy\ p(x|y)p(y). \tag{5.30}$$

As I will show in the next subsection, this is a useful tool in cosmology, since astrophysical and cosmological models have many parameters that we wish to marginalize over.

5.2.2 Bayesian Inference

When working with experimental data, one must choose a certain interpretation and framework to perform statistical operations. There are two interpretations of probability – the frequentist interpretation and the Bayesian interpretation. As the name suggests, the frequentist interpretation pertains to the frequency of outcomes of an experiment. The Bayesian interpretation refers to using currently available data to perform statistical operations. The key idea of the frequentist interpretation is that experiments are repeatable, while the fundamental concept of the Bayesian interpretation is information. Different branches of physics are generally dominated by different interpretations. For instance, majority of the statistics in particle physics is done from a frequentist interpretation, due to the repeatable experimental set-ups. Meanwhile astronomy/astrophysics/cosmology mainly

uses the Bayesian interpretation, since the "labs" in this case are not easily controllable. Hence for the statistical analysis in this thesis, I will adopt the Bayesian interpretation.

In a cosmological setting, we are often concerned with how theoretical models of astrophysical and cosmological phenomena relate to the vast amounts of cosmological data available to us. The frequentist vs. Bayesian interpretations debate occur once we invoke Bayes' rule using the data and the model as our parameters [136]. In general, if we denote the model as M and the data as D, then Bayes' rule gives

$$p(M|D) = \frac{p(D|M)p(M)}{p(D)}, \tag{5.31}$$

which is oftentimes called Bayes' theorem in literature[3]. In words, this describes how the probability of the model given the data depends on the probability of the data given the model, as well as the probability of the model and the probability of the data.

Adopting the usual convention, if the model is described by k parameters so that $\boldsymbol{\theta} = (\theta_1, \theta_2, \cdots, \theta_k)$ and $\mathbf{x}$ represents the data vector, then Bayes' theorem is written as

$$p(\boldsymbol{\theta}|\mathbf{x}) = \frac{p(\mathbf{x}|\boldsymbol{\theta})p(\boldsymbol{\theta})}{p(\mathbf{x})}, \tag{5.32}$$

where each of the factors have special names [126]:

- $p(\boldsymbol{\theta}|\mathbf{x})$ is the posterior probability of $\boldsymbol{\theta}$. This is the quantity that we are interested in for parameter inference.
- $p(\mathbf{x}|\boldsymbol{\theta})$ is the likelihood. It is the probability of the data given the model parameters. Most of the modelling and computation goes into this term, and in simplest cases this is all we need to maximize to acquire the peak of the posterior. The likelihood is a special function of $\boldsymbol{\theta}$ (it is not a pdf for $\boldsymbol{\theta}$ since it is normalized over $\boldsymbol{x}$ and not $\boldsymbol{\theta}$ [212]), labelled specially as $L(\mathbf{x}; \boldsymbol{\theta}) = p(\mathbf{x}|\boldsymbol{\theta})$.
- $p(\boldsymbol{\theta})$ is the prior. This term captures our previous knowledge about the parameters, either from theoretical arguments or prior experiments.
- $p(\mathbf{x})$ is the evidence or marginal likelihood. This is a term that ensures that the posterior is normalized to unity:

$$p(\mathbf{x}) = \int d\boldsymbol{\theta}\ p(\mathbf{x}|\boldsymbol{\theta})p(\boldsymbol{\theta}). \tag{5.33}$$

[3]Bayes' rule corresponds to the non-controversial mathematical identity (5.27). Bayes' theorem corresponds to the choice of interpretation using Bayes' rule with the model and data as the parameters.

In this relation we are marginalizing over the model parameters. This factor is usually not necessary in parameter inference and is usually ignored in calculations, but is important for model selection since there are multiple models [126].

In the simple cases where we have a flat prior (where $p(\boldsymbol{\theta})$ is a constant), and the evidence $p(\mathbf{x})$ is just a normalization factor for the posterior, then

$$p(\boldsymbol{\theta}|\mathbf{x}) \propto p(\mathbf{x}|\boldsymbol{\theta}) = L(\mathbf{x};\boldsymbol{\theta}). \tag{5.34}$$

Therefore as previously mentioned, to get the most probable result for the parameter, one just has to maximize the likelihood. One should note that flat priors are not necessarily the case, and oftentimes other priors such as Gaussian priors are used. With general priors, the above relationship is not as simple, and the peak of the likelihood does not necessarily coincide with the peak of the posterior.

To report an inferred value for the model parameters, one performs descriptive statistics on the posterior pdf. There are several methods to acquire the pdf. For a small number of model parameters, then one can easily calculate the likelihood function as a function of the model parameters by gridding in parameter space. However, in cosmological settings there are usually many model parameters, and the statistical modelling of the problem is non-trivial. In these cases, numerical methods such as Monte Carlo Markov Chain (MCMC) sampling is an effective way to acquire the posterior distribution[4]. By taking random walks in the parameter space and using some sort of acceptance condition (usually Metropolis-Hastings), one effectively samples from the posterior distribution. These samples can then be used to generate multidimensional histograms and density plots, allowing us to then perform descriptive statistics on.

There are several advantages of using Bayesian inference for model parameters [212]. One example is handling nuisance parameters, which are parameters that have an influence on the data but are not of interest for our purposes. By marginalizing over them, Bayesian inference easily handles these parameters. Another advantage is the use of the prior. By using either physically justified intuition or previous experimental results, the prior easily ensures physically sensible results for model parameters.

Bayesian inference can be summarized as: "Given a model with parameters $\boldsymbol{\theta}$ and some real data $\mathbf{x}$, what are the probability distributions $p(\boldsymbol{\theta}|\mathbf{x})$ for the model parameters given the data? From these probability distributions, what are the most likely values, and

[4]For a review on MCMC techniques and the different algorithms particularly in cosmological scenarios, see Refs. [96, 126, 136, 212].

what are the bars of error?" To conclude, Bayesian inference is a powerful technique to acquire inferred values of important cosmological parameters and their statistical significance, given different cosmological models. Lastly before moving on, note that the discussion in this subsection was focused on Bayesian methods for statistical inference of parameters. Bayesian statistics is a much more powerful tool than just for parameter inference and can also be used for other significant purposes in cosmology, such as model selection[5].

5.3 Cosmology with Standard Sirens

As previously mentioned in chapter 2, the Universe is homogeneous and isotropic on sufficiently large scales. However as we saw in chapter 3, the origins of structure in our Universe is quantum mechanical in nature. Due to the random nature of the fluctuations, although the Universe looks the same on large scales, it is generally inhomogeneous and anisotropic on smaller scales. Regions with higher energy densities or gravitational curvature in the very early Universe will have overdense regions in the late Universe, which will yield a higher number of galaxies compared to the average. Similarly, regions with lower energies in the very early Universe will correspond to underdense regions, and will have a fewer number of galaxies compared to the average. In this section I will introduce a statistical formalism to describe the distribution of matter in the Universe, and discuss how GWs are exciting prospects to probe this distribution.

5.3.1 Information from the Matter Density Field

As previously mentioned the large scale structure of the late Universe is conjectured to be of quantum mechanical origins in the very early Universe. Due to the random nature of these initial conditions, we use a random field from a statistical field theory perspective to model the underlying matter distribution [172, 90]. That is, if we denote $\boldsymbol{x}$ as a point in three-dimensional Euclidean space, a random scalar field is a set of random variables $\rho(\boldsymbol{x})$ with a set of distribution functions $P_n(\rho(\boldsymbol{x}_1), \ldots, \rho(\boldsymbol{x}_n))$, where $\boldsymbol{x}_i$ represents the i-th point from set of spatial points [90]. Given this, the n-point correlation function is given by

$$\langle \rho(\boldsymbol{x}_1) \cdots \rho(\boldsymbol{x}_n) \rangle = \int d\rho(\boldsymbol{x}_1) \cdots d\rho(\boldsymbol{x}_n)\ P_n(\rho(\boldsymbol{x}_1), \ldots, \rho(\boldsymbol{x}_n)) \rho(\boldsymbol{x}_1) \cdots \rho(\boldsymbol{x}_n), \tag{5.35}$$

[5]For interested readers, the use of Bayesian statistics for model selection can be found in Refs. [126, 212].

where $\langle\cdot\rangle$ represents the ensemble average. One can define the (matter) density field $\delta(\boldsymbol{x})$ as

$$\delta(\boldsymbol{x}) = \frac{\rho_m(\boldsymbol{x})}{\bar{\rho}_m} - 1, \tag{5.36}$$

where $\rho_m(\boldsymbol{x})$ is the matter density at $\boldsymbol{x}$ and $\bar{\rho}_m$ is the comoving average (or background) matter density. With this definition, points in space with higher densities than the background level are called overdensities, with $\delta(\boldsymbol{x}) > 0$, while regions in space with lower than average densities are called underdensities, with $\delta(\boldsymbol{x}) < 0$. As seen in Chapter 2, since the cosmological principle says that the Universe is homogeneous and isotropic, we require that the matter density field δ is statistically homogeneous and isotropic. In other words, its moments must be invariant under spatial transformations and rotations [172]. Therefore since the density field is a random statistical field,

$$\langle\delta(\boldsymbol{x}_i)\rangle = \langle\delta\rangle = 0, \tag{5.37}$$

and so its 1-point function, or its mean, is zero. In cosmology, two particular n-point functions of interest are the 2-point function and the 3-point function, given by

$$\langle\delta(\boldsymbol{x}_1)\delta(\boldsymbol{x}_2)\rangle = \xi^{(2)}(\boldsymbol{x}_1, \boldsymbol{x}_2), \tag{5.38}$$

$$\langle\delta(\boldsymbol{x}_1)\delta(\boldsymbol{x}_2)\delta(\boldsymbol{x}_3)\rangle = \xi^{(3)}(\boldsymbol{x}_1, \boldsymbol{x}_2, \boldsymbol{x}_3), \tag{5.39}$$

where $\xi^{(2)}(\boldsymbol{x}_1, \boldsymbol{x}_2)$ and $\xi^{(3)}(\boldsymbol{x}_1, \boldsymbol{x}_2, \boldsymbol{x}_3)$ are the 2-point and 3-point *connected* correlation functions respectively[6]. For the density field δ, we can also assert the cosmological principle, by enforcing homogeneity and isotropy. Homogeneity says that the statistics of the field should be invariant under spatial translations, so

$$\xi^{(2)}(\boldsymbol{x}_1, \boldsymbol{x}_2) = \xi^{(2)}(\boldsymbol{x}_1 - \boldsymbol{x}_2), \tag{5.40}$$

while isotropy says that the statistics of δ should be invariant under spatial rotations, and so

$$\xi^{(2)}(\boldsymbol{x}_1, \boldsymbol{x}_2) = \xi^{(2)}(|\boldsymbol{x}_1 - \boldsymbol{x}_2|). \tag{5.41}$$

Thus the two-point correlation function between two points for the matter density field only depends on the distance between the two points.

[6] In general, for generic statistical fields, the n-point correlation functions and the n-point connected correlation functions are not the same. In fact, the n-point connected correlation functions are defined so that the n-point correlation functions can be represented as a sum of these functions [90]. It is only in this case since $\langle\delta\rangle = 0$ that the two functions are equal.

While so far we have only worked with the three-dimensional Euclidean representation of statistical fields, it is also convenient to work in Fourier space. By defining the following convention for the Fourier transform:

$$\delta(\boldsymbol{k}) = \int d^3\boldsymbol{x}\ \delta(\boldsymbol{x}) e^{-i\boldsymbol{k}\cdot\boldsymbol{x}}, \tag{5.42}$$

and the inverse Fourier transform as

$$\delta(\boldsymbol{x}) = \int \frac{d^3\boldsymbol{k}}{(2\pi)^3} \delta(\boldsymbol{k}) e^{i\boldsymbol{k}\cdot\boldsymbol{x}}, \tag{5.43}$$

the power spectrum $P(k)$ is defined as

$$\langle \delta(\boldsymbol{k}) \delta^*(\boldsymbol{k}') \rangle = P(k)(2\pi)^3 \delta_D(\boldsymbol{k} - \boldsymbol{k}'), \tag{5.44}$$

where δ_D is the three-dimensional Dirac delta distribution in Fourier space. Similarly, the bispectrum $B(\boldsymbol{k}_1, \boldsymbol{k}_2, \boldsymbol{k}_3)$ is defined as

$$\langle \delta(\boldsymbol{k}_1) \delta(\boldsymbol{k}_2) \delta(\boldsymbol{k}_3) \rangle = B(\boldsymbol{k}_1, \boldsymbol{k}_2, \boldsymbol{k}_3)(2\pi)^3 \delta_D(\boldsymbol{k}_1 + \boldsymbol{k}_2 + \boldsymbol{k}_3). \tag{5.45}$$

The power spectrum and the bispectrum are the Fourier transforms of the 2-point and 3-point correlation functions respectively [90]:

$$\xi^{(2)}(r) = \frac{1}{2\pi^2} \int_0^\infty dk\ k^2 P(k) j_0(kr), \tag{5.46}$$

$$\xi^{(3)}(\boldsymbol{x}_1, \boldsymbol{x}_2, \boldsymbol{x}_3) = (2\pi^3) \int_{\boldsymbol{k}_1} \int_{\boldsymbol{k}_2} \int_{\boldsymbol{k}_3} \delta_D(\boldsymbol{k}_1 + \boldsymbol{k}_2 + \boldsymbol{k}_3) B(\boldsymbol{k}_1, \boldsymbol{k}_2, \boldsymbol{k}_3) e^{i[\boldsymbol{k}_1\cdot\boldsymbol{x}_1 + \boldsymbol{k}_2\cdot\boldsymbol{x}_2 + \boldsymbol{k}_3\cdot\boldsymbol{x}_3]}, \tag{5.47}$$

where $j_0(kr) = \sin(kr)/(kr)$ is the zeroth spherical Bessel function of the first kind. Note that this also means that the 2-point and 3-point correlation functions are inverse Fourier transforms of the power spectrum and the bispectrum.

One can also add another level of structure to the density field by asserting that it is a Gaussian random field (for reasons to be discussed in more detail shortly). Gaussian random fields with zero mean have distribution functions given by multivariate Gaussians:

$$P_n(\boldsymbol{y}) = \frac{1}{(2\pi)^{n/2}\sqrt{|\mathrm{C}^{-1}|}} \exp\left(-\frac{1}{2}\boldsymbol{y}^T \mathrm{C}^{-1} \boldsymbol{y}\right), \tag{5.48}$$

where $\boldsymbol{y}$ is the n-dimensional vector $\boldsymbol{y} = [\delta(\boldsymbol{x}_1), \cdots, \delta(\boldsymbol{x}_n)]^T$, $|\mathrm{C}^{-1}|$ is the determinant of C^{-1}, the inverse matrix of the symmetric and semipositive definite *covariance matrix* C, whose components are defined by

$$\mathrm{C}_{ij} = \langle \delta(\boldsymbol{x}_i)\delta(\boldsymbol{x}_j)\rangle = \xi^{(2)}(|\boldsymbol{x}_i - \boldsymbol{x}_j|). \tag{5.49}$$

Mo, van de Bosch, and White [172] state that there are at least three reasons why Gaussian random fields are of interest in cosmology:

1. Inflation produces a nearly Gaussian field from quantum fluctuations which retains its Gaussianity if the evolution is linear. Thus the initial conditions for the large scale structure is Gaussian.

2. The central limit theorem states that regardless of the (sufficiently well-defined) underlying distribution functions of the random variables, for a large number of samples, the distribution of the sum of these events asymptotes to a Gaussian distribution.

3. There is no strong evidence against the linear density field being non-Gaussian.

Since the primordial random field produced by inflation is almost perfectly Gaussian, the power spectrum nearly captures all of the statistical information, which is why in the context of inflation usually only the power spectrum is considered. However, despite the initial random field being almost perfectly Gaussian, the random field in the late time Universe from observations such as galaxy measurements is highly non-Gaussian [90]. Hence higher order n-point functions are required to provide a more complete description of the large scale structure, and the Gaussian random field formalism is only an approximation.

One should note that although the primordial random field is nearly Gaussian, there is a growing interest to search for non-Gaussian signatures in the primordial field. Non-Gaussian signatures in the primordial field can have several implications for the inflaton as well as other early Universe physics [168]. Information about non-Gaussianities is not only limited from the CMB, but large scale structure observations are also believed to have implications for the primordial non-Gaussianities [215, 89, 168].

5.3.2 Tracer Bias

As seen in the previous subsection, the matter density field δ is a very powerful statistical tool that offers rich information for both the early and late Universe. Unfortunately, it is difficult to capture the matter density field through direct observations and one must turn

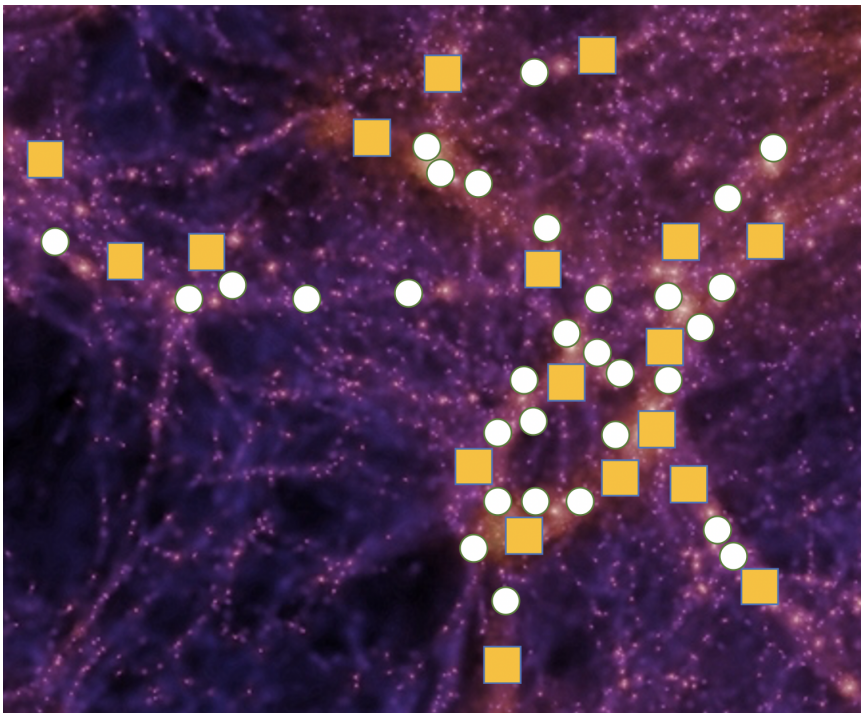

Figure 5.1: An example of possible observed samples from an underlying matter distribution. White circles correspond to one species of samples and the orange squares corresponds to another species of samples. These species can be any observable tracer of matter – for example galaxies and binary black hole mergers. The background image of the matter distribution is a modified image from the Millennium Simulation Project [210]. Bright regions in the image are overdense regions while dark regions are underdense regions. Note that this picture is not-to-scale.

to tracers of the density field instead. Tracers, such as galaxies, are physically observable objects that are related to the density field. Hence finding a distribution of the tracers can provide valuable information about the distribution of the matter density field. Since tracers are countable objects, their density fields are usually written with number densities instead. For instance, for galaxies, the *galaxy density field* δ_g at a point $\boldsymbol{x}$ is given by

$$\delta_g(\boldsymbol{x}) = \frac{n_g(\boldsymbol{x})}{\bar{n}_g} - 1, \tag{5.50}$$

where $n_g(\boldsymbol{x})$ is the number density of galaxies at $\boldsymbol{x}$ and $\bar{n}_g$ is the average number density of galaxies. Figure 5.1 shows a possible result of sampling from the matter distribution, where we end up with a finite number of detected tracers (hence why we often work with number densities).

In general, the density field for galaxies can be expanded as[7]

$$\delta_g(\boldsymbol{x}, \tau) = \sum_O b_O(\tau) O(\boldsymbol{x}, \tau), \tag{5.51}$$

where O is an operator that is comprised of the matter density field δ, the gravitational potential, galaxy masses, and general perturbation quantities, and b_O are bias parameters associated with each operator O [90]. It can be shown that since on sufficiently large scales, the governing mechanism for structure formation is gravity, the statistics of galaxies can be written locally and perturbatively as a functional of matter overdensities. Historically, this relation had the Taylor expanded form such that [111]:

$$\delta_g(\boldsymbol{x}) = f[\delta](\boldsymbol{x}) \approx \sum_{k=0}^{\infty} \frac{b_k}{k!} \delta^k. \tag{5.52}$$

We can assume $\langle \delta \rangle = \langle \delta_g \rangle = 0$ due to the cosmological principle and that taking the ensemble average of ρ and $n_g(\boldsymbol{x})$ should not depend on position in the Universe. In the limit where $|\delta| \ll 1$ and we can ignore higher orders of δ this justifies setting $b_0 = 0$. Thus in this limit, δ_g can be approximated as

$$\delta_g(\boldsymbol{x}) = b_1 \delta(\boldsymbol{x}), \tag{5.53}$$

where $b_1 = b$ is often referred to as the *linear galaxy bias* in this case. In general, this Taylor expanded form is a simplified expansion of the local matter density, and in general it should take on a form with more complicated terms as in Refs. [167, 90].

[7] Although there is a more general form of this expansion if one considers the influence of small-scale perturbations on the formations of galaxies, usually modelled by stochastic fields [172, 90]. For the work in this thesis, we will ignore stochastic effects from small-scales and focus only on large-scale effects.

In this case assuming we are in the linear bias regime, one can estimate the bias parameter by comparing the 2-point correlation function for galaxies with that for matter, so that

$$b_\xi(r)^2 = \frac{\langle \delta_g(\boldsymbol{x})\delta_g(\boldsymbol{y})\rangle}{\langle \delta(\boldsymbol{x})\delta(\boldsymbol{y})\rangle} = \frac{\xi_g^{(2)}(r)}{\xi^{(2)}(r)}, \tag{5.54}$$

where $r = |\boldsymbol{x} - \boldsymbol{y}|$ and $\xi_g^{(2)}(r)$ is the galaxy 2-point correlation function, called the galaxy-galaxy auto-correlation. In Fourier space, one can also find the linear bias parameter by comparing the two power spectra, so that

$$b_P(k)^2 = \frac{P_g(k)}{P(k)}, \tag{5.55}$$

where $P_g(k)$ is the galaxy power spectrum. Although these definitions are not generally equal are limited by the functions that define them, in the special case where we are in the deterministic local linear bias limit these definitions are equivalent and can therefore be used as a tool to estimate the local linear bias given these cosmological tools [147].

To summarize, the bias relates the density field of observable objects such as galaxies and clusters to the underlying matter density field.

5.3.3 Resolving Tensions with Standard Sirens

In the previous subsection, I discussed how biased tracers of the matter distribution can be used to extract information about the matter distribution. Although only galaxies and galaxy clusters were the most commonly used tracers, these are not the only tracers of matter. Since new avenues of cosmological exploration have been opened with the onset of GW astronomy, one can consider how GW sources can also act as tracers of the matter distribution. In particular, the binary mergers of compact objects discussed in section 5.1.2 are relatively new tracers of growing interest.

Before moving onto looking at these mergers from a cosmological perspective, one must modify the expressions in section 5.1.2, since at cosmological distances ($z \neq 0$), the quantities in expression (5.19) are redshifted due to the expansion of space as the GW signal propagates. In particular, the GW frequency f is modified so that

$$f \to f_0 = \frac{f}{(1+z)}, \tag{5.56}$$

where f_0 is the measured frequency. In this case, the observed amplitude depends on the usual quantities as [129, 85]:

$$h_{p,o} \sim \frac{\mathcal{M}_z^{5/3} f_0^{2/3}}{D_L}, \tag{5.57}$$

where $h_{p,o}$ is the observed amplitude and D_L is the luminosity distance to the source[8]. Again we left out explicit dependence on factors that are functions of angle at which the binary is viewed as well as the phase of the GW signal. Here the new quantity $\mathcal{M}_z$ is defined as

$$\mathcal{M}_z = (1+z)\frac{(m_1 m_2)^{3/5}}{(m_1+m_2)^{1/5}}, \tag{5.58}$$

referred to as the *redshifted chirp mass*. As previously mentioned in section 5.1.2, one also measures the frequency f_0 and the change in frequency $\dot{f}_0$ which can be used to break the degeneracy between D_L and $\mathcal{M}_z$ [199]. Since one only obtains the luminosity distance of the source and not the redshift, one requires additional information to extract information from these mergers. These binary mergers have been coined as *standard sirens* [129], aptly named for its analogous EM counterparts – Type Ia supernovae (SNe), a type of *standard candle*. The luminosity distance to these supernovae can be extracted if the observed luminosity is calibrated [187]. The calibration to other astronomical objects is often called the *cosmological distance ladder*, in which issues can arise even if one is very careful since incorrect assumptions in the astrophysical models can propagate throughout.

Standard sirens are of interest because they can provide distance measurements to cosmologically distant sources without use of the cosmological distance ladder. If an EM counterpart to the merger event is identified, then one can associate the merger to a host galaxy, thus acquiring a redshift to the source. Since the redshift and the luminosity distance to the source is known, one can make use of the redshift-distance relationship to extract important information required to infer cosmological parameters, such as the local Hubble parameter H_0 [129, 85].

The local Hubble parameter is a much debated topic in recent years, and is arguably one of the most popular topics in cosmology at the moment. The sides of the debate can be roughly divided into two halves – direct measurements from the late Universe and indirect measurements from the early Universe. The two most often quoted measurements are the measurements of $H_0 = 67.4 \pm 0.5$ km/s/Mpc from the Cosmic Microwave Background (CMB) by the Planck Collaboration [22] and the SH0ES measurement of $H_0 = 73.2 \pm 1.30$

[8]For a derivation of how the redshifted quantity results in the luminosity distance, see Ref. [77].

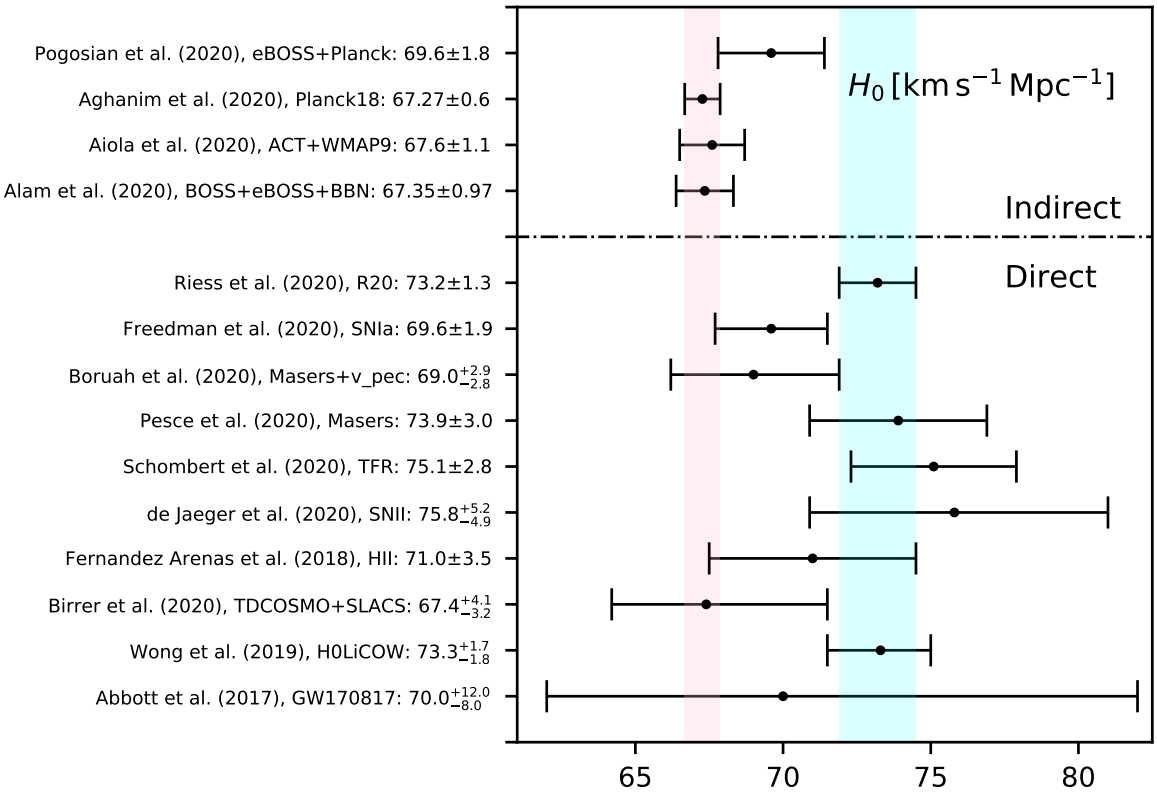

Figure 5.2: Recent reports of H_0 from various different datasets and methods. The blue band corresponds to the most recent H_0 value from the SH0ES team (R20) [194] while the pink band corresponds to the Planck 2018 measurement of H_0 [22]. Note that this is not a comprehensive collection, and it lists only some of the very many reports of H_0. This plot is a reduced version of the one in Ref. [91], produced by the sample code also from the same work, available at https://github.com/lucavisinelli/H0TensionRealm. Interested readers are encouraged to see Ref. [91] for a more complete figure and a comprehensive review of the topic. The method/datasets and measurement for each work are provided in Table 5.1 with references to the papers.

Direct (Late Universe)		Indirect (Early Universe)	
Method/Dataset	H_0 (km/s/Mpc)	Method/Dataset	H_0 (km/s/Mpc)
Cepheids-SNIa [194]	73.2 ± 1.3	eBOSS+Planck [188]	69.6 ± 1.8
TRGB-SNIa [110]	69.6 ± 1.9	Planck18 [22]	67.27 ± 0.6
Masers+v_{pec} [50]	$69.0^{2.9}_{-2.8}$	ACT+WMAP9 [24]	67.6 ± 1.1
Masers [186]	73.9 ± 3.0	BOSS+eBOSS+BBN [27]	67.35 ± 0.97
TFR [202]	75.1 ± 2.8		
SNII [88]	$75.8^{5.2}_{-4.9}$		
HII galaxies [103]	71.0 ± 3.5		
TDCOSMO+SLACS [46]	$67.4^{4.1}_{-3.2}$		
H0LiCOW [222]	$73.3^{1.7}_{-1.8}$		
Standard siren [3]	$70.0^{12.0}_{-8.0}$		

Table 5.1: Tabularized data for Figure 5.2. This is a reduced dataset taken from Ref. [91], with the only new addition being Ref. [50]. SNIa refers to Type Ia supernovae, TRGB is an acronym for Tip of the Red Giant Branch, and TFR is an acronym for the Tully-Fisher Relation. Note that this a very incomplete list of measurements only meant to capture the idea, and readers should see Ref. [91] for a more comprehensive review.

km/s/Mpc from SNe [195]. Note that these are not the most recent measurements of H_0, and several additional measurements and improvements have been made since these measurements. Figure 5.2 shows several recent measurements of H_0 from various different studies, including the first standard siren measurement of H_0 [3]. The datasets considered in Figure 5.2 are provided in Table 5.1. This table and figure are a heavily reduced version of the ones in Ref. [91].

Identification of the optical counterpart GRB 170817A allowed for the association of the GW signal detection from the binary neutron star merger GW170817 with the unique host galaxy NGC 4993, which yielded the first multi-messenger measurement for H_0 with a value of $H_0 = 70^{+12.0}_{-8.0}$ km s^{-1} Mpc^{-1} [3]. As shown in Figure 5.2, the error bars for this measurement are not competitive with the error bars from the more traditional methods. However, as additional GW events are detected one can expect that standard sirens can offer new insight on the ongoing Hubble debate. It is estimated that a sample size of ~ 50 binary neutron star mergers with optical counterparts can provide a $\sim 2\%$ estimate of H_0 [76, 102]. In addition, while the first neutron star-black hole mergers have just been detected [10], an optimistic estimate[9] shows that they may provide a 1.5-2.4% estimate of H_0 by the year 2030 [101]. Therefore as more standard sirens with electromagnetic counterparts are detected, we will gain access to information previously not available to us, making the next few years very exciting for mutli-messenger astronomy. However over the last six years, only one siren with an EM counterpart (GW170817) has been confidently detected[10]. In a crude approximation, if we assume 5 years for a detection of one merger with an EM counterpart, then it would take over 200 years to get a sample size of ~ 50 mergers necessary for the $\sim 2\%$ estimate of H_0.

While the prospects for standard sirens are promising, it is expected that we will not be able to detect an electromagnetic counterpart for majority of the detected mergers, making it difficult to acquire the redshift of the source. Thus even as one gains access to the GW data from numerous sirens, they will not be usable to measure the Hubble parameter in the standard way. In particular, so far, since BBH mergers have higher intrinsic luminosities compared to BNS systems or NS-BH systems [5, 8], they are detected a a much higher rate. Meanwhile, they are theoretically less likely to have electromagnetic counterparts. Thus in order to extract cosmological information from these *dark sirens* [11] alternative methods must be utilized. In other words, since dark sirens are much more common in nature, they

[9] The authors of Ref. [101] state that this level of precision is heavily dependent on the modelling for these types of mergers.

[10] Although candidates of binary mergers with astrophysical counterparts have been reported [9].

[11] Yet another *dark* quantity in astronomy... This "dark" should not be confused with the "dark" used for dark matter or for dark energy.

could potentially provide a valuable key to unlock cosmological mysteries in the future.

In his seminal paper, Schutz [203] outlined a method that allowed for association of a siren with its host galaxy through statistical methods. In this method, by considering each galaxy in the siren's sky localization error as a potential host, one can calculate H_0. Then by combining these estimates using statistical methods, one can extract a final measurement of H_0. This method was used with the binary neutron star merger GW170817 (which had an optical counterpart but was ignored to imitate a dark siren) to give an estimate of H_0 [108]. Since then, several works have made use of this concept to acquire statistical estimates of H_0 using actual dark sirens [208, 107].

Recently, an alternative method for inferring cosmological parameters from dark sirens was proposed [180, 175, 176, 43]. In these works, rather than associating each siren a host galaxy and computing statistical inferences for H_0 for each host, they make use of the fact that sirens and galaxies are both tracers of the underlying matter distribution. For visualization, in Figure 5.1 one could consider the orange squares to be sirens and the white circles to be galaxies. In this case, one can then make use of the statistical properties of the density field, and consider the cross-correlation of the galaxies with dark sirens. In the next chapter, I will present my current work on a new approach to this method which is built from the most basic assumptions. By using Poisson statistics to model the sampling of galaxies and sirens from the matter distribution, we present a novel method to infer H_0 without the use of any inverse covariance matrices.

Chapter 6

A Novel Method for Cosmological Parameter Inference Using Dark Sirens

6.1 Introduction

The first detection of gravitational waves (GWs) from a binary black hole merger by the LIGO Scientific and Virgo Collaboration [2] marked the emergence of a new era of multi-messenger astronomy. GWs provide new information previously unavailable from electromagnetic (EM) data, opening up entirely new avenues for astronomy, astrophysics, and cosmology. Since GWs from binary mergers provide an absolute distance measurement to the source via the luminosity distance [203], if the redshift to the source is also known, then one can use the redshift-distance relationship to extract information regarding cosmological parameters. These binary mergers are often called standard sirens [129, 85] in analogy to observations of Type Ia supernovae (SNe) [185, 195], which are called standard candles.

Ideally, an electromagnetic counterpart to the GW event is identified in which the host galaxy and hence the redshift is obtained. Therefore, in this case the siren can be used to acquire independent measurements of cosmological parameters. A recent topic of debate in the cosmological community has been determining the true value of the local expansion rate of the Universe, known as the Hubble parameter H_0. In particular, the SH0ES measurement of H_0 from SNe [195] is believed to be in tension with the measurement of H_0 from the Cosmic Microwave Background (CMB) by the Planck Collaboration [22]. Meanwhile,

the GW signal detection from the binary neutron star (BNS) merger GW170817 with an electromagnetic counterpart GRB 170817A allowed for identification of the unique host galaxy NGC 4993, which yielded the first standard siren measurement for H_0 with a value of $H_0 = 70^{+12.0}_{-8.0}$ km s^{-1} Mpc^{-1} [3]. Although this measurement is completely independent from CMB and SNe measurements and sits right in between SH0ES and Planck measurements, at this time it is not competitive with them because of its large error bar. However, it is expected that ~ 50 detections of BNS mergers with electromagnetic counterparts will provide a 2% measurement of H_0 [76, 102], which can play a significant role in resolving the ongoing tension.

Despite the promising avenues for cosmology with standard sirens, majority of these events are expected to either be missing an electromagnetic counterpart or have low chances of one being detected – making it difficult to obtain the redshift distance to the source. These standard sirens without electromagnetic counterparts are sometimes called dark sirens in literature, which we shall adopt for this work. One prominent method to perform the analysis for dark sirens is to identify the host galaxy via the "statistical method" [203]. In this method, the bright galaxies in the GW localization region are potential hosts to the merger. By assuming that each galaxy is the host for the GW event, one can acquire statistical estimates of H_0, which when statistically combined gives a final H_0 best estimate. This statistical method is expected to be much more useful for BBH mergers since they are not expected to have electromagnetic counterparts although they are detected at higher rates. This method was recently utilized with GW170817[1] to acquire an estimate for H_0 consistent with the electromagnetic counterpart measurement, although less precise [108]. The principle of the statistical method was also used for the binary black hole (BBH) merger GW170814 to acquire the first estimate for H_0 from a BBH using a redshift catalog from the Dark Energy Survey (DES), albeit with very large error bars [208]. Applying a variation of this method and correlating GW data from the GWTC-2 catalog [11] and the GLADE galaxy catalog [86] Ref. [107] has been able to get the tightest estimate for H_0 using only dark sirens to date. With the vast amount of incoming data from LIGO and Virgo, there are expected to be a large number of BBH events since the detection rates for BBH mergers are generally higher than for BNS mergers due to the higher intrinsic luminosity of BBHs. Consequently, they are also expected to have a larger observable volume. However, Schutz's statistical method is limited by the number of potential hosts in the siren's sky localization region. For sirens at higher redshifts, the number of potential hosts are expected to be too large for this method, and not all potential hosts may be detected.

[1] Although an electromagnetic counterpart for GW170817 has been detected, in this analysis the authors did not take into account the identification of the host galaxy.

Recently, an alternate method to extract information about cosmological parameters from dark sirens was proposed [180, 175, 176, 43]. In this method, rather than determining the potential host galaxies statistically, it takes advantage of the fact that both galaxies and sirens are tracers of the underlying matter distribution. Hence one can make use of the correlation function to statistically infer cosmological parameters. In this work, we present a different method that also makes use of the dark matter distribution. However in our method, we relieve several assumptions in the derivation of the posterior that the authors in Ref. [176] considered for the sirens. In particular, we do not assume that the power spectrum for the cross-correlations of galaxies and dark sirens is Gaussian. We start by assuming that the galaxies and sirens are sampled from a random Poisson process, and show that one can construct a data vector comprised of biases rather than overdensities. We find that there is no need to calculate the inverse of the covariance matrix that usually appears in Gaussian posteriors for cross-correlations, and instead one can work with just the covariance matrix of the matter density field instead. This can have several computational advantages, since the matrix inversion is an expensive part of the usual posterior calculation. In section 6.2 we will provide the derivations for the likelihood using Poisson sampling and present the posterior for cosmological parameter inference. In section 6.3 we will discuss the generation of mock catalogs for this work. In section 6.4 we will present the main results of our simulations and show that this can be a new tool for cosmological parameter inference. Finally, we will make our concluding remarks in section 6.5.

6.2 Methods

6.2.1 Modelling via Poisson Statistics

In this subsection we will derive the relevant likelihood for our purposes. A discrete random variable X is said to have a Poisson distribution if its probability density function (pdf) p is given by

$$p(X = k) = e^{-\lambda}\frac{\lambda^k}{k!}, \tag{6.1}$$

where k is the number of occurrences and $\lambda > 0$ is a positive parameter, usually related to the rate of a Poisson process. Now to model galaxies and sirens with Poisson sampling of nonlinear functions of the matter density field δ, we start by gridding up the comoving space volume with cells of volume ΔV. Then at a comoving position $\boldsymbol{r}$, we consider the

expected number of a species x in a volume of ΔV, given by

$$\langle n_x(\boldsymbol{r})\rangle \Delta V = g_x[1+\delta(\boldsymbol{r}), r]\Delta V, \tag{6.2}$$

where $n_x(\boldsymbol{r})$ represents the number density of species x at position $\boldsymbol{r}$ and g_x is a general non-linear function of the matter density function δ. Since a random variable X following a Poisson distribution has the property $\lambda = E(X)$, the probability of obtaining k_x number of events of species x at position $\boldsymbol{r}$ given a matter distribution δ with cosmological parameters Θ_c is

$$p(k_x(\boldsymbol{r})|\delta, \Theta_c) = e^{-\langle n_x(\boldsymbol{r})\rangle \Delta V} \frac{[\langle n_x(\boldsymbol{r})\rangle \Delta V]^{k_x(\boldsymbol{r})}}{k_x(\boldsymbol{r})!}. \tag{6.3}$$

Thus the joint probability of having $k_g(\boldsymbol{r})$ galaxies at position $\boldsymbol{r}$ and $k_{GW}(\boldsymbol{R})$ sirens at position $\boldsymbol{R}$ assuming the set of cosmological parameters Θ_c is given by[2]

$$\begin{aligned} p(k_g(\boldsymbol{r}), k_{GW}(\boldsymbol{R})|\delta, \Theta_c) &= p(k_g(\boldsymbol{r})|\delta, \Theta_c) p(k_{GW}(\boldsymbol{R})|\delta, \Theta_c) \\ &= e^{-\langle n_g(\boldsymbol{r})\rangle \Delta V} \frac{[\langle n_g(\boldsymbol{r})\rangle \Delta V]^{k_g(\boldsymbol{r})}}{k_g(\boldsymbol{r})!} e^{-\langle n_{GW}(\boldsymbol{r})\rangle \Delta V} \frac{[\langle n_{GW}(\boldsymbol{r})\rangle \Delta V]^{k_{GW}(\boldsymbol{r})}}{k_{GW}(\boldsymbol{r})!}, \end{aligned} \tag{6.4}$$

where the subscript g corresponds to the galaxies and the subscript GW corresponds to the sirens. We consider ΔV is sufficiently small such that the chances of having two of the same species (either both galaxies or both sirens) in one cell are very slim. Hence we only take the leading order terms $k_x = 0, 1$. In the following, we grid up the total volume with cells of volume ΔV and label the cells with $m = 1, \ldots, N_{cells}$. Then the probability of finding a total of N_g galaxies and N_{GW} sirens located at locations $\{\boldsymbol{r}^i\}$ and $\{\boldsymbol{R}^a\}$ is given by

$$\begin{aligned} p(\{\boldsymbol{r}^i\}, \{\boldsymbol{R}^a\}|\delta, \Theta_c) &= \prod_{m=1}^{N_{cells}} p(k_g(\boldsymbol{r}^m), k_{GW}(\boldsymbol{R}^m)|\delta, \Theta_c) \\ &= \prod_{i=1}^{N_{cells}} p(k_g(\boldsymbol{r}^i)|\delta, \Theta_c) \prod_{a=1}^{N_{cells}} p(k_{GW}(\boldsymbol{R}^a)|\delta, \Theta_c). \end{aligned} \tag{6.5}$$

[2]Note that the sirens are not taken as a subsample of galaxies but sampled separately from δ.

Introducing the notation $\langle N_g(\delta)\rangle$ to represent the expected total number of galaxies and $\langle N_{GW}(\delta)\rangle$ as the expected total number of sirens, we can expand this as

$$p(\{\boldsymbol{r}^i\},\{\boldsymbol{R}^a\}|\delta,\Theta_c) = \exp\left[-\langle N_g(\delta)\rangle - \langle N_{GW}(\delta)\rangle\right] \times \left[\prod_{i=1}^{N_g} g_g[1+\delta(\boldsymbol{r}^i), r^i]\Delta V\right]\left[\prod_{a=1}^{N_{GW}} g_{GW}[1+\delta(\boldsymbol{R}^a), R^a]\Delta V\right]. \quad (6.6)$$

This term can be marginalized over all possible realizations of matter densities δ that would be produced by the cosmology with the set of parameters Θ_c so that

$$p(\{\boldsymbol{r}^i\},\{\boldsymbol{R}^a\}|\Theta_c) \approx \int D\delta\; p(\{\boldsymbol{r}^i\},\{\boldsymbol{R}^a\}|\{\delta\},\Theta_c)p(\{\delta\}|\Theta_c), \quad (6.7)$$

where $p(\{\delta\}|\Theta_c)$ is the probability functional for δ given the cosmology. Here we have introduced the notation

$$\int D\delta = \int \prod_{i=1}^{N_{cells}} d\delta^i, \quad (6.8)$$

where $\delta^i = \delta(\boldsymbol{r}^m)$ for brevity. To simplify further, we can expand the nonlinear functions g_x for each species x by making an expansion as

$$\langle n_x(\boldsymbol{r})\rangle\Delta V \approx g_x(1,r)\Delta V\left[1 + b_x(r)\delta(\boldsymbol{r}) + \mathcal{O}(\delta^2)\right], \quad (6.9)$$

which to leading order can also be approximated as an exponential (see (A.1) for more details). To first order, this also allows us to write (see (A.2) for more details):

$$\langle N_x(\delta)\rangle \approx \bar{N}_x + \mathcal{O}(\delta^2). \quad (6.10)$$

Disregarding any higher order effects[3] from δ, the independent probabilities for each species x has terms that can be separated as:

$$e^{-\langle N_x(\delta)\rangle}\prod_{i=1}^{N_x} g_x[1+\delta(\boldsymbol{r}^i), r^i]\Delta V = e^{-\bar{N}_x}\left(\prod_{i=1}^{N_x}\bar{n}_x(r^i)\Delta V\right)e^{\sum_{i=1}^{N_x} b_x(r^i)\delta(\boldsymbol{r}^i)}. \quad (6.11)$$

Then excluding the pre-factor that is independent of δ for now, the integration over δ in the conditional probability can be written as

$$p(\{\boldsymbol{r}^i\},\{\boldsymbol{R}^a\}|\Theta_c) \propto \int D\delta\;\; \exp\left(\sum_{i=1}^{N_g} b_g(r^i)\delta(\boldsymbol{r}^i) + \sum_{a=1}^{N_{GW}} b_{GW}(R^a)\delta(\boldsymbol{R}^a)\right)p(\{\delta\}|\Theta_c). \quad (6.12)$$

[3]This means that we are working in the linear bias regime, although these expressions can be left general for nonlinear bias terms.

Defining the column vector

$$\boldsymbol{\delta} = (\delta(r^1), \ldots, \delta(r^{N_{cells}}), \delta(R^1), \ldots, \delta(R^{N_{cells}})), \tag{6.13}$$

to be the matter density vector with its components the matter densities at each cell and the bias vector

$$\boldsymbol{b} = (b_g(r^1), \ldots, b_g(r^{N_{cells}}), b_{GW}(R^1), \ldots, b_{GW}(R^{N_{cells}})), \tag{6.14}$$

so that the biases at cells without any events are zero, the exponential terms in the expression (6.12) can be simplified and written into a compact matrix multiplication as

$$p(\{\boldsymbol{r}^i\}, \{\boldsymbol{R}^a\}|\Theta_c) \propto \int \prod_{m=1}^{N_{cells}} d\delta^m \; e^{\boldsymbol{b}^T\boldsymbol{\delta}} p(\{\delta\}|\Theta_c). \tag{6.15}$$

Then assuming that δ is a Gaussian statistical field, the probability functional $p(\{\delta\}|\Theta_c)$ is given by

$$p(\{\delta\}|\Theta_c) = \sqrt{\frac{1}{(2\pi)^{N_{cells}}|\mathrm{C}^{-1}|}} e^{-\frac{1}{2}\boldsymbol{\delta}^T\mathrm{C}^{-1}\boldsymbol{\delta}}, \tag{6.16}$$

where $|\mathrm{C}^{-1}|$ is the determinant of the inverse covariance matrix. The covariance matrix C is defined in the usual way as

$$\mathrm{C}_{ij} = \langle\delta(\boldsymbol{r}^i)\delta(\boldsymbol{r}^j)\rangle = \xi^{(2)}(|\boldsymbol{r}^i - \boldsymbol{r}^j|), \tag{6.17}$$

where $\xi^{(2)}(r)$ is the expected 2-point correlation function for δ. Applying an integration identity for N-dimensional Gaussian integrals with a linear term, we can evaluate the integral on δ as:

$$p(\{\boldsymbol{r}^i\}, \{\boldsymbol{R}^a\}|\Theta_c) \propto \int \prod_{m=1}^{N_{cells}} d\delta^i \sqrt{\frac{1}{(2\pi)^{N_{cells}}|\mathrm{C}^{-1}|}} e^{-\frac{1}{2}\boldsymbol{\delta}^T\mathrm{C}^{-1}\boldsymbol{\delta}+\boldsymbol{b}^T\boldsymbol{\delta}} = e^{\frac{1}{2}\boldsymbol{b}^T\mathrm{C}\boldsymbol{b}}. \tag{6.18}$$

Therefore, the desired conditional probability can be estimated as

$$p(\{\boldsymbol{r}^i\},\{\boldsymbol{R}^a\}|\Theta_c) \approx \left(e^{-\bar{N}_g}\prod_{i=1}^{N_g}\bar{n}_g(r^i)\Delta V\right)\left(e^{-\bar{N}_{GW}}\prod_{a=1}^{N_{GW}}\bar{n}_{GW}(R^a)\Delta V\right)$$
$$\times\exp\left[\frac{1}{2}\sum_{i,j=1}^{N_g}b_g(r^i)\mathrm{C}_{ij}b_g(r^j)\right]$$
$$\times\exp\left[\frac{1}{2}\sum_{a,b=1}^{N_{GW}}b_{GW}(R^a)\mathrm{C}_{ab}b_{GW}(R^b)\right]$$
$$\times\exp\left[\sum_{i,a=1}^{N_g,N_{GW}}b_g(r^i)\mathrm{C}_{ia}b_{GW}(R^a)\right]. \tag{6.19}$$

As will be shown in the next subsection, the final posterior will depend on this conditional probability. This conditional probability does not require inverting the covariance matrix which is usually the case. Furthermore, this likelihood is still very generic and includes auto-correlation functions as well but in the following section we will make several assumptions in order to only consider the impact of the cross-correlation between the galaxies and sirens for statistical inference.

6.2.2 General Posterior for Parameter Inference

The final posterior we wish to compute is given by Bayes' theorem (ignoring the evidence factor $p(\{x^a_{GW}\},\{x^i_g\})$, typical for parameter inference) :

$$p(\Theta_c|\{x^a_{GW}\},\{x^i_g\}) = p(\Theta_c)p(\{x^a_{GW}\},\{x^i_g\}|\Theta_c), \tag{6.20}$$

where x^a_{GW} is the data for the GW sources $a = 1,\ldots,N_{GW}$ and x^i_g is the data for galaxies $i = 1,\ldots,N_g$. Here, $p(\Theta_c)$ is the prior for the set of cosmological parameters Θ_c that we will statistically infer. Let us assume that we have processed the galaxy data into a readable form $x^i_g = (z^i,\Omega^i_g)$, where z^i is the redshift and Ω^i_g angular position for a galaxy with label i.In this case, we can write the posterior as

$$p(\Theta_c|\{x^a_{GW}\},\{z^i,\Omega^i_g\}) = p(\Theta_c)p(\{x_{GW}\},\{z^i,\Omega^i_g\}|\Theta_c). \tag{6.21}$$

For now for simplicity in our model we assume that data format for x^a_{GW} is simply given as (D^a_L, Ω^a_{GW}) [4] then we can compute the likelihood above as

$$\begin{aligned} p(\{x^a_{GW}\},\{x_g\}|\Theta_c) &= p(\{D^a_L,\Omega^a_{GW}\},\{z^i,\Omega^i_g\}|\Theta_c) \\ &= \int D\boldsymbol{R}^a\ D\boldsymbol{r}^i\ p(\{D^a_L,\Omega^a_{GW}\},\{\boldsymbol{R}^a\},\{z^i,\Omega^i_g\},\{\boldsymbol{r}^i\}|\Theta_c) \\ &= \int D\boldsymbol{R}^a\ D\boldsymbol{r}^i\ p(\{D^a_L,\Omega^a_{GW}\},\{z^i,\Omega^i_g\}|\{\boldsymbol{R}^a\},\{\boldsymbol{r}^i\},\Theta_c)\ p(\{\boldsymbol{R}^a\},\{\boldsymbol{r}^i\}|\Theta_c) \\ &= \int D\boldsymbol{R}^a\ D\boldsymbol{r}^i p(\{D^a_L,\Omega^a_{GW}\}|\{\boldsymbol{R}^a\},\Theta_c)p(\{z^i,\Omega^i_g\}|\{\boldsymbol{r}^i\},\Theta_c)\ p(\{\boldsymbol{R}^a\},\{\boldsymbol{r}^i\}|\Theta_c), \end{aligned} \tag{6.22}$$

where to get to the last line we used the fact that obtaining the luminosity distance and angular position of the sirens experimentally is independent of the galaxy positions, and vice versa. Note that we introduced the notation as before for products of integrals:

$$\int D\boldsymbol{r}^i = \int \prod_{i=1}^{N_g} d\boldsymbol{r}^i, \quad \int D\boldsymbol{R}^a = \int \prod_{a=1}^{N_{GW}} d\boldsymbol{R}^a, \tag{6.23}$$

and integration should be done over the 3D comoving volume for both samples. Furthermore, since we assumed that the auto-correlation between the sirens is negligible as they are rare and far from each other, we can write

$$p(\{D^a_L,\Omega^a_{GW}\}|\{\boldsymbol{R}^a\},\Theta_c)p(\{\boldsymbol{R}^a\}|\{\boldsymbol{r}^i\},\Theta_c) = \prod_{a=1}^{N_{GW}} p(D^a_L,\Omega^a_{GW}|\boldsymbol{R}^a,\Theta_c)p(\boldsymbol{R}^a|\{\boldsymbol{r}^i\},\Theta_c) \tag{6.24}$$

where we substituted $p(\{\boldsymbol{R}^a\}|\{\boldsymbol{r}^i\},\Theta_c)p(\{\boldsymbol{r}^i\}|\Theta_c)$ for $p(\{\boldsymbol{R}^a\},\{\boldsymbol{r}^i\}|\Theta_c)$. This finally leads to

$$\begin{aligned} p(\{x^a_{GW}\},\{x_g\}|\Theta_c) = \int D\boldsymbol{r}^i\ p(\{z^i,\Omega^i_g\}|\{\boldsymbol{r}^i\},\Theta_c)\ p(\{\boldsymbol{r}^i\}|\Theta_c) \\ \times \prod_{a=1}^{N_{GW}} \int d\boldsymbol{R}^a\ p(D^a_L,\Omega^a_{GW}|\boldsymbol{R}^a,\Theta_c)\ p(\boldsymbol{R}^a|\{\boldsymbol{r}^i\},\Theta_c). \end{aligned} \tag{6.25}$$

[4] When working with the actual data format from gravitational wave experiments such as LIGO and Virgo, one needs to incorporate an additional step to turn the data x_{GW} into D^a_L, Ω^a_{GW} by including an additional factor $P(x^a_{GW}|D^a_L,\Omega^a_{GW})$ in the likelihood as in Ref. [108].

We can now identify different terms in this result one-by-one by comparing with our estimator from last section while implementing some corrections to take into account anticipated experimental errors. Expanding out the factor dependent on redshift we get

$$\begin{aligned} p(\{z^i, \Omega_g^i\}|\{\boldsymbol{r}^i\}, \Theta_c) p(\{\boldsymbol{r}^i\}|\Theta_c) &= p(\{z^i, \Omega_g^i\}, \{\boldsymbol{r}^i\}|\Theta_c) \\ &= p(\{\boldsymbol{r}^i|\{z^i, \Omega_g^i\}, \Theta_c) p(\{z^i, \Omega_g^i\}|\Theta_c). \end{aligned} \tag{6.26}$$

In what follows we ignore the error in the galaxies' sky localization as well as redshift distortions by taking

$$p(\{\boldsymbol{r}^i\}|\{z^i, \Omega_g^i\}, \Theta_c) = \prod_{i=1}^{N_g} \delta^{(3)}(\boldsymbol{r}^i - \hat{\boldsymbol{r}}(z^i, \Omega_g^i, \Theta_c)). \tag{6.27}$$

In other words we assume that given the data $\{z^i, \Omega_g^i\}$ and cosmological parameters, one can directly calculate the position of galaxies in comoving space using the redshift-distance relation. Then

$$p(\{x_{GW}^a\}, \{x_g\}|\Theta_c) = p(\{z^i, \Omega_g^i\}|\Theta_c) \prod_{a=1}^{N_{GW}} \int d\boldsymbol{R}^a \; p(D_L^a, \Omega_{GW}^a|\boldsymbol{R}^a, \Theta_c) \; p(\boldsymbol{R}^a|\hat{\boldsymbol{r}}(z^i, \Omega_g^i, \Theta_c), \Theta_c). \tag{6.28}$$

Note that if galaxies were independent then it would identically result to

$$p(\{z^i, \Omega_g^i\}|\Theta_c) = \prod_{i=1}^{N_g} p(z^i, \Omega_g^i|\Theta_c), \tag{6.29}$$

and since the likelihood is marginalised over all realizations of δ, this factor would be independent of the positions $\boldsymbol{r}$ and could be absorbed in the normalization and prior. However, as we saw in last section in Eq.(6.19), there were additional contributions to the likelihood from the auto-correlation function for galaxies that can in principle be used to optimise the estimator. Inspecting the likelihood in Eq.(6.19) and comparing with Bayes' theorem,

$$p(\{\boldsymbol{r}^i\}, \{\boldsymbol{R}^a\}|\Theta_c) = p(\{\boldsymbol{R}^a\}|\{\boldsymbol{r}^i\}, \Theta_c) \; p(\{\boldsymbol{r}^i\}|\Theta_c). \tag{6.30}$$

the second factor $p(\{\boldsymbol{r}^i\}|\Theta_c)$ on the right hand side is a factor that we identify as the auto-correlation for the galaxies corresponding to $\exp\left[\frac{1}{2}\sum_{i,j=1}^{N_g} b_g(r^i) \mathrm{C}_{ab} b_g(r^j)\right]$ in Eq.(6.19). As we just saw in Eq.(6.28) this term leads to the auto-correlation term in the redshift

space as $p(\{z^i, \Omega_g^i\}|\Theta_c)$. However, our goal here is not to use the information of the auto-correlation of the galaxies, which can be done regardless of sirens, instead we like to extract cosmological constraints only based on the cross-correlations of the galaxies with sirens. Therefore, we will proceed assuming we can absorb this term as a pre-factor and will correct for it (to some extent) through our numerical de-biasing scheme discussed in the next section. Thus the posterior using only the cross-correlation can be written as

$$p(\Theta_c|\{x^a_{GW}\},\{x^i_g\}) \propto p(\Theta_c) \prod_{a=1}^{N_{GW}} \int d\boldsymbol{R}^a \ \exp\left[\sum_{i=1}^{N_g} b_g(r^i) \mathrm{C}_{ia} b_{GW}(R^a)\right] p(D^a_L, \Omega^a_{GW}|\boldsymbol{R}^a, \Theta_c). \tag{6.31}$$

To account for uncertainty in the luminosity distance and sky localization of the sirens, we model the errors for these using a Gaussian for simplicity[5]:

$$p(D^a_L, \Omega^a_{GW}|\boldsymbol{R}^a, \Theta_c) \propto \exp\left[-\frac{(D^a_L - \hat{D}_L(\boldsymbol{R}^a, \Theta_c))^2}{2(\sigma^a_{D_L})^2}\right] \times \exp\left[-\frac{(\Omega^a_{GW} - \hat{\Omega}_{GW}(\boldsymbol{R}^a, \Theta_c))^2}{2(\sigma_{\Omega_{GW}})^2}\right], \tag{6.32}$$

where $\hat{D}_L(\boldsymbol{R}^a, \Theta_c)$ is the luminosity distance calculated using $\boldsymbol{R}^a$ and Θ_c as inputs:

$$\hat{D}_L(\boldsymbol{R}^a, \Theta_c) = (1 + z(\boldsymbol{R}^a, \Theta_c))|\boldsymbol{R}^a|, \tag{6.33}$$

and $\hat{\Omega}_{GW}(\boldsymbol{R}^a, \Theta_c)$ just extracts the angular position in the sky for the siren. For the standard deviations of the two Gaussians, we have that $\sigma^a_{D_L}$ is the 1-sigma error in luminosity distance and $\sigma^a_{\Omega_{GW}}$ is the 1-sigma error in sky localization. The error in luminosity distance is taken to be a fractional error:

$$\sigma^a_{D_L} = \frac{1}{2}\Delta D^a_L, \tag{6.34}$$

where ΔD_L is the 68% error for the luminosity distance for each source. In addition, to be consistent with the notation in Ref. [176], we use the following relationship for the sky localization error given that $\Delta\Omega_{GW}$ is the 68% interval:

$$\sigma_{\Omega_{GW}} = \left[-\frac{\Delta\Omega_{GW}}{2\pi \ln(0.32)}\right]^{1/2}. \tag{6.35}$$

[5]We comment that this is a rather simplistic modelling of the error for sirens. A realistic modelling of error for the sirens would also make use of other information than just the spatial positions of the sirens.

6.3 Catalogs

For this work, we used a modified mock galaxy catalog initially generated using the `VELMASS` simulation suite [193]. The `VELMASS` suite is made up by 10 cosmological simulations, in which 9 of these use the same initial phases while probing variations of cosmological parameters, and 1 of them uses the same parameters as the central simulation while varying different initial phases. The central simulation assumes Planck 2015 [18] values for cosmological parameters: $\Omega_m = 0.315$, $\Omega_b = 0.049$, $H_0 = 68$ km s^{-1} Mpc^{-1}, $\sigma_8 = 0.81$, $n_s = 0.97$, and $Y_{\rm He} = 0.248$. While the `VELMASS` suite is designed to test the robustness of analysis tools to different variations in parameter and initial phase space, we will just use the central simulation results. The simulation volume is 2000 h^{-1} Mpc with 2048^3 dark matter particles, which was initalized at a redshift of $z = 50$ and evolved to present time using `GADGET2` [209]. Then the `ROCKSTAR` halo finder algorithm [41] was used to extract the halos from the simulation, providing a halo catalogue. For full details of the simulation, we refer readers to Ref [193].

For our purposes, we use a subsample of this full simulation, by limiting the volume to 500 h^{-1} Mpc. This leaves a total of 2403465 haloes in the catalog. We also make a mass cut for $M > 5 \times 10^{13} M_\odot$, where $M_\odot$ is the solar mass, so that we only consider the more massive galaxies. This reduces the number of galaxies in our sample to 80622. We then cut this sample into two halves randomly, leaving 40311 galaxies in each half, and selected one of them to be the actual galaxy catalog we work with. For this work, we have not considered any error in galaxy positions, hence the simulated positions will be the true positions for galaxies.

The GW samples in this work are generated using the mock galaxy catalog described above. After cutting the full catalog as described above, the other half was used as the potential hosts for the mergers. After randomly picking 300 of the galaxies to be the hosts, the remainder of the potential hosts were thrown out and not used in the cross-correlation process, completely hiding the hosts of the mergers. At this point the GW samples are still "error-free" samples since they are taken at the exact positions of the host galaxies.

For each of the catalogs, the comoving coordinates were converted into the necessary observed quantities using a true value of $h_{true} = 0.68$ as described in Appendix A.2. In other words, the transformations into observable quantities were:

$$\boldsymbol{r}^i = (x^i, y^i, z^i) \to (z^i, \Omega_g^i), \tag{6.36}$$

$$\boldsymbol{R}^a = (X^a, y^a, z^a) \to (D_L^a, \Omega_{GW}^a), \tag{6.37}$$

for galaxies and sirens respectively. To convert these quantities, while one can use the exact integral relations to acquire the redshift z, as we are limiting the detection volume to the

low redshift regime ($z \lesssim 0.2$), we will use the power law expansions discussed in Appendix A.2. For higher redshift values, one must use the full integral for the redshift-distance relation assuming some fiducial cosmology.

Next, to generate the mocked positional error in the observational measurements, the sirens were sampled randomly from a Gaussian probability function with the mean as the true position of the sirens and varying standard deviations for the luminosity distance errors and sky localization errors. In line with Ref. [176], the 68% sky localization errors were taken to be $\Delta\Omega_{GW} = 10$, 25, and 100 square degrees. The error in luminosity distances were taken so that the 68% fractional errors for each source were $\Delta D_L^a/D_L^a = 0.01$, 0.05, and 0.1. Hence this new catalog has sources that are offset from the true positions to imitate experimental uncertainty and error. For this work we did not consider any positional errors on the galaxy positions due to redshift space distortions or peculiar velocities.

Finally, to assert experimental thresholds from "realistic" galaxy and GW surveys where a more spherical volume is observed rather than a box, we imposed a cutoff in the redshift for galaxies and the luminosity distance for sirens[6]. In this work we choose rather arbitrary cutoff values of $D_L^c = 900$ Mpc for the sirens and $z^c = 0.2$ for the galaxies. Since we have not considered any line-of-sight errors for the galaxies, the number of galaxies inside this volume of observable redshifts stays fixed with $N_g = 29218$. For sirens however, since we are considering an error in luminosity distance prior to the luminosity distance cutoff, the number of sirens inside the volume of observable luminosity distances will change. Hence for each result for the posterior in the section 6.4, we will list the number of sirens inside this volume. We will also consider the effects of changing the number of sirens N_{GW} on the posterior in section 6.4.

We can compute the linear bias for the galaxies and GWs by computing an estimator for the 2-point correlation function. By using a modified version of the two-point correlation function from `astroML` [214], we obtain $\xi_{gg}^{(2)}(r)$ and $\xi_{GWGW}^{(2)}(r)$ so that the constant biases can be approximated as

$$b_g^2 = \left\langle \frac{\xi_{gg}^{(2)}(r)}{\xi^{(2)}(r)} \right\rangle, \quad b_{GW}^2 = \left\langle \frac{\xi_{GWGW}^{(2)}(r)}{\xi^{(2)}(r)} \right\rangle, \tag{6.38}$$

where $\xi^{(2)}(r)$ is the two-point correlation function for matter from `CAMB` [152]. We found that $b_g = b_{GW} = 2$ was a good fit to the sample bias, which makes sense since the galaxies and sirens are produced from the same halo catalog. Hence in what follows, the biases b_g

[6]Note that this a simplification. A realistic dataset will also depend on other criteria such as signal to noise ratios that will depend on direction and will not in general be isotropic.

$\Delta D_L/D_L$	$\Delta\Omega_{GW}$ (sq. deg)	N_{GW}
0.01	10	180
	25	179
	100	176
0.05	10	182
	25	178
	100	172
0.10	10	181
	25	181
	100	173

Table 6.1: Number of GW sirens N_{GW} given after accounting for experimental error and D_L cutoff for varying values of error for D_L and sky localization Ω_{GW}. These correspond to the number of sirens in Figures 6.1, 6.2, and 6.3. Note that for simplicity, since we are not considering any uncertainty for galaxies, $N_g = 29218$ remains fixed.

and b_{GW} that show up in the likelihood will be 2 whenever there is a source and 0 when the cell is empty.

6.4 Results

Now that the Bayesian framework has been constructed, we can look to infer cosmological parameters. In this analysis we will limit our set of cosmological parameters Θ_c only to Hubble parameter H_0 and leave the exploration of other parameters for future work[7]. We also will work with h, the dimensionless version of H_0, defined by

$$H_0 = 100\ h\ \text{km/s/Mpc}. \tag{6.39}$$

[7]Our work in the previous section is more general and one could consider multiple parameters to infer.

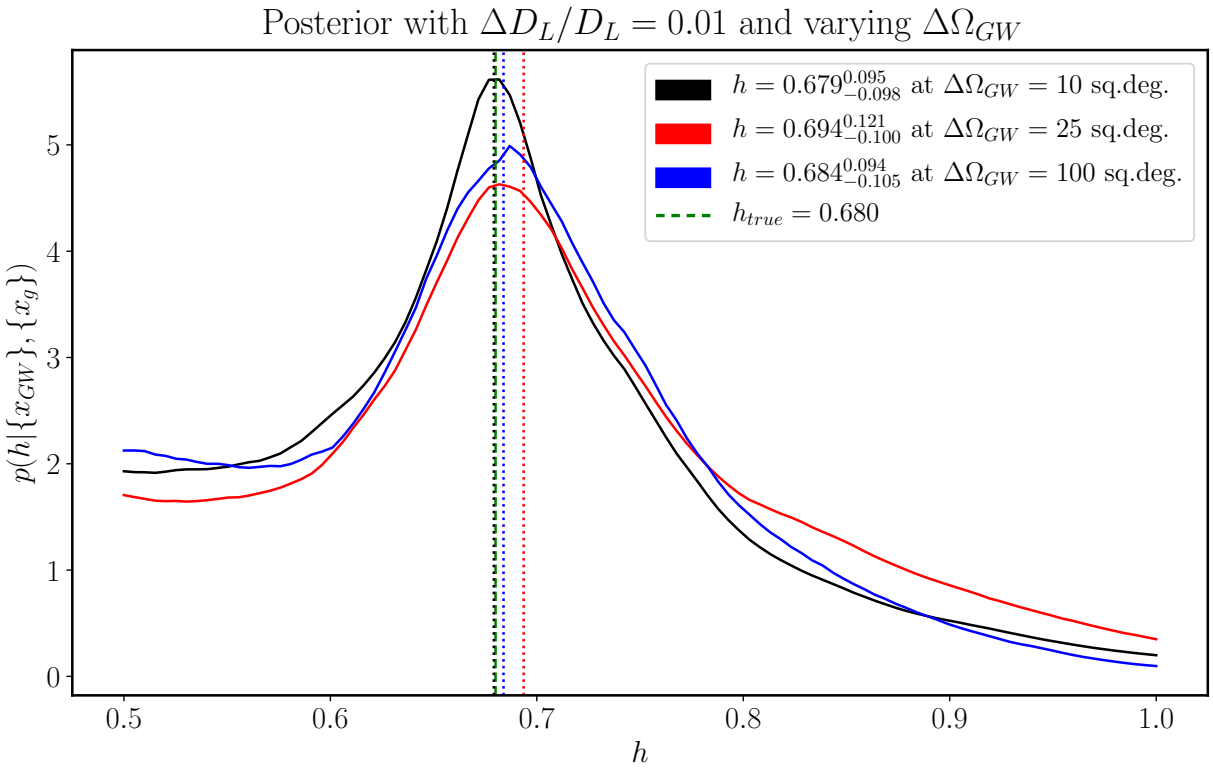

Figure 6.1: Posterior calculation for inferring H_0 given a catalog of sirens and galaxies using our method with a constant luminosity distance error of $\Delta D_L/D_L = 0.01$ for each siren with luminosity D_L. The sky localization errors are varying in this plot, with the black curve for $\Delta\Omega_{GW} = 10$ square degrees, the red curve for $\Delta\Omega_{GW} = 25$ square degrees, and the blue curve for $\Delta\Omega_{GW} = 100$ square degrees. The dotted lines represent the median (50th-percentile) values, which are the reported values in the legend. The uncertainties reported are the 16th and 84th-percentiles corresponding to the 1σ error bars.

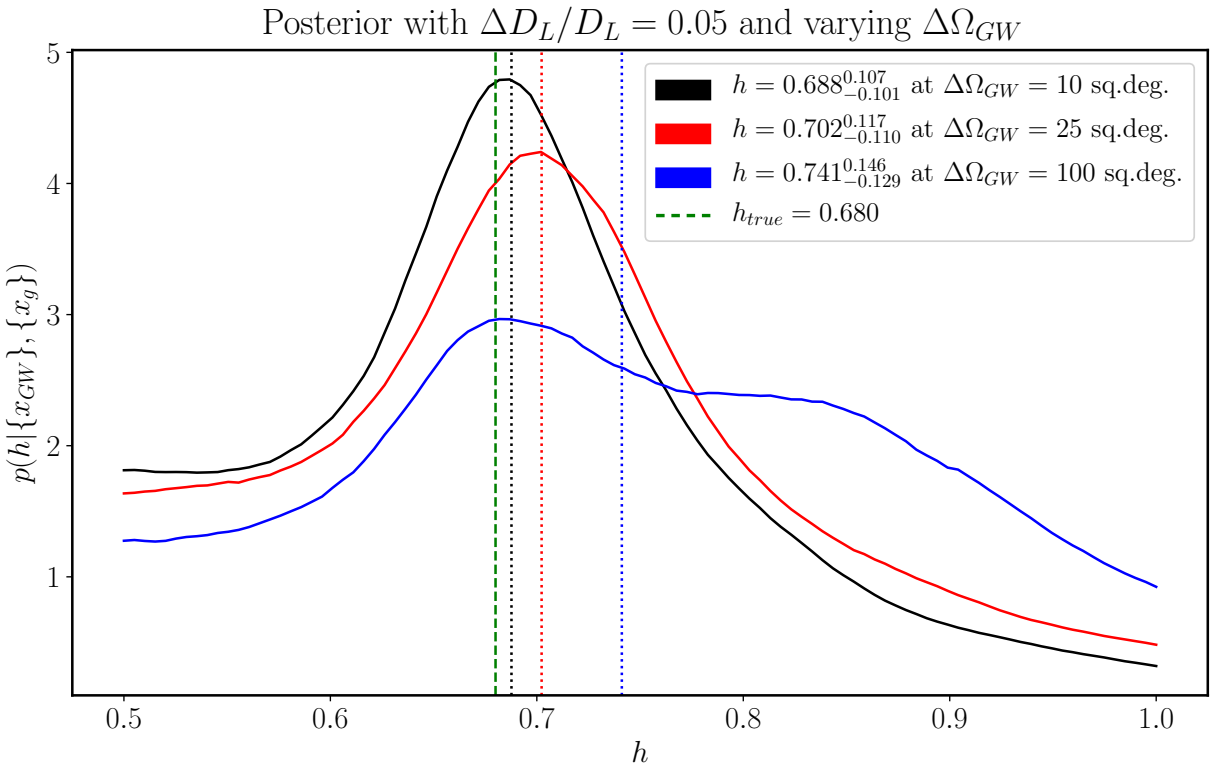

Figure 6.2: Posterior calculation for inferring H_0 given a catalog of sirens and galaxies using our method with a constant luminosity distance error of $\Delta D_L/D_L = 0.05$ for each siren with luminosity D_L. The sky localization errors are varying in this plot, with the black curve for $\Delta\Omega_{GW} = 10$ square degrees, the red curve for $\Delta\Omega_{GW} = 25$ square degrees, and the blue curve for $\Delta\Omega_{GW} = 100$ square degrees. The dotted lines represent the median (50th-percentile) values, which are the reported values in the legend. The uncertainties reported are the 16th and 84th-percentiles corresponding to the 1σ error bars.

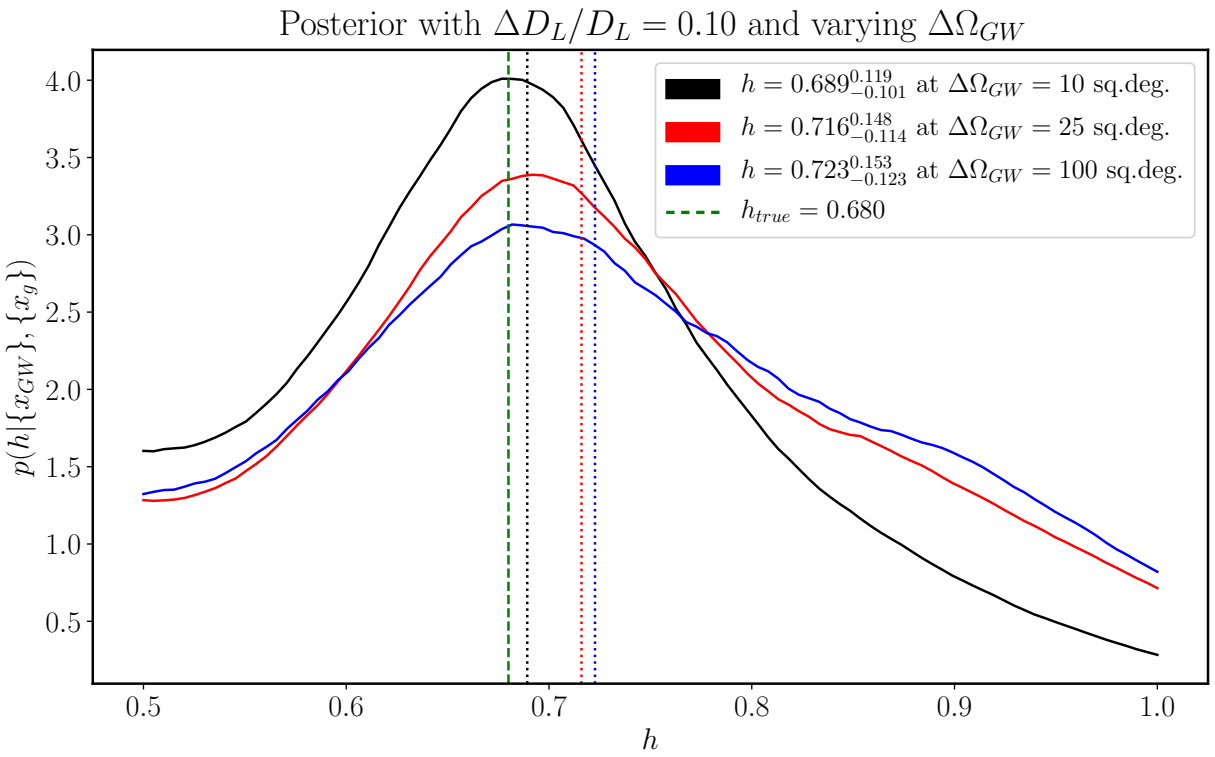

Figure 6.3: Posterior calculation for inferring H_0 given a catalog of sirens and galaxies using our method with a constant luminosity distance error of $\Delta D_L/D_L = 0.1$ for each siren with luminosity D_L. Note that this is the largest fractional luminosity distance error that we consider in this work. The sky localization errors are varying in this plot, with the black curve for $\Delta\Omega_{GW} = 10$ square degrees, the red curve for $\Delta\Omega_{GW} = 25$ square degrees, and the blue curve for $\Delta\Omega_{GW} = 100$ square degrees. The dotted lines represent the median (50th-percentile) values, which are the reported values in the legend. The uncertainties reported are the 16th and 84th-percentiles corresponding to the 1σ error bars.

Therefore, we have effectively set $\Theta_c = \{h\}$. Next, disregarding the auto-correlation terms for both galaxies and sirens, the posterior can be written as

$$p(h|\{x^a_{GW}\},\{x^i_g\}) \propto p(h) \prod_{a=1}^{N_{GW}} \int d\boldsymbol{R}^a \ \exp\left[\sum_{i=1}^{N_g} b_g(r^i) \mathrm{C}_{ia} b_{GW}(R^a)\right] \times \exp\left[-\frac{(D^a_L - \hat{D}_L(\boldsymbol{R}^a,h))^2}{2(\sigma^a_{D_L})^2}\right] \times \exp\left[-\frac{(\Omega^a_{GW} - \hat{\Omega}_{GW}(\boldsymbol{R}^a,h))^2}{2(\sigma_{\Omega_{GW}})^2}\right], \tag{6.40}$$

where $p(h)$ is the prior for h that we take as a flat prior in the range $[0.5, 1.0]$. To obtain the elements of the covariance matrix or 2-point correlation function, we compute the Fourier transform of the power spectrum:

$$\mathrm{C}_{ij} = \xi^{(2)}(|\boldsymbol{r}^i - \boldsymbol{r}^j|) = \frac{1}{2\pi^2}\int_0^\infty dk \ k^2 P(k) j_0(kr), \tag{6.41}$$

where $r = |r^i - r^j|$ and $P(k)$ is the matter power spectrum that we can acquire through `CAMB`[8] [152]. Here $j_0(kr) = \sin(kr)/(kr)$ is the zeroth order spherical Bessel function of the first kind.

Note that in our derivation of the Likelihood for Cross-correlation, there were also pre-factors that did not depend on position of sirens but still depended on h. If constant, such terms could be absorbed into the normalization but since they depend on h, they are essentially introducing additional effects in the prior. Similarly, varying h will also change the boundary of our sample volumes, which can also introduce additional h-dependent h-biases which is independent of the cross-correlation. We examined the impact of these terms more numerically by producing a random sample of galaxies and sirens taken from a three-dimensional uniform distribution. For example one of the features we noticed was that for higher values of h the likelihood for random sample was increasing as a non-linear function.

Therefore we implemented a de-biasing algorithm through calculating the likelihood given "catalogs" comprised of randomly sampled points from a uniform distribution inside the luminosity distance volume. Since for a given random distribution there is always the possibility that the distribution of sampled points can be clustered in a way that drastically influences the likelihood, we took an average over several bias calculations with a

[8] http://camb.info

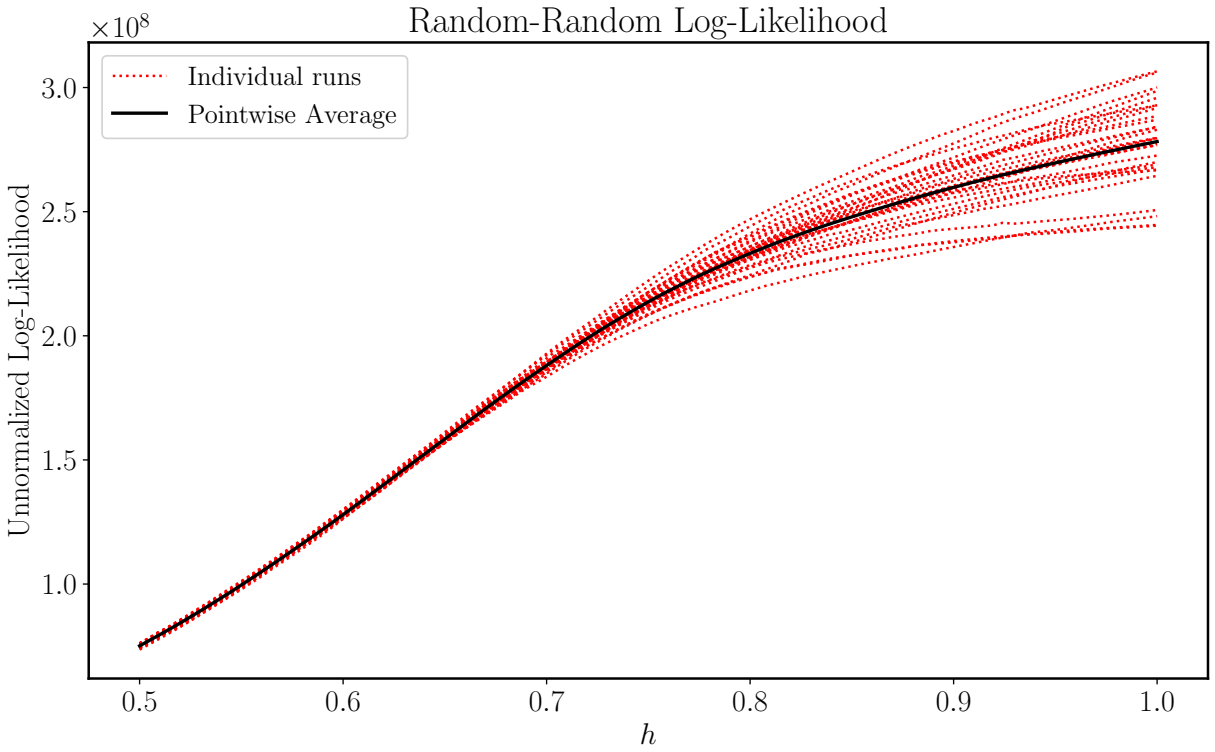

Figure 6.4: Likelihood calculation for inferring H_0 given 30 different randomly sampled catalog of $N_{GW} = 180$ sirens and $N_g = 30000$ galaxies from a uniform distribution in the volume restricted by the luminosity cutoff $D_L^c = 900$ Mpc. The red dotted lines represent the likelihood results for each run while the black solid line represents the pointwise mean taken from the 30 runs.

different random sample each time. Then this function was factored out from the likelihood, numerically removing the underlying bias, so that we obtain an unbiased estimate for h. Ideally, if one could estimate this function analytically, it would not only result in a better modelling of the posterior, but would also reduce the amount of computation to get to the final posterior since we can avoid taking several likelihood calculations. Figure 6.4 shows our bias calculation for 30 different randomly sampled catalogs of $N_{GW} = 180$ sirens and $N_g = 30000$ galaxies from a uniform distribution. By assuming that the leading order effects of the bias can be absorbed as a multiplicative prefactor in the posterior, this bias computation was then subtracted off from the final log-likelihood computation[9].

Figures 6.1, 6.2 and 6.3 present our final posterior calculations for inferring H_0 with the bias numerically removed, for a variety of different error assumptions. The number of sirens in each calculation is provided in Table 6.1. The result displayed in Figure 6.1 indicate that for a small luminosity distance error of $\Delta D_L/D_L = 0.01$, the sky localization error does not affect the posterior shape too much. However, as the luminosity distance error increases (Figures 6.2 and 6.3), the larger sky localization errors result in posterior shapes that were significantly more spread out compared to their more localized counterparts. Although the peaks are sharper for smaller errors as expected, the error bars reported through the 16% and 84% percentiles remain quite large, which we suspect is due to the fact that our likelihood is non-Gaussian and the behaviour of the tails can increase the error[10]. A better understanding of the underlying bias may also give more insight to why the tails do not fall off to zero.

In addition to changing the sky localization error and error in luminosity distance for the sirens, we also see how the number of sirens N_{GW} is important in determining the posterior shape. Figure 6.5 shows the difference in posterior shape for h when changing N_{GW} while leaving the luminosity distance error and sky localization error fixed. As expected, for this catalog the spread of the posterior increased as the number of sirens decreased, a pattern consistent with Ref. [176].

[9]Some of the bias present in our method will be due to a Malmquist bias, where one usually corrects for this by dividing out a volumetric distance prior $p_0(R) \propto R^2$ as in Ref. [108]. However, there are additional bias effects that are not all from volumetric effects. Hence for now we treat all of the bias as a prefactor in the posterior so that it can be removed numerically, and leave more careful considerations of the de-biasing scheme for future work.

[10]Note that in general for non-Gaussian likelihood/posteriors the tails will increase the error but often times in the literature, likelihood is only estimated around the peak as a Gaussian distribution, therefore this error is underestimated [35].

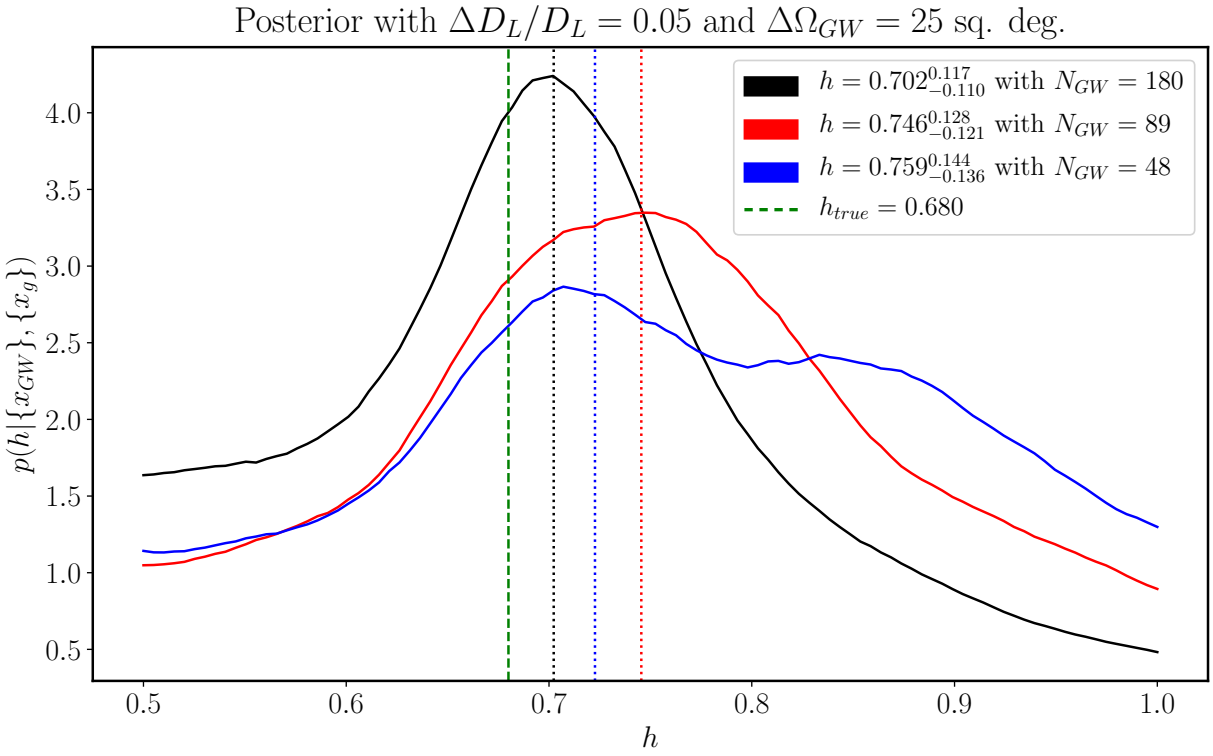

Figure 6.5: Posterior calculation for inferring H_0 given a catalog of sirens and galaxies using our method with a fixed luminosity distance error of $\Delta D_L/D_L = 0.05$ and sky localization error of $\Omega_{GW} = 25$ sq. deg. for each siren with luminosity D_L. The only difference between the curves plotted are the number of sirens in each consider catalog N_{GW}. The dotted lines represent the median (50th-percentile) values, which are the reported values in the legend. The uncertainties reported are the 16th and 84th-percentiles corresponding to the 1σ error bars.

6.5 Conclusion

To summarize, in this work we presented a statistical framework to infer cosmological parameters given a dataset for gravitational wave detections from dark sirens and electromagnetic data from galaxies. By assuming that the sirens and galaxies are Poisson-sampled events of the underlying matter distribution, we showed that one can perform a real-space cross-correlation with the galaxies and sirens to infer h (and hence H_0). Since dark sirens on cosmological scales are rare events we think Possion sampling is theoretically more suited to describe their statistics. From a computational perspective, the advantage of this method is that although one computes element of the covariance method via the Fourier transform of the matter power spectrum, there is no need to invert the covariance matrix due to the set-up of our posterior. Matrix inverses are generally very expensive in computational work, and oftentimes hoard a lot of memory. Since our method lacks the need for an inverse, the only memory hog would be to calculate the distances between each galaxy-siren pair (and potentially galaxy-galaxy and siren-siren pairs if the auto-correlations are considered). While keeping discrete counts for each siren is desired due to the sparse number of sirens in the catalog, one possible avenue to pursue in the future is to smooth the galaxy distribution due to their abundance and work with larger cells of comoving volumes for the galaxies instead.

Furthermore, so far we have tested our method with very simple Gaussian models for error and ignored effects such as redshift space distortion and errors in galaxy surveys. The next stage would be to test this method given sets of mock data with more realistic GW and galaxies error, and finally test if this method could give an unbiased estimate for H_0 given the current available data. In particular, it would be interesting to see how well our statistical model can handle sky localization probability maps such as `BAYESTAR` [207]. For future work, we hope to properly implement astrophysical effects in the posterior similar to Refs. [108, 176, 43] which would improve our statistical inference.

Last but not least, implementing our work in section 6.2 to increase the number of parameters to infer is not difficult. Currently with only H_0 to infer, we are computing the posterior by directly computing the likelihood and the necessary terms on a linearly spaced grid in H_0. As one increases the number of parameters to infer, a more convenient method would be to run Monte Carlo Markov Chain (MCMC) simulations to sample the parameter space. We leave this generalization for future work.

Chapter 7

Conclusion

In this thesis, we investigated recent developments in modern cosmology for very different epochs in our cosmological history. In chapter 2 a gentle introduction to general relativity and cosmology was discussed, in which we saw how the Einstein Field Equations of general relativity can be used to describe the evolution of our Universe when equipped with the appropriate spacetime background. In chapter 3 we looked closer into the very beginnings of Universe, zooming in to the very first seconds that we call the very early Universe. By looking at the current paradigm called inflation, I discussed some of the very many successes of the model as well as the criticisms. This led to a discussion about one of the many alternatives to inflation known as a cosmological bounce. In chapter 4, I presented a specific bouncing scenario generated by Cuscuton gravity, in which I showed the first considerations for observables of the theory through the power spectrum. Shifting gears in chapter 5, we discussed the exciting developments in gravitational wave cosmology and the promising outlook for multi-messenger astronomy in the near future. In chapter 6, we looked a new framework built from the ground-up to infer cosmological parameters by taking advantage of fact that sirens are tracers of the underlying matter distribution in the Universe.

With the recent advancements in observational technology and the massive amounts of incoming data, the future prospects for cosmology look brighter than ever. As measurements become more precise and next-generation observatories and interferometers are developed, we will unlock previously unavailable information regarding our Universe. Whether it be fundamental physics, general relativity, or the recent ongoing Hubble tension, future cosmological observations will have significant implications for our understanding of various different fields of physics and mathematics. Cosmology is truly at the forefront of modern physics, with its apex yet to come.

References

[1] LIGO Scientific collaboration, *LIGO: The Laser interferometer gravitational-wave observatory*, *Rept. Prog. Phys.* **72** (2009) 076901 [0711.3041].

[2] LIGO Scientific, Virgo collaboration, *Observation of Gravitational Waves from a Binary Black Hole Merger*, *Phys. Rev. Lett.* **116** (2016) 061102 [1602.03837].

[3] LIGO Scientific, Virgo, 1M2H, Dark Energy Camera GW-E, DES, DLT40, Las Cumbres Observatory, VINROUGE, MASTER collaboration, *A gravitational-wave standard siren measurement of the Hubble constant*, *Nature* **551** (2017) 85 [1710.05835].

[4] LIGO Scientific, Virgo collaboration, *GW170817: Observation of Gravitational Waves from a Binary Neutron Star Inspiral*, *Phys. Rev. Lett.* **119** (2017) 161101 [1710.05832].

[5] LIGO Scientific, Virgo collaboration, *GWTC-1: A Gravitational-Wave Transient Catalog of Compact Binary Mergers Observed by LIGO and Virgo during the First and Second Observing Runs*, *Phys. Rev. X* **9** (2019) 031040 [1811.12907].

[6] LIGO Scientific, Virgo collaboration, *Searches for Gravitational Waves from Known Pulsars at Two Harmonics in 2015-2017 LIGO Data*, *Astrophys. J.* **879** (2019) 10 [1902.08507].

[7] LIGO Scientific, Virgo collaboration, *Upper Limits on the Stochastic Gravitational-Wave Background from Advanced LIGO's First Observing Run*, *Phys. Rev. Lett.* **118** (2017) 121101 [1612.02029].

[8] LIGO Scientific, Virgo collaboration, *GWTC-2: Compact Binary Coalescences Observed by LIGO and Virgo During the First Half of the Third Observing Run*, *Phys. Rev. X* **11** (2021) 021053 [2010.14527].

[9] LIGO Scientific, VIRGO collaboration, *GWTC-2.1: Deep Extended Catalog of Compact Binary Coalescences Observed by LIGO and Virgo During the First Half of the Third Observing Run*, 2108.01045.

[10] LIGO Scientific, VIRGO, KAGRA collaboration, *Observation of gravitational waves from two neutron star-black hole coalescences*, *Astrophys. J. Lett.* **915** (2021) L5 [2106.15163].

[11] LIGO Scientific, Virgo collaboration, *Population Properties of Compact Objects from the Second LIGO-Virgo Gravitational-Wave Transient Catalog*, *Astrophys. J. Lett.* **913** (2021) L7 [2010.14533].

[12] LIGO Scientific, Virgo, KAGRA collaboration, *Upper Limits on the Isotropic Gravitational-Wave Background from Advanced LIGO's and Advanced Virgo's Third Observing Run*, 2101.12130.

[13] A. Achúcarro and G. A. Palma, *The string swampland constraints require multi-field inflation*, *JCAP* **02** (2019) 041 [1807.04390].

[14] A. Adams, N. Arkani-Hamed, S. Dubovsky, A. Nicolis and R. Rattazzi, *Causality, analyticity and an IR obstruction to UV completion*, *JHEP* **10** (2006) 014 [hep-th/0602178].

[15] Planck collaboration, *Planck 2013 results. XVI. Cosmological parameters*, *Astron. Astrophys.* **571** (2014) A16 [1303.5076].

[16] Planck collaboration, *Planck 2013 results. XXII. Constraints on inflation*, *Astron. Astrophys.* **571** (2014) A22 [1303.5082].

[17] Planck collaboration, *Planck 2013 results. XXIII. Isotropy and statistics of the CMB*, *Astron. Astrophys.* **571** (2014) A23 [1303.5083].

[18] Planck collaboration, *Planck 2015 results. XIII. Cosmological parameters*, *Astron. Astrophys.* **594** (2016) A13 [1502.01589].

[19] N. Afshordi, D. J. Chung, M. Doran and G. Geshnizjani, *Cuscuton Cosmology: Dark Energy meets Modified Gravity*, *Phys. Rev. D* **75** (2007) 123509 [astro-ph/0702002].

[20] N. Afshordi, D. J. Chung and G. Geshnizjani, *Cuscuton: A Causal Field Theory with an Infinite Speed of Sound*, *Phys. Rev. D* **75** (2007) 083513 [hep-th/0609150].

[21] A. Agarwal and N. Afshordi, *Thermal Tachyacoustic Cosmology*, *Phys. Rev. D* **90** (2014) 043528 [1406.0575].

[22] Planck collaboration, *Planck 2018 results. VI. Cosmological parameters*, *Astron. Astrophys.* **641** (2020) A6 [1807.06209].

[23] P. Agrawal, G. Obied, P. J. Steinhardt and C. Vafa, *On the Cosmological Implications of the String Swampland*, *Phys. Lett. B* **784** (2018) 271 [1806.09718].

[24] ACT collaboration, *The Atacama Cosmology Telescope: DR4 Maps and Cosmological Parameters*, *JCAP* **12** (2020) 047 [2007.07288].

[25] Planck collaboration, *Planck 2018 results. X. Constraints on inflation*, 1807.06211.

[26] eBOSS collaboration, *The Completed SDSS-IV extended Baryon Oscillation Spectroscopic Survey: Cosmological Implications from two Decades of Spectroscopic Surveys at the Apache Point observatory*, 2007.08991.

[27] eBOSS collaboration, *Completed SDSS-IV extended Baryon Oscillation Spectroscopic Survey: Cosmological implications from two decades of spectroscopic surveys at the Apache Point Observatory*, *Phys. Rev. D* **103** (2021) 083533 [2007.08991].

[28] A. Albrecht and P. J. Steinhardt, *Cosmology for Grand Unified Theories with Radiatively Induced Symmetry Breaking*, *Phys. Rev. Lett.* **48** (1982) 1220.

[29] LISA collaboration, *Laser Interferometer Space Antenna*, 1702.00786.

[30] R. L. Arnowitt, S. Deser and C. W. Misner, *The Dynamics of general relativity*, *Gen. Rel. Grav.* **40** (2008) 1997 [gr-qc/0405109].

[31] NANOGrav collaboration, *The NANOGrav 12.5 yr Data Set: Search for an Isotropic Stochastic Gravitational-wave Background*, *Astrophys. J. Lett.* **905** (2020) L34 [2009.04496].

[32] A. Ashoorioon, R. Casadio, M. Cicoli, G. Geshnizjani and H. J. Kim, *Extended Effective Field Theory of Inflation*, *JHEP* **02** (2018) 172 [1802.03040].

[33] I. Babic, C. Burgess and G. Geshnizjani, *Keeping an Eye on DBI: Power-counting for small-c_s Cosmology*, *JCAP* **05** (2020) 023 [1910.05277].

[34] E. Babichev, V. Mukhanov and A. Vikman, *k-Essence, superluminal propagation, causality and emergent geometry*, *JHEP* **02** (2008) 101 [0708.0561].

[35] B. A. Bassett and N. Afshordi, *Non-Gaussian Posteriors arising from Marginal Detections*, 1005.1664.

[36] L. Battarra and J.-L. Lehners, *Quantum-to-classical transition for ekpyrotic perturbations*, *Phys. Rev. D* **89** (2014) 063516 [1309.2281].

[37] D. Battefeld and P. Peter, *A Critical Review of Classical Bouncing Cosmologies*, *Phys. Rept.* **571** (2015) 1 [1406.2790].

[38] D. Baumann, *Primordial Cosmology*, *PoS* **TASI2017** (2018) 009 [1807.03098].

[39] A. Bedroya, R. Brandenberger, M. Loverde and C. Vafa, *Trans-Planckian Censorship and Inflationary Cosmology*, *Phys. Rev. D* **101** (2020) 103502 [1909.11106].

[40] A. Bedroya and C. Vafa, *Trans-Planckian Censorship and the Swampland*, *JHEP* **09** (2020) 123 [1909.11063].

[41] P. S. Behroozi, R. H. Wechsler and H.-Y. Wu, *The ROCKSTAR Phase-space Temporal Halo Finder and the Velocity Offsets of Cluster Cores*, *The Astrophysical Journal* **762** (2013) 109 [1110.4372].

[42] V. Belinsky, I. Khalatnikov and E. Lifshitz, *Oscillatory approach to a singular point in the relativistic cosmology*, *Adv. Phys.* **19** (1970) 525.

[43] S. Bera, D. Rana, S. More and S. Bose, *Incompleteness Matters Not: Inference of H_0 from Binary Black Hole–Galaxy Cross-correlations*, *Astrophys. J.* **902** (2020) 79 [2007.04271].

[44] A. Bhoonah, J. Bramante, S. Nerval and N. Song, *Gravitational Waves From Dark Sectors, Oscillating Inflatons, and Mass Boosted Dark Matter*, *JCAP* **04** (2021) 043 [2008.12306].

[45] N. Birrell and P. Davies, *Quantum Fields in Curved Space*, Cambridge Monographs on Mathematical Physics. Cambridge Univ. Press, Cambridge, UK, 2, 1984, 10.1017/CBO9780511622632.

[46] S. Birrer et al., *TDCOSMO - IV. Hierarchical time-delay cosmography – joint inference of the Hubble constant and galaxy density profiles*, *Astron. Astrophys.* **643** (2020) A165 [2007.02941].

[47] A. Borde and A. Vilenkin, *Eternal inflation and the initial singularity*, *Phys. Rev. Lett.* **72** (1994) 3305 [gr-qc/9312022].

[48] A. Borde and A. Vilenkin, *Singularities in inflationary cosmology: A Review*, *Int. J. Mod. Phys. D* **5** (1996) 813 [gr-qc/9612036].

[49] A. Borde and A. Vilenkin, *Violations of the weak energy condition in inflating space-times*, *Phys. Rev. D* **56** (1997) 717 [gr-qc/9702019].

[50] S. S. Boruah, M. J. Hudson and G. Lavaux, *Peculiar velocities in the local Universe: comparison of different models and the implications for H_0 and dark matter*, 2010.01119.

[51] S. S. Boruah, H. J. Kim and G. Geshnizjani, *Theory of Cosmological Perturbations with Cuscuton*, *JCAP* **07** (2017) 022 [1704.01131].

[52] S. S. Boruah, H. J. Kim, M. Rouben and G. Geshnizjani, *Cuscuton bounce*, *JCAP* **08** (2018) 031 [1802.06818].

[53] L. Boyle, K. Finn and N. Turok, *CPT-Symmetric Universe*, *Phys. Rev. Lett.* **121** (2018) 251301 [1803.08928].

[54] R. Brandenberger, K. Dasgupta and Z. Wang, *Reheating after S-Brane Ekpyrosis*, 2007.01203.

[55] R. Brandenberger and P. Peter, *Bouncing Cosmologies: Progress and Problems*, *Found. Phys.* **47** (2017) 797 [1603.05834].

[56] R. Brandenberger and Z. Wang, *Ekpyrotic cosmology with a zero-shear S-brane*, *Phys. Rev. D* **102** (2020) 023516 [2004.06437].

[57] R. Brandenberger and Z. Wang, *Nonsingular Ekpyrotic Cosmology with a Nearly Scale-Invariant Spectrum of Cosmological Perturbations and Gravitational Waves*, *Phys. Rev. D* **101** (2020) 063522 [2001.00638].

[58] R. H. Brandenberger, *Lectures on the theory of cosmological perturbations*, *Lect. Notes Phys.* **646** (2004) 127 [hep-th/0306071].

[59] R. H. Brandenberger, *Cosmology of the Very Early Universe*, *AIP Conf. Proc.* **1268** (2010) 3 [1003.1745].

[60] R. H. Brandenberger, *Is the spectrum of gravitational waves the "Holy Grail" of inflation?*, *Eur. Phys. J. C* **79** (2019) 387 [1104.3581].

[61] R. H. Brandenberger and J. Martin, *The Robustness of inflation to changes in superPlanck scale physics*, *Mod. Phys. Lett. A* **16** (2001) 999 [astro-ph/0005432].

[62] R. H. Brandenberger and J. Martin, *Trans-Planckian Issues for Inflationary Cosmology*, *Class. Quant. Grav.* **30** (2013) 113001 [1211.6753].

[63] R. H. Brandenberger, A. Nayeri, S. P. Patil and C. Vafa, *String gas cosmology and structure formation*, *Int. J. Mod. Phys. A* **22** (2007) 3621 [hep-th/0608121].

[64] R. H. Brandenberger and C. Vafa, *Superstrings in the Early Universe*, *Nucl. Phys. B* **316** (1989) 391.

[65] T. D. Brennan, F. Carta and C. Vafa, *The String Landscape, the Swampland, and the Missing Corner*, *PoS* **TASI2017** (2017) 015 [1711.00864].

[66] E. I. Buchbinder, J. Khoury and B. A. Ovrut, *New Ekpyrotic cosmology*, *Phys. Rev. D* **76** (2007) 123503 [hep-th/0702154].

[67] C. Burgess, *Intro to Effective Field Theories and Inflation*, 1711.10592.

[68] Y.-F. Cai, D. A. Easson and R. Brandenberger, *Towards a Nonsingular Bouncing Cosmology*, *JCAP* **08** (2012) 020 [1206.2382].

[69] Y.-F. Cai, E. McDonough, F. Duplessis and R. H. Brandenberger, *Two Field Matter Bounce Cosmology*, *JCAP* **10** (2013) 024 [1305.5259].

[70] Y.-F. Cai, T. Qiu, R. Brandenberger, Y.-S. Piao and X. Zhang, *On Perturbations of Quintom Bounce*, *JCAP* **03** (2008) 013 [0711.2187].

[71] Y. Cai, H.-G. Li, T. Qiu and Y.-S. Piao, *The Effective Field Theory of nonsingular cosmology: II*, *Eur. Phys. J. C* **77** (2017) 369 [1701.04330].

[72] Y. Cai and Y.-S. Piao, *A covariant Lagrangian for stable nonsingular bounce*, *JHEP* **09** (2017) 027 [1705.03401].

[73] Y. Cai, Y. Wan, H.-G. Li, T. Qiu and Y.-S. Piao, *The Effective Field Theory of nonsingular cosmology*, *JHEP* **01** (2017) 090 [1610.03400].

[74] B. Caron et al., *The Virgo interferometer*, *Class. Quant. Grav.* **14** (1997) 1461.

[75] S. M. Carroll, *Spacetime and Geometry*. Cambridge University Press, 7, 2019.

[76] H.-Y. Chen, M. Fishbach and D. E. Holz, *A two per cent Hubble constant measurement from standard sirens within five years*, *Nature* **562** (2018) 545 [1712.06531].

[77] X. Chen, *Distortion of Gravitational-wave Signals by Astrophysical Environments*, 9, 2020, 2009.07626.

[78] N. Christensen, *Stochastic Gravitational Wave Backgrounds*, *Rept. Prog. Phys.* **82** (2019) 016903 [1811.08797].

[79] W. G. Cook, I. A. Glushchenko, A. Ijjas, F. Pretorius and P. J. Steinhardt, *Supersmoothing through Slow Contraction*, 2006.01172.

[80] P. Creminelli, M. A. Luty, A. Nicolis and L. Senatore, *Starting the Universe: Stable Violation of the Null Energy Condition and Non-standard Cosmologies*, *JHEP* **12** (2006) 080 [hep-th/0606090].

[81] P. Creminelli, A. Nicolis and M. Zaldarriaga, *Perturbations in bouncing cosmologies: Dynamical attractor versus scale invariance*, *Phys. Rev. D* **71** (2005) 063505 [hep-th/0411270].

[82] P. Creminelli, D. Pirtskhalava, L. Santoni and E. Trincherini, *Stability of Geodesically Complete Cosmologies*, *JCAP* **11** (2016) 047 [1610.04207].

[83] P. Creminelli and L. Senatore, *A Smooth bouncing cosmology with scale invariant spectrum*, *JCAP* **11** (2007) 010 [hep-th/0702165].

[84] C. Cutler and E. E. Flanagan, *Gravitational waves from merging compact binaries: How accurately can one extract the binary's parameters from the inspiral wave form?*, *Phys. Rev. D* **49** (1994) 2658 [gr-qc/9402014].

[85] N. Dalal, D. E. Holz, S. A. Hughes and B. Jain, *Short GRB and binary black hole standard sirens as a probe of dark energy*, *Phys. Rev. D* **74** (2006) 063006 [astro-ph/0601275].

[86] G. Dálya, G. Galgóczi, L. Dobos, Z. Frei, I. S. Heng, R. Macas et al., *GLADE: A galaxy catalogue for multimessenger searches in the advanced gravitational-wave detector era*, *Mon. Not. Roy. Astron. Soc.* **479** (2018) 2374 [1804.05709].

[87] T. Damour and A. Vilenkin, *Gravitational radiation from cosmic (super)strings: Bursts, stochastic background, and observational windows*, *Phys. Rev. D* **71** (2005) 063510 [hep-th/0410222].

[88] T. de Jaeger, B. E. Stahl, W. Zheng, A. V. Filippenko, A. G. Riess and L. Galbany, *A measurement of the Hubble constant from Type II supernovae*, *Mon. Not. Roy. Astron. Soc.* **496** (2020) 3402 [2006.03412].

[89] V. Desjacques and U. Seljak, *Primordial non-Gaussianity from the large scale structure*, *Class. Quant. Grav.* **27** (2010) 124011 [1003.5020].

[90] V. Desjacques, D. Jeong and F. Schmidt, *Large-Scale Galaxy Bias*, *Phys. Rept.* **733** (2018) 1 [1611.09787].

[91] E. Di Valentino, O. Mena, S. Pan, L. Visinelli, W. Yang, A. Melchiorri et al., *In the Realm of the Hubble tension − a Review of Solutions*, 2103.01183.

[92] M. Dias, J. Frazer, A. Retolaza and A. Westphal, *Primordial Gravitational Waves and the Swampland*, *Fortsch. Phys.* **67** (2019) 2 [1807.06579].

[93] D. A. Dobre, A. V. Frolov, J. T. Gálvez Ghersi, S. Ramazanov and A. Vikman, *Unbraiding the Bounce: Superluminality around the Corner*, *JCAP* **03** (2018) 020 [1712.10272].

[94] S. Dodelson, *Modern Cosmology*. Academic Press, Amsterdam, 2003.

[95] S. Dubovsky, T. Gregoire, A. Nicolis and R. Rattazzi, *Null energy condition and superluminal propagation*, *JHEP* **03** (2006) 025 [hep-th/0512260].

[96] J. Dunkley, M. Bucher, P. G. Ferreira, K. Moodley and C. Skordis, *Fast and reliable mcmc for cosmological parameter estimation*, *Mon. Not. Roy. Astron. Soc.* **356** (2005) 925 [astro-ph/0405462].

[97] G. Dvali, A. Kehagias and A. Riotto, *Inflation and Decoupling*, 2005.05146.

[98] D. A. Easson, I. Sawicki and A. Vikman, *G-Bounce*, *JCAP* **11** (2011) 021 [1109.1047].

[99] D. A. Easson, I. Sawicki and A. Vikman, *When Matter Matters*, *JCAP* **07** (2013) 014 [1304.3903].

[100] W. E. East, M. Kleban, A. Linde and L. Senatore, *Beginning inflation in an inhomogeneous universe*, *JCAP* **09** (2016) 010 [1511.05143].

[101] S. M. Feeney, H. V. Peiris, S. M. Nissanke and D. J. Mortlock, *Prospects for Measuring the Hubble Constant with Neutron-Star–Black-Hole Mergers*, *Phys. Rev. Lett.* **126** (2021) 171102 [2012.06593].

[102] S. M. Feeney, H. V. Peiris, A. R. Williamson, S. M. Nissanke, D. J. Mortlock, J. Alsing et al., *Prospects for resolving the Hubble constant tension with standard sirens*, *Phys. Rev. Lett.* **122** (2019) 061105 [1802.03404].

[103] D. Fernández Arenas, E. Terlevich, R. Terlevich, J. Melnick, R. Chávez, F. Bresolin et al., *An independent determination of the local Hubble constant*, *Mon. Not. Roy. Astron. Soc.* **474** (2018) 1250 [1710.05951].

[104] P. Ferreira and J. Magueijo, *Observing the temperature of the Big Bang through large scale structure*, *Phys. Rev. D* **78** (2008) 061301 [0708.0429].

[105] A. Fertig, J.-L. Lehners, E. Mallwitz and E. Wilson-Ewing, *Converting entropy to curvature perturbations after a cosmic bounce*, *JCAP* **10** (2016) 005 [1607.05663].

[106] F. Finelli and R. Brandenberger, *On the generation of a scale invariant spectrum of adiabatic fluctuations in cosmological models with a contracting phase*, *Phys. Rev. D* **65** (2002) 103522 [hep-th/0112249].

[107] A. Finke, S. Foffa, F. Iacovelli, M. Maggiore and M. Mancarella, *Cosmology with LIGO/Virgo dark sirens: Hubble parameter and modified gravitational wave propagation*, 2101.12660.

[108] LIGO Scientific, Virgo collaboration, *A Standard Siren Measurement of the Hubble Constant from GW170817 without the Electromagnetic Counterpart*, *Astrophys. J. Lett.* **871** (2019) L13 [1807.05667].

[109] E. E. Flanagan and S. A. Hughes, *The Basics of gravitational wave theory*, *New J. Phys.* **7** (2005) 204 [gr-qc/0501041].

[110] W. L. Freedman, B. F. Madore, T. Hoyt, I. S. Jang, R. Beaton, M. G. Lee et al., *Calibration of the Tip of the Red Giant Branch (TRGB)*, 2002.01550.

[111] J. N. Fry and E. Gaztanaga, *Biasing and hierarchical statistics in large scale structure*, *Astrophys. J.* **413** (1993) 447 [astro-ph/9302009].

[112] D. Garfinkle, W. C. Lim, F. Pretorius and P. J. Steinhardt, *Evolution to a smooth universe in an ekpyrotic contracting phase with w ¿ 1*, *Phys. Rev. D* **78** (2008) 083537 [0808.0542].

[113] M. Gasperini and G. Veneziano, *Pre - big bang in string cosmology*, *Astropart. Phys.* **1** (1993) 317 [hep-th/9211021].

[114] M. Gasperini and G. Veneziano, *The Pre - big bang scenario in string cosmology*, *Phys. Rept.* **373** (2003) 1 [hep-th/0207130].

[115] G. Geshnizjani and N. Ahmadi, *Can non-local or higher derivative theories provide alternatives to inflation?*, *JCAP* **11** (2013) 029 [1309.4782].

[116] G. Geshnizjani and W. H. Kinney, *Theoretical implications of detecting gravitational waves*, *JCAP* **08** (2015) 008 [1410.4968].

[117] G. Geshnizjani, W. H. Kinney and A. Moradinezhad Dizgah, *General conditions for scale-invariant perturbations in an expanding universe*, *JCAP* **11** (2011) 049 [1107.1241].

[118] H. Gomes and D. C. Guariento, *Hamiltonian analysis of the cuscuton*, *Phys. Rev. D* **95** (2017) 104049 [1703.08226].

[119] C. Grojean and G. Servant, *Gravitational Waves from Phase Transitions at the Electroweak Scale and Beyond*, *Phys. Rev. D* **75** (2007) 043507 [hep-ph/0607107].

[120] H.-K. Guo, K. Sinha, D. Vagie and G. White, *Phase Transitions in an Expanding Universe: Stochastic Gravitational Waves in Standard and Non-Standard Histories*, *JCAP* **01** (2021) 001 [2007.08537].

[121] A. H. Guth, *The Inflationary Universe: A Possible Solution to the Horizon and Flatness Problems*, *Adv. Ser. Astrophys. Cosmol.* **3** (1987) 139.

[122] A. H. Guth, *Eternal inflation and its implications*, *J. Phys. A* **40** (2007) 6811 [hep-th/0702178].

[123] A. H. Guth, D. I. Kaiser and Y. Nomura, *Inflationary paradigm after Planck 2013*, *Phys. Lett. B* **733** (2014) 112 [1312.7619].

[124] M. C. Guzzetti, N. Bartolo, M. Liguori and S. Matarrese, *Gravitational waves from inflation*, *Riv. Nuovo Cim.* **39** (2016) 399 [1605.01615].

[125] C. R. Harris, K. J. Millman, S. J. van der Walt, R. Gommers, P. Virtanen, D. Cournapeau et al., *Array programming with NumPy*, *Nature* **585** (2020) 357.

[126] A. Heavens, *Statistical techniques in cosmology*, *arXiv e-prints* (2009) arXiv:0906.0664 [0906.0664].

[127] WMAP collaboration, *First year Wilkinson Microwave Anisotropy Probe (WMAP) observations: The Angular power spectrum*, *Astrophys. J. Suppl.* **148** (2003) 135 [astro-ph/0302217].

[128] D. W. Hogg, *Distance measures in cosmology*, astro-ph/9905116.

[129] D. E. Holz and S. A. Hughes, *Using gravitational-wave standard sirens*, *Astrophys. J.* **629** (2005) 15 [astro-ph/0504616].

[130] R. A. Hulse and J. H. Taylor, *Discovery of a pulsar in a binary system.*, *Astrophys. J.* **195** (1975) L51.

[131] A. Ijjas, W. G. Cook, F. Pretorius, P. J. Steinhardt and E. Y. Davies, *Robustness of slow contraction to cosmic initial conditions*, 2006.04999.

[132] A. Ijjas, J.-L. Lehners and P. J. Steinhardt, *General mechanism for producing scale-invariant perturbations and small non-Gaussianity in ekpyrotic models*, *Phys. Rev. D* **89** (2014) 123520 [1404.1265].

[133] A. Ijjas and P. J. Steinhardt, *Classically stable nonsingular cosmological bounces*, *Phys. Rev. Lett.* **117** (2016) 121304 [1606.08880].

[134] A. Ijjas and P. J. Steinhardt, *Fully stable cosmological solutions with a non-singular classical bounce*, *Phys. Lett. B* **764** (2017) 289 [1609.01253].

[135] A. Ijjas, P. J. Steinhardt and A. Loeb, *Inflationary paradigm in trouble after Planck2013*, *Phys. Lett. B* **723** (2013) 261 [1304.2785].

[136] Ž. Ivezić, A. Connolly, J. VanderPlas and A. Gray, *Statistics, Data Mining, and Machine Learning in Astronomy: A Practical Python Guide for the Analysis of Survey Data*, Princeton Series in Modern Observational Astronomy. Princeton University Press, 2014.

[137] A. Iyonaga, K. Takahashi and T. Kobayashi, *Extended Cuscuton: Formulation*, *JCAP* **12** (2018) 002 [1809.10935].

[138] S. Kawamura et al., *The Japanese space gravitational wave antenna DECIGO*, *Class. Quant. Grav.* **23** (2006) S125.

[139] S. Kawamura et al., *Current status of space gravitational wave antenna DECIGO and B-DECIGO*, 2006.13545.

[140] J. Khoury, B. A. Ovrut, P. J. Steinhardt and N. Turok, *The Ekpyrotic universe: Colliding branes and the origin of the hot big bang*, *Phys. Rev. D* **64** (2001) 123522 [hep-th/0103239].

[141] J. Khoury and F. Piazza, *Rapidly-Varying Speed of Sound, Scale Invariance and Non-Gaussian Signatures*, *JCAP* **07** (2009) 026 [0811.3633].

[142] T. W. B. Kibble, *Topology of Cosmic Domains and Strings*, *J. Phys. A* **9** (1976) 1387.

[143] J. L. Kim and G. Geshnizjani, *Spectrum of Cuscuton Bounce*, *JCAP* **03** (2021) 104 [2010.06645].

[144] W. H. Kinney, S. Vagnozzi and L. Visinelli, *The zoo plot meets the swampland: mutual (in)consistency of single-field inflation, string conjectures, and cosmological data*, *Class. Quant. Grav.* **36** (2019) 117001 [1808.06424].

[145] T. Kobayashi, *Generic instabilities of nonsingular cosmologies in Horndeski theory: A no-go theorem*, *Phys. Rev. D* **94** (2016) 043511 [1606.05831].

[146] K. D. Kokkotas, *Gravitational waves*, *Acta Phys. Polon. B* **38** (2007) 3891.

[147] A. V. Kravtsov and A. A. Klypin, *Origin and evolution of halo bias in linear and nonlinear regimes*, *Astrophys. J.* **520** (1999) 437 [astro-ph/9812311].

[148] A. Le Tiec and J. Novak, *Theory of Gravitational Waves*, in *An Overview of Gravitational Waves: Theory, Sources and Detection*, G. Auger and E. Plagnol, eds., (2017), 1607.04202, DOI.

[149] J.-L. Lehners, *Ekpyrotic and Cyclic Cosmology*, *Phys. Rept.* **465** (2008) 223 [0806.1245].

[150] J.-L. Lehners, P. McFadden, N. Turok and P. J. Steinhardt, *Generating ekpyrotic curvature perturbations before the big bang*, *Phys. Rev. D* **76** (2007) 103501 [hep-th/0702153].

[151] J.-L. Lehners and P. J. Steinhardt, *Non-Gaussianity Generated by the Entropic Mechanism in Bouncing Cosmologies Made Simple*, *Phys. Rev. D* **80** (2009) 103520 [0909.2558].

[152] A. Lewis, A. Challinor and A. Lasenby, *Efficient computation of CMB anisotropies in closed FRW models*, *Astrophys. J.* **538** (2000) 473 [astro-ph/9911177].

[153] M. Li, *Note on the production of scale-invariant entropy perturbation in the Ekpyrotic universe*, *Phys. Lett. B* **724** (2013) 192 [1306.0191].

[154] M. Libanov, S. Mironov and V. Rubakov, *Generalized Galileons: instabilities of bouncing and Genesis cosmologies and modified Genesis*, *JCAP* **08** (2016) 037 [1605.05992].

[155] A. R. Liddle and S. M. Leach, *How long before the end of inflation were observable perturbations produced?*, *Phys. Rev. D* **68** (2003) 103503 [astro-ph/0305263].

[156] E. Lifshitz and I. Khalatnikov, *Investigations in relativistic cosmology*, *Adv. Phys.* **12** (1963) 185.

[157] W.-C. Lin and W. H. Kinney, *Trans-Planckian Censorship and k-inflation*, *Phys. Rev. D* **101** (2020) 123534 [1911.03736].

[158] A. D. Linde, *Chaotic Inflation*, *Phys. Lett. B* **129** (1983) 177.

[159] A. D. Linde, *Eternal Chaotic Inflation*, *Mod. Phys. Lett. A* **1** (1986) 81.

[160] A. D. Linde, *A New Inflationary Universe Scenario: A Possible Solution of the Horizon, Flatness, Homogeneity, Isotropy and Primordial Monopole Problems*, *Adv. Ser. Astrophys. Cosmol.* **3** (1987) 149.

[161] A. D. Linde, *Prospects of inflation*, *Phys. Scripta T* **117** (2005) 40 [hep-th/0402051].

[162] M. Maggiore et al., *Science Case for the Einstein Telescope*, *JCAP* **03** (2020) 050 [1912.02622].

[163] J. Magueijo, *Speedy sound and cosmic structure*, *Phys. Rev. Lett.* **100** (2008) 231302 [0803.0859].

[164] J. Magueijo and L. Pogosian, *Could thermal fluctuations seed cosmic structure?*, *Phys. Rev. D* **67** (2003) 043518 [astro-ph/0211337].

[165] J. M. Maldacena, *Non-Gaussian features of primordial fluctuations in single field inflationary models*, *JHEP* **05** (2003) 013 [astro-ph/0210603].

[166] J. Martin and R. H. Brandenberger, *The TransPlanckian problem of inflationary cosmology*, *Phys. Rev. D* **63** (2001) 123501 [hep-th/0005209].

[167] P. McDonald and A. Roy, *Clustering of dark matter tracers: generalizing bias for the coming era of precision lss*, *Journal of Cosmology and Astroparticle Physics* **2009** (2009) 020–020.

[168] P. D. Meerburg et al., *Primordial Non-Gaussianity*, 1903.04409.

[169] S. Mironov, V. Rubakov and V. Volkova, *Cosmological scenarios with bounce and Genesis in Horndeski theory and beyond: An essay in honor of I.M. Khalatnikov on the occasion of his 100th birthday*, 1906.12139.

[170] S. Mironov, V. Rubakov and V. Volkova, *Subluminal cosmological bounce beyond Horndeski*, *JCAP* **05** (2020) 024 [1910.07019].

[171] S. Mironov, V. Rubakov and V. Volkova, *Superluminality in DHOST theory with extra scalar*, 2011.14912.

[172] H. Mo, F. C. van den Bosch and S. White, *Galaxy Formation and Evolution*. 2010.

[173] V. Mukhanov and S. Winitzki, *Introduction to quantum effects in gravity*. Cambridge University Press, 6, 2007.

[174] V. F. Mukhanov, H. Feldman and R. H. Brandenberger, *Theory of cosmological perturbations. Part 1. Classical perturbations. Part 2. Quantum theory of perturbations. Part 3. Extensions*, *Phys. Rept.* **215** (1992) 203.

[175] S. Mukherjee and B. D. Wandelt, *Beyond the classical distance-redshift test: cross-correlating redshift-free standard candles and sirens with redshift surveys*, 1808.06615.

[176] S. Mukherjee, B. D. Wandelt, S. M. Nissanke and A. Silvestri, *Accurate precision Cosmology with redshift unknown gravitational wave sources*, *Phys. Rev. D* **103** (2021) 043520 [2007.02943].

[177] A. Notari and A. Riotto, *Isocurvature perturbations in the ekpyrotic universe*, *Nucl. Phys. B* **644** (2002) 371 [hep-th/0205019].

[178] G. Obied, H. Ooguri, L. Spodyneiko and C. Vafa, *De Sitter Space and the Swampland*, 1806.08362.

[179] E. O'Callaghan, S. Chadburn, G. Geshnizjani, R. Gregory and I. Zavala, *The effect of extra dimensions on gravity wave bursts from cosmic string cusps*, *JCAP* **09** (2010) 013 [1005.3220].

[180] M. Oguri, *Measuring the distance-redshift relation with the cross-correlation of gravitational wave standard sirens and galaxies*, *Phys. Rev. D* **93** (2016) 083511 [1603.02356].

[181] H. Ooguri and C. Vafa, *On the Geometry of the String Landscape and the Swampland*, *Nucl. Phys. B* **766** (2007) 21 [hep-th/0605264].

[182] E. Palti, *The Swampland: Introduction and Review*, *Fortsch. Phys.* **67** (2019) 1900037 [1903.06239].

[183] A. A. Penzias and R. W. Wilson, *A Measurement of excess antenna temperature at 4080-Mc/s*, *Astrophys. J.* **142** (1965) 419.

[184] Supernova Cosmology Project collaboration, *Discovery of a supernova explosion at half the age of the Universe and its cosmological implications*, *Nature* **391** (1998) 51 [astro-ph/9712212].

[185] Supernova Cosmology Project collaboration, *Measurements of* Ω *and* Λ *from 42 high redshift supernovae*, *Astrophys. J.* **517** (1999) 565 [astro-ph/9812133].

[186] D. W. Pesce et al., *The Megamaser Cosmology Project. XIII. Combined Hubble constant constraints*, *Astrophys. J. Lett.* **891** (2020) L1 [2001.09213].

[187] M. M. Phillips, *The absolute magnitudes of Type IA supernovae*, *Astrophys. J. Lett.* **413** (1993) L105.

[188] L. Pogosian, G.-B. Zhao and K. Jedamzik, *Recombination-independent determination of the sound horizon and the Hubble constant from BAO*, *Astrophys. J. Lett.* **904** (2020) L17 [2009.08455].

[189] E. Poisson, *A Relativist's Toolkit: The Mathematics of Black-Hole Mechanics*. Cambridge University Press, 12, 2009, 10.1017/CBO9780511606601.

[190] A. M. Price-Whelan, B. M. Sipőcz, H. M. Günther, P. L. Lim, S. M. Crawford, S. Conseil et al., *The astropy project: Building an open-science project and status of the v2.0 core package*, *The Astronomical Journal* **156** (2018) 123.

[191] T. Qiu, J. Evslin, Y.-F. Cai, M. Li and X. Zhang, *Bouncing Galileon Cosmologies*, *JCAP* **10** (2011) 036 [1108.0593].

[192] J. Quintin and D. Yoshida, *Cuscuton gravity as a classically stable limiting curvature theory*, *JCAP* **02** (2020) 016 [1911.06040].

[193] D. K. Ramanah, T. Charnock and G. Lavaux, *Painting halos from cosmic density fields of dark matter with physically motivated neural networks*, *Phys. Rev. D* **100** (2019) 043515 [1903.10524].

[194] A. G. Riess, S. Casertano, W. Yuan, J. B. Bowers, L. Macri, J. C. Zinn et al., *Cosmic Distances Calibrated to 1% Precision with Gaia EDR3 Parallaxes and Hubble Space Telescope Photometry of 75 Milky Way Cepheids Confirm Tension with ΛCDM*, *Astrophys. J. Lett.* **908** (2021) L6 [2012.08534].

[195] A. G. Riess, S. Casertano, W. Yuan, L. M. Macri and D. Scolnic, *Large Magellanic Cloud Cepheid Standards Provide a 1% Foundation for the Determination of the Hubble Constant and Stronger Evidence for Physics beyond ΛCDM*, *Astrophys. J.* **876** (2019) 85 [1903.07603].

[196] T. P. Robitaille, E. J. Tollerud, P. Greenfield, M. Droettboom, E. Bray, T. Aldcroft et al., *Astropy: A community python package for astronomy*, *Astronomy & Astrophysics* **558** (2013) A33.

[197] V. Rubakov, *The Null Energy Condition and its violation*, *Usp. Fiz. Nauk* **184** (2014) 137 [1401.4024].

[198] S. Sarangi and S. H. H. Tye, *Cosmic string production towards the end of brane inflation*, *Phys. Lett. B* **536** (2002) 185 [hep-th/0204074].

[199] B. S. Sathyaprakash and B. F. Schutz, *Physics, Astrophysics and Cosmology with Gravitational Waves*, *Living Rev. Rel.* **12** (2009) 2 [0903.0338].

[200] I. Sawicki and A. Vikman, *Hidden Negative Energies in Strongly Accelerated Universes*, *Phys. Rev. D* **87** (2013) 067301 [1209.2961].

[201] Supernova Search Team collaboration, *The High Z supernova search: Measuring cosmic deceleration and global curvature of the universe using type Ia supernovae*, *Astrophys. J.* **507** (1998) 46 [astro-ph/9805200].

[202] J. Schombert, S. McGaugh and F. Lelli, *Using the Baryonic Tully–Fisher Relation to Measure H o*, *Astron. J.* **160** (2020) 71 [2006.08615].

[203] B. F. Schutz, *Determining the Hubble Constant from Gravitational Wave Observations*, *Nature* **323** (1986) 310.

[204] B. F. Schutz and F. Ricci, *Gravitational Waves, Sources, and Detectors*, 1005.4735.

[205] L. Senatore, *Lectures on Inflation*, in *Theoretical Advanced Study Institute in Elementary Particle Physics: New Frontiers in Fields and Strings*, pp. 447–543, 2017, DOI [1609.00716].

[206] X. Siemens, V. Mandic and J. Creighton, *Gravitational wave stochastic background from cosmic (super)strings*, *Phys. Rev. Lett.* **98** (2007) 111101 [astro-ph/0610920].

[207] L. P. Singer and L. R. Price, *Rapid Bayesian position reconstruction for gravitational-wave transients*, *Phys. Rev. D* **93** (2016) 024013 [1508.03634].

[208] DES, LIGO Scientific, Virgo collaboration, *First Measurement of the Hubble Constant from a Dark Standard Siren using the Dark Energy Survey Galaxies and the LIGO/Virgo Binary–Black-hole Merger GW170814*, *Astrophys. J. Lett.* **876** (2019) L7 [1901.01540].

[209] V. Springel, *The Cosmological simulation code GADGET-2*, *Mon. Not. Roy. Astron. Soc.* **364** (2005) 1105 [astro-ph/0505010].

[210] V. Springel et al., *Simulating the joint evolution of quasars, galaxies and their large-scale distribution*, *Nature* **435** (2005) 629 [astro-ph/0504097].

[211] P. J. Steinhardt, *Natural inflation*, in *The Very Early Universe, ed. by G. Gibbons, S. Hawking and S. Siklos*, p. 251–66, Cambridge University Press, (1983).

[212] R. Trotta, *Bayesian Methods in Cosmology*, 1, 2017, 1701.01467.

[213] C.-Y. Tseng, *Decoherence problem in an ekpyrotic phase*, *Phys. Rev. D* **87** (2013) 023518 [1210.0581].

[214] J. VanderPlas, A. J. Connolly, Z. Ivezic and A. Gray, *Introduction to astroML: Machine learning for astrophysics*, in *Proceedings of Conference on Intelligent Data Understanding (CIDU*, pp. 47–54, Oct., 2012, DOI [1411.5039].

[215] L. Verde, *Non-Gaussianity from Large-Scale Structure Surveys*, *Advances in Astronomy* **2010** (2010) 768675 [1001.5217].

[216] A. Vilenkin and E. P. S. Shellard, *Cosmic Strings and Other Topological Defects*. Cambridge University Press, 7, 2000.

[217] A. Vilenkin, *The Birth of Inflationary Universes*, *Phys. Rev. D* **27** (1983) 2848.

[218] P. Virtanen, R. Gommers, T. E. Oliphant, M. Haberland, T. Reddy, D. Cournapeau et al., *SciPy 1.0: Fundamental Algorithms for Scientific Computing in Python*, *Nature Methods* **17** (2020) 261.

[219] S. Weinberg, *Cosmology*. 2008.

[220] J. M. Weisberg and J. H. Taylor, *Relativistic binary pulsar B1913+16: Thirty years of observations and analysis*, *ASP Conf. Ser.* **328** (2005) 25 [astro-ph/0407149].

[221] E. Witten, *Cosmic Separation of Phases*, *Phys. Rev. D* **30** (1984) 272.

[222] K. C. Wong et al., *H0LiCOW – XIII. A 2.4 per cent measurement of H0 from lensed quasars: 5.3σ tension between early- and late-Universe probes*, *Mon. Not. Roy. Astron. Soc.* **498** (2020) 1420 [1907.04869].

APPENDICES

Appendix A

Further Calculations for Dark Sirens

A.1 Expansions of Non-Linear Functions of the Density Field

We can expand the nonlinear functions g_x for each species x by making an exponential expansion (corresponding to expression (6.9) in the main text):

$$\begin{aligned}\langle n_x(\boldsymbol{r})\rangle \Delta V &= g_x(1+\delta(\boldsymbol{r}), r)\Delta V \\ &= g_x(1, r)\Delta V \exp(b_x(\boldsymbol{r})\delta(\boldsymbol{r})) \\ &\approx g_x(1, r)\Delta V \left[1 + b_x(r)\delta(\boldsymbol{r}) + \mathcal{O}(\delta^2)\right]. \end{aligned} \tag{A.1}$$

And so expression (6.10) can be expanded in detail as:

$$\begin{aligned}\langle N_x(\delta)\rangle &= \sum_{m=1}^{N_{cells}} \langle n_x(\boldsymbol{r}^m)\rangle \Delta V \\ &\approx \sum_{m=1}^{N_{cells}} g_x(1, r^m)\Delta V \left[1 + b_x(r^m)\delta(\boldsymbol{r}^m) + \mathcal{O}(\delta^2)\right] \\ &= \bar{N}_x + \sum_{r_m} g_x(1, r^m)\Delta V \left[b_x(r^m) \underbrace{\sum_{\hat{r}_m} \delta(r^m, \hat{r}^m)}_{=0} + \mathcal{O}(\delta^2) \right] \\ &\approx \bar{N}_x + \mathcal{O}(\delta^2), \end{aligned} \tag{A.2}$$

where we used $\hat{r}$ to indicate the angular direction of the vector $\boldsymbol{r}$, and the fact that at a fixed radius,

$$\langle \delta(r^m) \rangle \sim \sum_{\hat{r}_m} \delta(r^m, \hat{r}^m) \sim 0. \tag{A.3}$$

A.2 Distance Conversions

A.2.1 Converting Distance to Redshift

To compute the redshift, we introduce the usual decceleration parameter

$$q_0 = -\frac{1}{H_0^2}\frac{d^2a}{dt^2} = \frac{1}{2}\Omega_m - \Omega_\Lambda, \tag{A.4}$$

after assuming that $\Omega_r \sim 0$ and $w_{\rm DE} = -1$. In the purpose of our calculations, $\Omega_m = 0.3$ and $\Omega_\Lambda = 0.7$ as a rough estimate[1]. Assuming that our sources are at a low enough redshift (ie. $z \lesssim 0.2$), one can perform the power law expansion for the comoving distance (keeping c in) [219]:

$$\frac{H_0}{c} r = z - \frac{1}{2}(1 + q_0)z^2 + \mathcal{O}(z^3), \tag{A.5}$$

to which we can solve at second order for z to get

$$z(r) \approx \frac{1 - \sqrt{1 - 2rH_0(1 + q_0)/c}}{1 + q_0}, \tag{A.6}$$

giving a second order approximation of the redshift z given a comoving distance r.

A.2.2 Converting Comoving Distance to Luminosity Distance

Recall that the luminosity distance D_L of a source is related to the comoving distance r by

$$D_L = (1 + z)r, \tag{A.7}$$

[1] Although these are cosmological parameters that one can introduce into the set of cosmological parameters to be inferred with the statistical model.

where z is the redshift of the source. Using (A.6), this then lets us write D_L as a function of r approximately as

$$D_L(r) = (1 + z(r))r \approx \left[1 + \frac{1 - \sqrt{1 - 2rH_0(1 + q_0)/c}}{1 + q_0}\right] r. \tag{A.8}$$

A.2.3 Converting Luminosity Distance to Comoving Distance

This time, writing D_L as a power series [219],

$$\frac{H_0}{c} D_L = z + \frac{1}{2}(1 - q_0)z^2 + \mathcal{O}(z^3), \tag{A.9}$$

to which we can find the roots (to second order) again

$$z(D_L) = \frac{-1 + \sqrt{1 + 2D_L H_0(1 - q_0)/c}}{1 - q_0}. \tag{A.10}$$

These will be the redshifts that we compute with each value of h given the luminosity distances of the GW sources. Then we substitute back into the relationship for r and d_L to get:

$$r(D_L) = \frac{D_L}{1 + z} \approx \left[1 + \frac{-1 + \sqrt{1 + 2D_L H_0(1 - q_0)/c}}{1 - q_0}\right]^{-1} D_L. \tag{A.11}$$

A.3 68% Interval for 2D Gaussian

By definition, the solid angle can be written as

$$\Omega = \frac{A}{r^2}, \tag{A.12}$$

where r is the radius of the spherical shell and A is the spherical surface area of a patch for solid angle A. In the large distance regime where r is very large (as in most cases for astronomy), for a small solid angle $\Delta\Omega$, we can approximate the spherical surface area with a flat circle of radius ℓ so that

$$\Delta\Omega = \frac{\pi\ell^2}{r^2} = \pi\theta^2, \tag{A.13}$$

where $\theta = \ell/r$ is the approximated small angle. Hence if $\Delta\Omega$ is the 68% interval for the solid angle, we can translate it to a standard deviation in either transverse coordinates or one-dimensional angle θ by using the probability function in two dimensions:

$$P(x,y) = \frac{1}{2\pi\sigma_x\sigma_y}\exp\left(-\frac{x^2}{2\sigma_x^2}\right)\exp\left(-\frac{y^2}{2\sigma_y^2}\right) = \frac{1}{2\pi\sigma_\ell^2}\exp\left(-\frac{\ell^2}{2\sigma_\ell^2}\right), \tag{A.14}$$

where we used the fact that $\ell^2 = x^2 + y^2$ and the isotropic condition $\sigma_\ell = \sigma_x = \sigma_y$. Then, we can integrate this in polar coordinates to find the 68%-percentile around the mean:

$$0.68 = \frac{1}{2\pi\sigma_\ell^2}\int_0^{2\pi}\int_0^{\ell}\ell d\ell\ \exp\left(-\frac{\ell^2}{2\sigma_\ell^2}\right) = 1 - \exp\left(-\frac{\ell^2}{2\sigma_\ell^2}\right). \tag{A.15}$$

Isolating for σ_ℓ^2 and using (A.13) gives

$$\sigma_\ell^2 = \frac{\Delta\Omega r^2}{-2\pi\ln(0.32)}, \tag{A.16}$$

or in angles $\sigma_\theta = \sigma_\ell/r$,

$$\sigma_\theta^2 = \frac{\Delta\Omega}{-2\pi\ln(0.32)}. \tag{A.17}$$